STATIC LOAD VERSUS SETTLEMENT FOR GEOMETRIC SHAPES ON COHESIONLESS SOIL

by Theo A. Bryc and Lymon C. Reese

Department of Civil Engineering

The University of Texas

Austin, Texas

a report to

National Aeronautics and Space Administration

Langley Research Center

Hampton, Virginia

May 1965

STATIC LOAD VERSUS SETTLEMENT

FOR GEOMETRIC SHAPES ON COHESIONLESS SOIL

by

Raja A. Iliya
Lymon C. Reese

Prepared for

NATIONAL AERONAUTICS AND SPACE ADMINISTRATION

Langley Research Center
Hampton, Virginia

Contract   NsG-604

THE UNIVERSITY OF TEXAS

DEPARTMENT OF CIVIL ENGINEERING

Austin, Texas

May   1965

ABSTRACT

2 7 7 3 6

The bearing capacities and settlements of rigid-surface, spherical and conical foundation elements on sand of medium density were observed experimentally in static tests. Results were compared with those established by this investigation for circular plates loaded under the same conditions on the same type of sand. Equations for determining the bearing capacity of a cone and sphere were developed by theory and were supported by the experimental results.

The bearing capacity and settlement, as a function of the thickness of soil layer, were investigated to establish depth of soil beyond which values of either stay constant.

This investigation led to the conclusion that the bearing capacity of foundation elements with circular projected areas is a function of the cross-sectional diameter in the plane of the ground surface and varied directly with respect to this diameter.

As an example of this point, it was observed that the bearing capacity of two spheres of differing spherical diameters was the same if the cross-sectional areas at the plane of the ground surface were the same. *Author*

TABLE OF CONTENTS

Page

SYMBOLS AND NOTATIONS

A   Area, ft^2 or $in.^2$

B   Diameter or width of the footing, ft or in.

B_c Cross-sectional diameter of cone

B_p Diameter of plate whose surface area equals the surface contact area of a cone

c   Unit cohesion of the soil, lb/ft^2

c_a Adhesion force, lb/ft^2

D   Spherical diameter, ft or in.

D_f The vertical distance between the surface of the ground and the base of the footing, ft

E   Young's modulus of the solid, $lb/in.^2$

I_ρ Influence value of shape pertaining to settlement

k_s Coefficient of subgrade reaction, $tons/ft^3$

$\overset{o}{k_s}$ Coefficient of subgrade reaction for a circular plate, $tons/ft^3$

$\overline{k}_{s_1}$ Coefficient of subgrade reaction for a 1-ft square plate, $tons/ft^3$

$\overset{o}{k}_{s_1}$ Coefficient of subgrade reaction for a 1-ft diameter plate, $tons/ft^3$

N_c Dimensionless bearing capacity coefficient

N_γ Dimensionless bearing capacity coefficient

N_q Dimensionless bearing capacity coefficient

p   Pressure per unit of surface area, lb/ft^2 or $lb/in.^2$

P_p Passive earth pressure without adhesion component

q Load per unit of area, lb/ft^2 or $lb/in.^2$

q_n Net foundation pressure, lb/ft^2 or $lb/in.^2$

q_0 Ultimate bearing capacity, lb/ft^2 or $lb/in.^2$

q'_0 Ultimate bearing capacity for local shear failures, lb/ft^2 or $lb/in.^2$

r Radius of footing or one-half of the width, ft or in.

W Total weight of soil mass, or weight per unit of length, lb or lb/ft

y Settlement, ft or in.

α Half the vertex angle of a cone, degrees

γ Unit weight of soil, lb/ft^3

ϵ Unit axial strain, in./in.

μ Poisson's ratio

σ Normal stress, lb/ft^2 or $lb/in.^2$

σ_1 Major principal stress, lb/ft^2 or $lb/in.^2$

σ_3 Minor principal stress, lb/ft^2 or $lb/in.^2$

τ Shearing stress, lb/ft^2 or $lb/in.^2$

ϕ Angle of internal friction, degrees

ψ Angle of rise of lower boundary of central zone under a loaded

strip footing, degrees

LIST OF TABLES

---

[*]Superscript numbers refer to the References.

xi

LIST OF FIGURES

CHAPTER ONE

INTRODUCTION

1.1 General

An important and major part of soil mechanics deals with foundations; their shapes, sizes, position with respect to ground surface, bearing capacity of the soil and settlement.

Proper design of foundations is most essential, and should be studied thoroughly to assure the safety and soundness of the superstructures to be supported on the foundations. Two main requirements must be satisfied; namely, failure of the foundation by plunging must be avoided, and settlement must be maintained within the limits imposed by the superstructure that is supported.

In this investigation, the theories and techniques of soil mechanics are employed in a study related to the landing of spacecraft on soil. In particular, a study is made of the behavior under static loading of various shapes of landing heads.

Such a study requires the use of models, since in general the prototype is too large to be handled in the laboratory. Models of various scale ratios were used in order to develop expressions for behavior which can be employed to predict the behavior of prototypes under static loading.

1.2 Objectives of Investigation

The main objective is the load-settlement study of statically loaded foundation elements to develop expressions for predicting the load-settlement relationships for circular plates, spheres, and 60 degree cones.

1

In this investigation, models of the shapes of possible landing heads of spacecraft were studied both theoretically and experimentally, with the objective in mind of developing non-dimensional expressions for predicting the load-settlement behavior.

Since experimental studies in this investigation involved the use of models, another study of importance which was undertaken concerned the depth or thickness of the foundation soil. Knowledge was desired concerning the depth at which there was no appreciable influence from the boundaries of the container. A thorough study was done through load tests using a 2.22-in. diameter plate as a foundation element.

1.3 Scope of Investigation

Though a landing spacecraft probably would cause dynamic loading as the result of impact, the scope of this investigation is limited to static loading tests on three types of foundation elements; namely, plates, spheres, and cones. Moreover, the foundation elements tested and the respective soil beds were limited by the means of handling and performing such tests within the soil mechanics laboratories. The soil beds were eight times the diameter of the plate in depth, width and length, thus placing a limitation on the elements to be tested as the soil beds became too heavy to be handled in the laboratory.

1.4 Foundation Elements Selected

The foundation elements selected were circular, conical, and spherical in shape. (See Fig. 1.) The circular plates formed the basis for establishing the theory and the experimental procedures; and the observed data from plates were compared with that from spheres and cones for the same
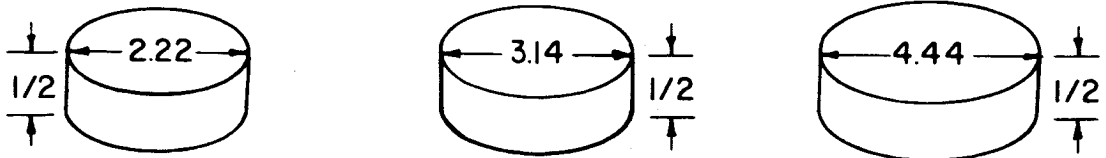
CIRCULAR PLATES
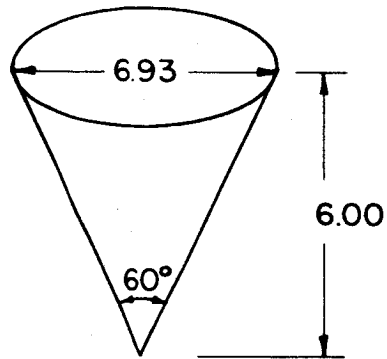
CONE
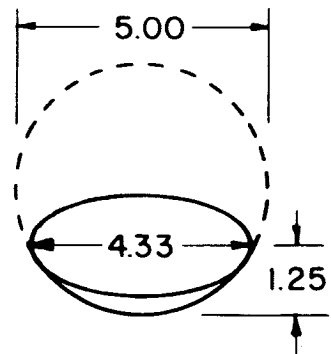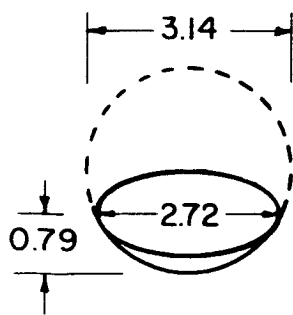
SPHERES

NOTE—ALL DIMENSIONS ARE IN INCHES

FIG. I FOUNDATION ELEMENTS

conditions of foundation soil.

The plates were of three sizes: 2.22 in., 3.14 in., and 4.44 in. in diameter, with surface areas in contact with the soil of ratios of 1 to 2 to 4 respectively. All three plates were machined from aluminum blocks having 1/2-in. thickness. The deflections of the plates within the range of applied loads are negligible and therefore the plates may be considered as rigid footings.

The spheres chosen were of two sizes; 3.14 in. and 5 in. in spherical diameter. At various embedments within the soil, the spheres furnish cross-sectional areas, as well as surface contact areas, equivalent to those of the plates. Therefore, the two spheres formed a basis for comparative study with the circular plates, and also permitted a study of the effect of the spherical diameter on the load-settlement relationship.

The conical element chosen was a right circular cone with the half angle at the vertex equal to 30 degrees with the vertical. One cone, 6 in. high, was used. The cone and spheres were solid aluminum castings and were similarly considered to be rigid footings.

1.5 Foundation Medium Used

The foundation medium used was clean, dry sand that was kept at room conditions. It was brought from the Colorado River basin in Austin, Texas. The sand was sifted on a "Rotex" sifter, style No. 12, with a pulley speed of 520 to 560 rpm. The sifter had two U. S. Standard sieves, No. 30 and No. 200. The output, passing sieve No. 30 but retained on sieve No. 200, was collected for use in this investigation. A sieve analysis to determine the grain size distribution is given in Chap. IV, Art. 4.1.

Examined under a magnifying lens, the sand grains were found to be of rather smooth, round shapes. Moreover, the sand was found to be quite rich in silica.

CHAPTER TWO

THEORETICAL CONSIDERATIONS

2.1 Introduction

The load-settlement relationships for the three types of foundation

elements were studied both theoretically and experimentally.

Figure 2 shows a typical load-settlement curve for a plate that was

loaded at a shallow depth, i.e., the depth of the soil to the bottom of the

plate did not exceed twice the diameter or width of the plate.

As seen from Fig. 2, the ultimate load that the ground can sustain

is clearly indicated by the fairly abrupt passing of the curve into a

vertical tangent, at which stage the failure of the earth support may be

identified. This type of failure is called general shear failure.[22] (Refer

to Fig. 3.)

On the other hand, if the load-settlement curve does not exhibit a peak

load as for the shallow foundation (Fig. 2) but continues to descend on a slope,

as shown by the curve of Fig. 3; then the failure of the earth support is

arbitrarily specified, in accordance with accepted conceptions, as soon as

the curve passes into a steep and fairly straight tangent. Such a type of

failure is called local shear failure.[22]

The load which causes the failure of the earth support is called the

total or ultimate bearing capacity, and when used per unit of bearing area,

it is called the bearing capacity of the soil.

Therefore, the load-settlement relationship involves the knowledge of

the bearing capacity of the soil and the settlement of the foundation element.

6

FIG. 2. TYPICAL LOAD–SETTLEMENT CURVE FOR A SHALLOW PLATE.

LOAD q

q'_o q_o

SETTLEMENT Y

GENERAL SHEAR

LOCAL SHEAR
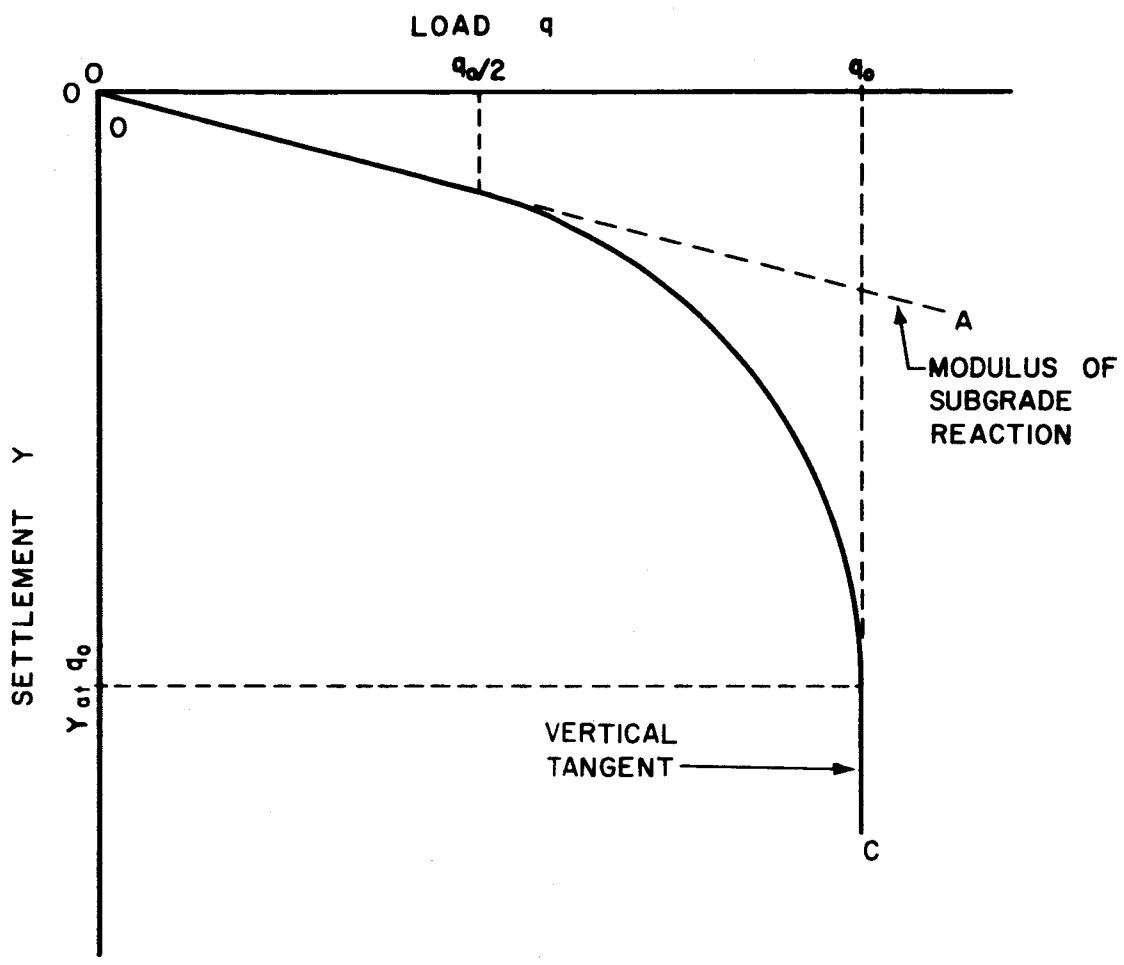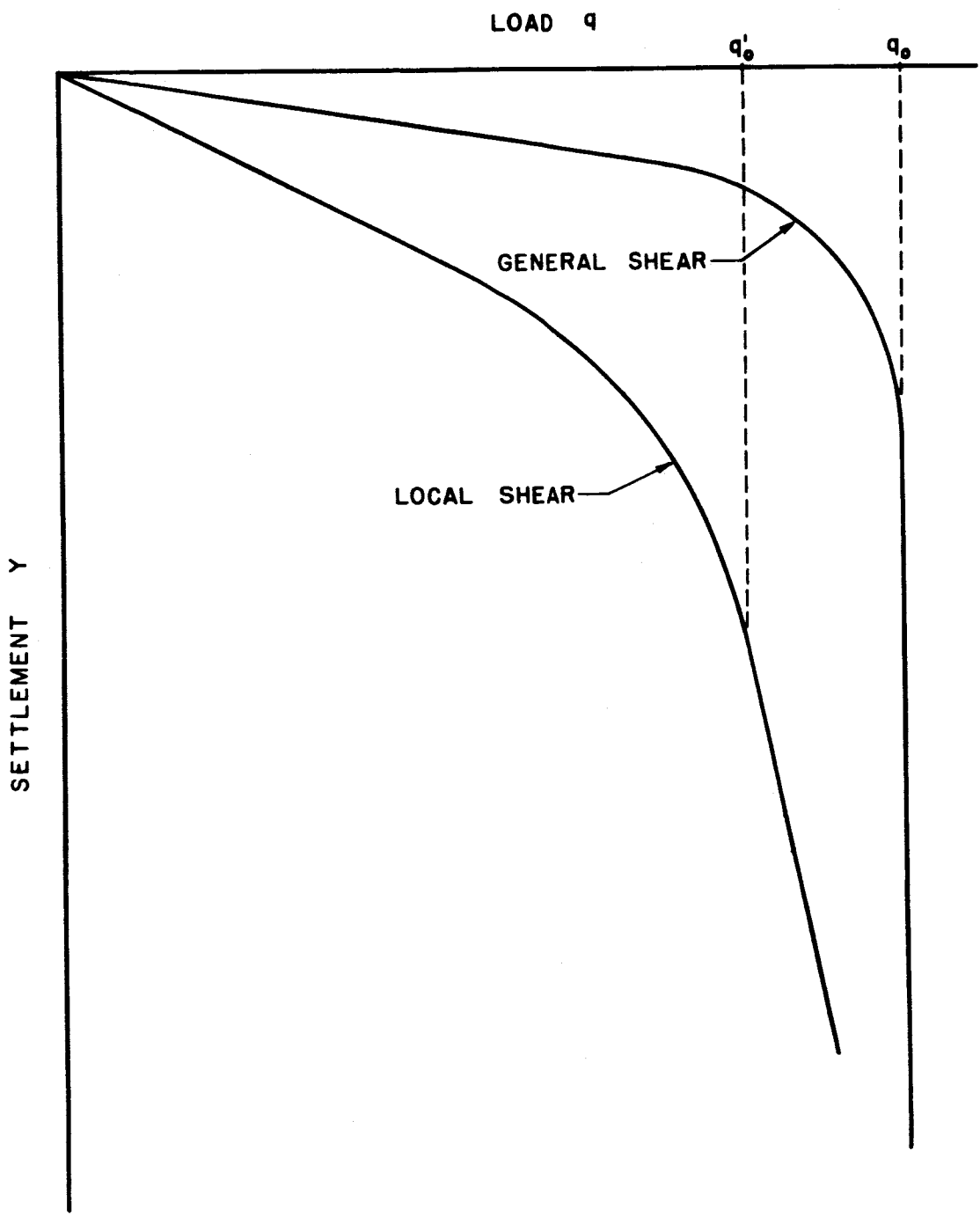
FIG. 3. ILLUSTRATION SHOWING CASES OF SHEAR FAILURE

Referring to the typical load-settlement curve, Fig. 2, the early part of the curve is almost a straight line extending to about one-half the value of the ultimate load. Then it deviates through a curved section to pass on to the vertical tangent. The slope of the straight line section is called the modulus of subgrade reaction.[21]

In this chapter, the theoretical considerations involved in the following load-settlement relationships are briefly discussed:

    A. Bearing capacity

    B. Settlement analysis

    C. Theory of subgrade reaction.

2.2 The Bearing Capacity of Foundations

    A. Introduction

The bearing capacity of foundations is influenced by the following factors:[8]

    (1) Mechanical properties of the soil:

        (a) Density

        (b) Shearing strength

        (c) Deformation characteristics

        (d) Size and shape of grains

    (2) Physical definitions of loaded area:

        (a) Size

        (b) Shape

        (c) Roughness of base

        (d) Depth below ground surface

    (3) The initial stresses in the soil

    (4) Water conditions in the ground.

These factors clearly indicate that the rather widespread idea that the bearing capacity depends mainly on the characteristics of the soil in question is incorrect. While the main difficulty in bearing capacity problems is that of evaluating soil properties, there are many other factors to be considered. Therefore, it is erroneous to use the bearing capacity tables of some building codes that only list the type of soil with no allowance or modification for certain designated conditions.

B. Theory of Bearing Capacity for Shallow Footings

A number of theories have been presented which furnish expressions for the ultimate bearing capacity. It is worth noting the theory of Prandtl, which was originally set up for metals.

Figure 4 shows a cross-section illustrating Prandtl's plastic equilibrium theory[16] for long, loaded areas of width B on the surface of the soil. The figure shows the three zones which exist after failure is reached. Zone I moves downward with the footing, pushing Zone II into a radial motion. Zone III, in turn, is pushed up and out. On the basis of these assumptions Prandtl developed an expression for ultimate bearing capacity q_0 , dependent principally on the angle of internal friction ϕ as defined in Mohr-Coulomb.[28] Since soils have the characteristic of compressibility, no close agreement was reached between soils and Prandtl's hypothesis. However, the general concepts of the mechanics of failure as given by this theory are reasonably correct.

Terzaghi[23, 25] in 1943 presented a more general solution for the ultimate bearing capacity of long footings. Figure 5 shows the failure zones and surfaces assumed by this theory.

Terzaghi's method contains various assumptions which are discussed in
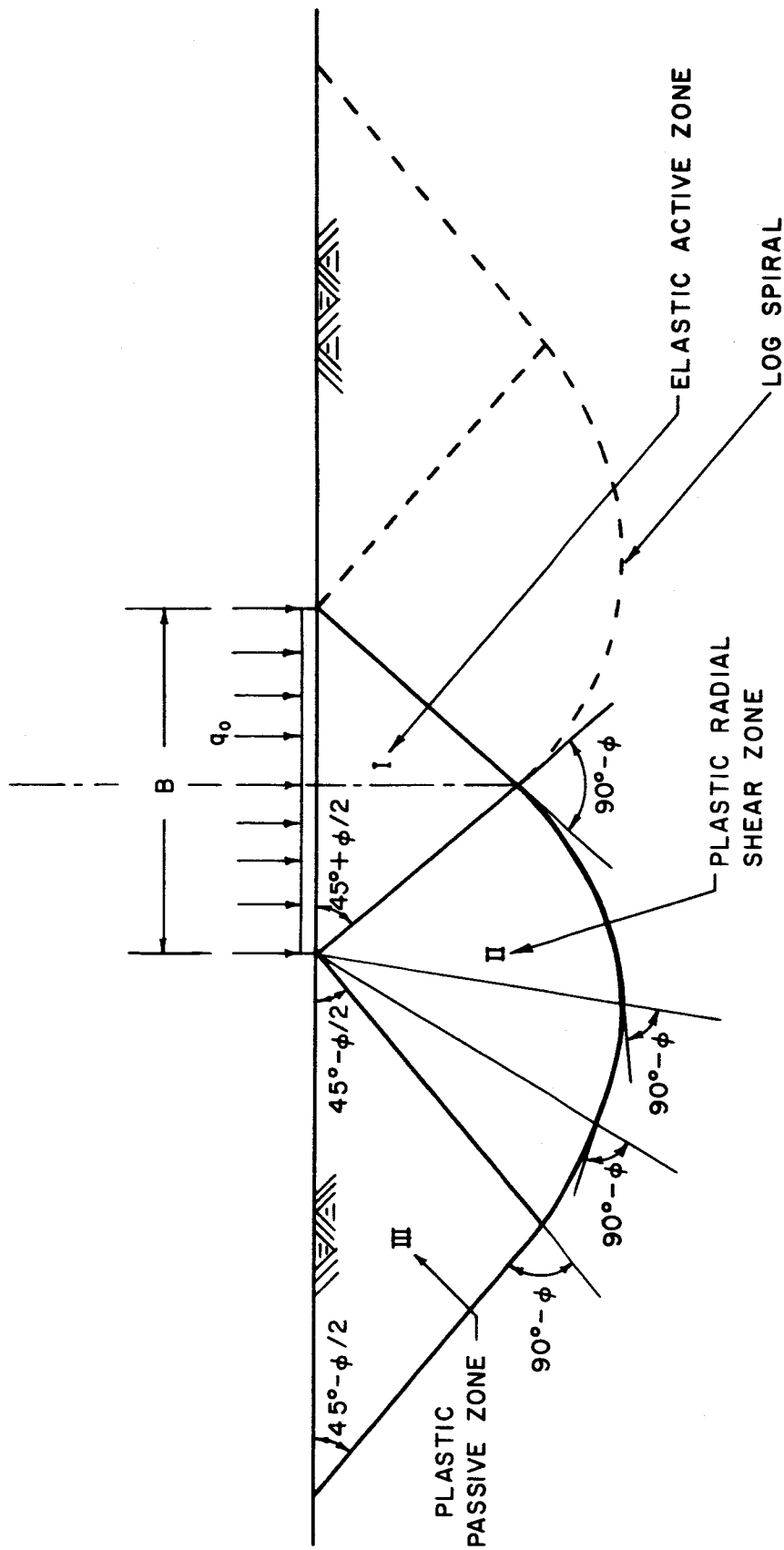
FIG. 4 PRANDTL'S PLASTIC EQUILIBRIUM THEORY FOR LONG AREAS
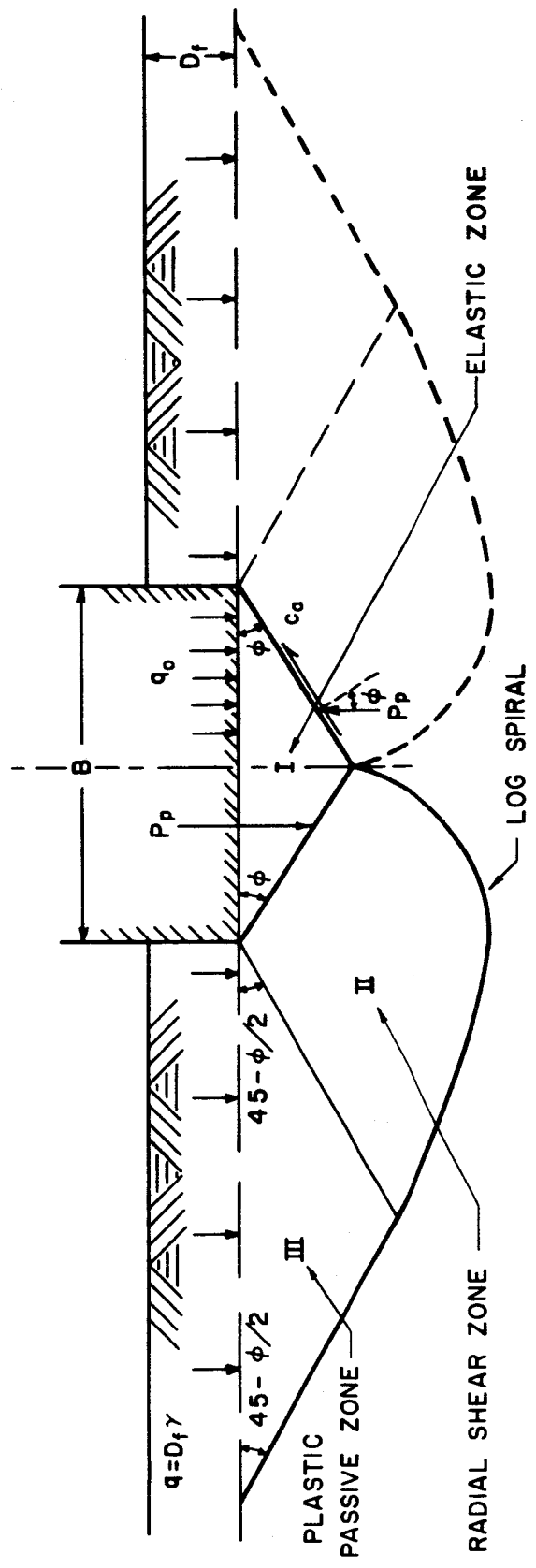
FIG. 5. TERZAGHI'S PLASTIC EQUILIBRIUM THEORY FOR CONTINUOUS FOOTINGS

Chap. V in comparing results from theory to the data from experiments. However, all the assumptions used by this theory are quite reasonable, and results from this approach should be quite accurate for most cases.

For the benefit of the reader, the general equations for bearing capacity from Terzaghi's theory are presented here. Some aspects of these equations are discussed in detail in Chap. V.

Terzaghi[17, 23] showed that for general shear failure the ultimate bearing capacity of long footings at, or below, the surface of any soil is given by

$$q_0 = c(N_c) + \gamma B(0.5 N_\gamma) + \gamma D_f(N_q) \tag{1}$$

where the dimensionless N coefficients N_c, N_γ, and N_q are bearing capacity factors that depend only on the value of the angle of internal friction ϕ, and where

  D_f = the vertical distance between the surface of the ground and the base of the footing

  γ = unit weight of the soil

  c = cohesion per unit of area

  B = width of the footing.

Figure 6 shows the relationships between the bearing capacity coefficients and the angle of internal friction.[17, 23]

The above expression represents the two-dimensional case. From an analysis of experimental data Terzaghi obtained the following expressions for the ultimate bearing capacity for round, shallow footings,[18, 26]

$$q_0 = 1.3c(N_c) + 0.3\gamma B(N_\gamma) + \gamma D_f(N_q). \tag{2}$$
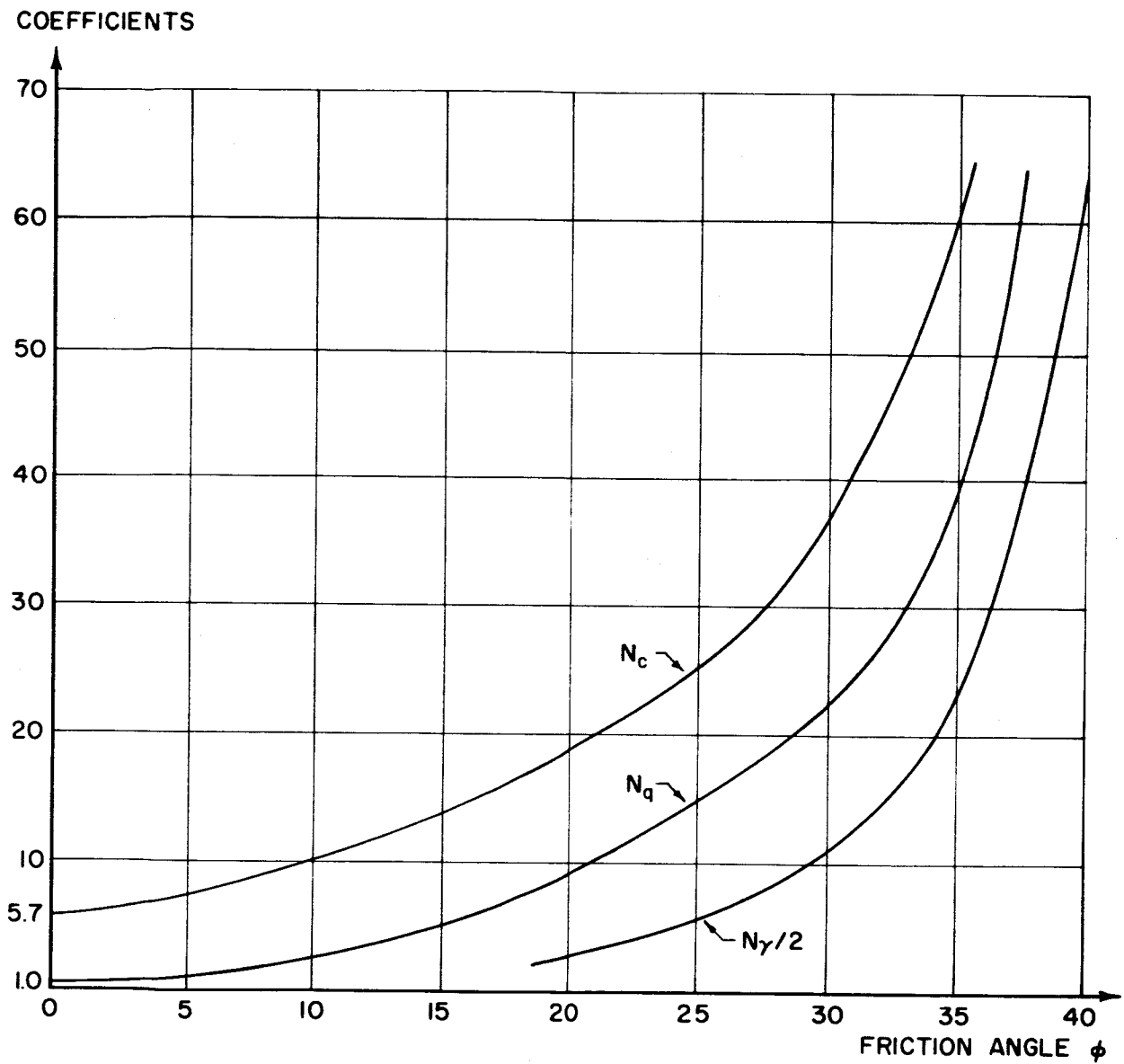
COEFFICIENTS

FIG. 6. COEFFICIENTS OF THE TERZAGHI EXPRESSIONS FOR ULTIMATE BEARING CAPACITY

An expression for the ultimate bearing capacity of purely cohesive soils may be determined by setting the friction angle equal to zero. Similarly, an expression for cohesionless soils may be determined by setting the cohesion c equal to zero. Therefore, the expressions for the ultimate bearing capacity for circular footings placed on the surface of the soil ($D_f = 0$), are given according to Terzaghi's theory by

$$q_0 = 1.3c(N_c) \text{ for purely cohesive soils} \tag{3}$$

and

$$q_0 = 0.3\gamma B(N_\gamma) \text{ for purely cohesionless soils.} \tag{4}$$

It may be noted here that the ultimate bearing capacity for purely cohesive soils is entirely related to the cohesion c and the coefficient N_c which is a constant. Therefore, the value of q_0 as expressed in Eq. 3 is constant for a given cohesive soil regardless of the size and shape of footing.

On the other hand, the ultimate bearing capacity for cohesionless soils is related to the diameter B as well as the coefficient N_γ which is a function of ϕ. Therefore, the value of q_0 as expressed in Eq. 4 for a given cohesionless soil is not constant but is directly proportional to the diameter B.

In this investigation, (refer to Chap. V), a theoretical approach similar to that above was used to develop bearing capacity expressions for the conical and spherical foundation elements on cohesionless soils.

Many other theories on bearing capacity[5, 8, 13, 15] have been presented

in the literature. These theories offer only slight modifications to the theories of Prandtl and Terzaghi. Therefore, only these two theories are discussed and Terzaghi's theory is employed later as the basis for comparison with the experimentally observed data.

2.3 Settlement Analysis of Surface Footings

For rigid footings resting on the surface of the soils where no tilting is allowed, the settlement must be uniform. The generally accepted pressure distribution under such footings is shown in Fig. 7 for both types of soils, cohesionless and cohesive.[20]

In sand, under uniform settlement, the high resistance to compression in the soil below the center of the footing, as compared to the lack of resistance to compression below the edges, must result in a relatively large pressure under the center and no pressure at the edges, as shown in Fig. 7(a). The shearing strain, developed below the edges of the footing due to difference in soil subsidence, is caused by a vertical force from the footing. In sands, owing to the lack of rigidity, little or no force is required to develop shearing strains at the edges of a surface footing; whereas in cohesive soils a large force is required. This explains the larger edge pressure distribution for clay as shown in Fig. 7 (b).

In estimating the settlement of a foundation on a clay soil, it is important to realize that the total movement is composed of two main portions, the immediate settlement and the consolidation settlement.

The immediate settlement is considered to be due to deformation of the soil without volume change, by lateral yielding, and thus is taken as the elastic settlement. It is considered to be the more important component

RIGID FOOTING

SETTLEMENT

PRESSURE DISTRIBUTION

(a.)

RIGID FOOTING

SETTLEMENT

PRESSURE DISTRIBUTION

(b.)
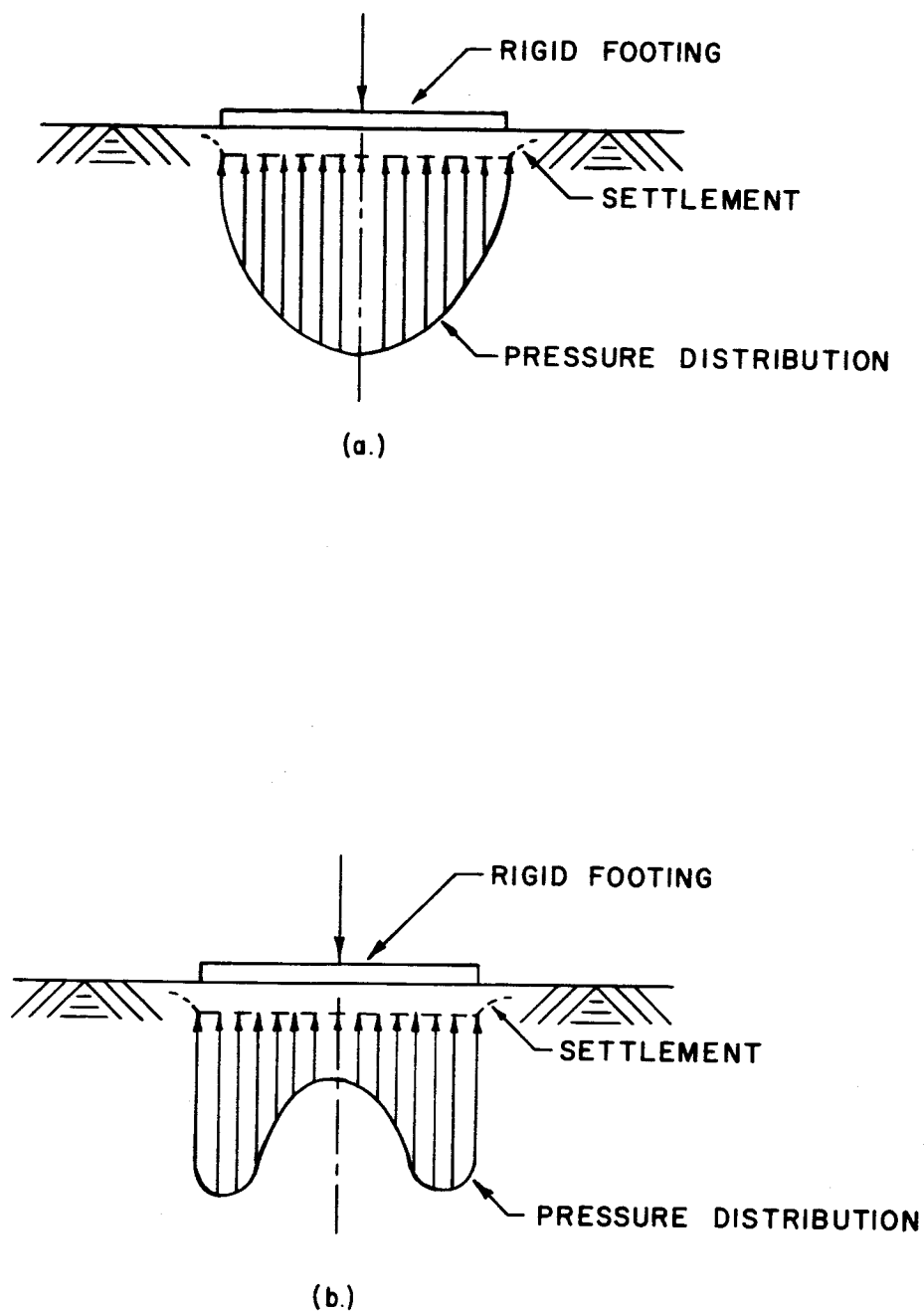
FIG. 7. PRESSURE DISTRIBUTION UNDER RIGID FOOTING'S (a.) ON SAND (b.) ON CLAY

for loads which are small in relation to the ultimate bearing capacity. However, Meyerhoff[9] stated that the immediate settlement appears to contain two fairly distinct components, resulting from elastic and plastic deformations, with settlements due to plastic deformations forming up to one-quarter of the total movement.

From the theory of elasticity,[24] the immediate settlement of a loaded area on the surface of a semi-infinite solid is given by the expression

$$y = q_n B \frac{1-\mu^2}{E} I_\rho \tag{5}$$

where

q_n = net foundation pressure

B = breadth or diameter of the loaded area

μ = Poisson's ratio

E = Young's modulus of the soil

I_ρ = influence value depending on the shape and rigidity of the loaded area.

For saturated clays there is no volume change if there is no dissipation of pore pressure. Therefore, Poisson's ratio may be used as 0.5 in the calculations of settlements. The value of E is taken from the stress-strain curve obtained in the undrained triaxial test.

As shown by Skempton,[15] Eq. 5 can be re-arranged, for convenience, in the form

$$\frac{y}{B} = \frac{q_n}{q_0} \frac{q_0}{c} I_\rho \frac{1-\mu^2}{E/c} \tag{6}$$

where

q_0 = ultimate bearing capacity

c = apparent cohesion of the clay.

The ultimate bearing capacity of clays (for the condition of $\phi = 0$) as previously discussed is expressed by

$$q_0 = c(N_c) + \gamma D_f(N_q). \tag{7}$$

Note that the middle term in Terzaghi's general expression[17, 23] dropped out due to the value of $N_\gamma = 0$ for $\phi = 0$. Since for surface footings D_f is zero, the expression is reduced to the general form of

$$q_0 = cN_c \tag{8}$$

or

$$N_c = \frac{q_0}{c}. \tag{9}$$

The value of I_ρ as shown by Timoshenko[27] and others[12, 15] for circular footings at the surface is

$$I_\rho = \frac{\pi}{4},$$

then for a rigid circular plate at the surface, by substitution in Eq. 6

$$\frac{y}{B} = \frac{q_n}{q_0} N_c \frac{\frac{\pi}{4}\left[1 - (0.5)^2\right]}{E/c}. \tag{10}$$

Now, by definition from the undrained triaxial compression test, the relation between stress and strain is

$$\epsilon = \frac{\left(\sigma_1 - \sigma_3\right)}{E} \tag{11}$$

where

ϵ = axial strain

$\sigma_1 - \sigma_3$ = deviator stress

E = Young's modulus using the secant at the stress condition

equal to $\left(\sigma_1 - \sigma_3\right)$.

Equation 11 may be written in the form

$$\epsilon = \frac{\left(\sigma_1 - \sigma_3\right)}{\left(\sigma_1 - \sigma_3\right)_f} \quad \frac{\left(\sigma_1 - \sigma_3\right)_f}{c} \quad \frac{1}{E/c} \; , \tag{12}$$

where the f denotes failure condition. For undrained testing, the failure condition for saturated clays is represented by

$$\left(\sigma_1 - \sigma_3\right)_f = 2c \tag{13}$$

or

$$\frac{\left(\sigma_1 - \sigma_3\right)_f}{c} = 2. \tag{14}$$

Substituting in Eq. 12

$$\epsilon = \frac{\left(\sigma_1 - \sigma_3\right)}{\left(\sigma_1 - \sigma_3\right)_f} \quad \frac{2}{E/c} \tag{15}$$

Assuming similarity between stress-strain curves from triaxial tests and load-settlement curves from bearing capacity studies as shown in Fig. 8, the following relation may be stated.

$$\frac{q_n}{q_0} = \frac{\left(\sigma_1 - \sigma_3\right)}{\left(\sigma_1 - \sigma_3\right)_f} \tag{16}$$

Solving Eqs. 10, 15 and 16 simultaneously, Eq. 17 is obtained.

$$\frac{\epsilon}{2} = \frac{y}{B} \frac{1}{N_c} \frac{1}{\pi/4\left[1 - (0.5)^2\right]} \tag{17}$$

Therefore,

$$\frac{y}{B} = 0.2945 \, N_c \, \epsilon \tag{18}$$

or

$$y = 0.2945 \, B \, N_c \, \epsilon \tag{19}$$

Equation 19 has been derived here for circular plates; equations for plates of different shapes can be derived similarly by using the proper influence factor I_ρ.

Therefore, as discussed by Lee,[6] this approach leads to a general procedure for predicting plate settlements from unconfined compression tests of a saturated clay. Referring to Fig. 8, the steps for predicting plate settlements are as follows.

1. From the compression test, plot the stress-strain relationship.

22
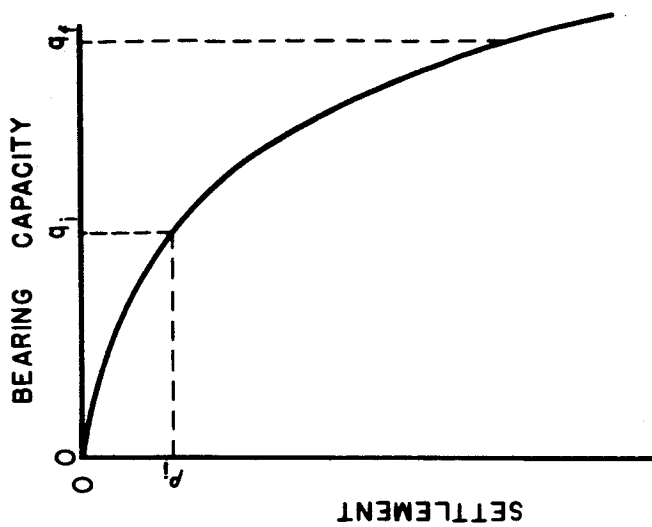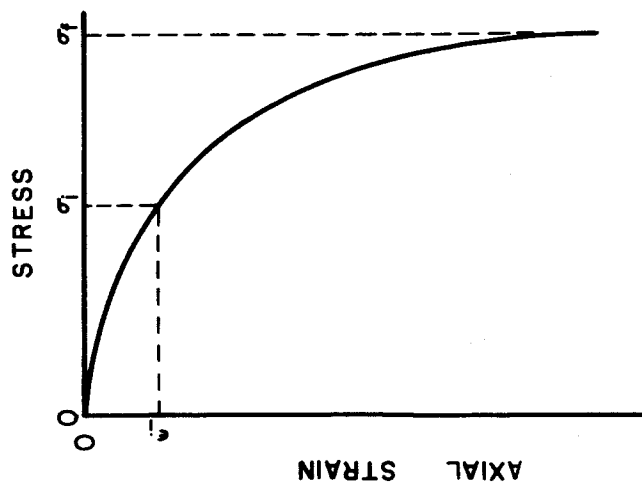
FIG. 8.

2. For any value of stress σ , obtain the corresponding strain ϵ .

3. Using Eq. 19 and substituting the value of N_c , determine the

settlement y for the value of ϵ , corresponding to the applied

stress, and plot results. The value of N_c may be obtained from

the theories of Terzaghi,[23] Skempton,[15] or Meyerhoff.[8]

Equation 19 cannot be expected to yield accurate results in the high

range of $\dfrac{q_n}{q_o}$ since at loads near the ultimate bearing capacity a consid-

erable zone of the clay beneath the footing is subjected to strains greater

than those at the ultimate stress in the compression test.

It is of interest to note that Skempton[15] has shown the greater part

of the settlement is due to strains in the clay within a depth of not more

than four times the diameter below the base of the footing. At the greater

depths, the shear stresses are less than about 5 per cent of the net founda-

tion pressure q_n .

As noted in the above discussion, the theory as expressed in Eq. 19

was developed for a saturated clay. No comparable theory exists for a cohe-

sionless soil; however, as discussed later some aspects of the settlement

of a plate on cohesionless soil were considered in this investigation.

2.4 The Theory of Subgrade Reaction

Referring to Fig. 2 which shows the typical load-settlement curve for

a shallow plate, the slope of the straight-line portion of the curve is the

subject of the theory of subgrade reaction.

The theory of subgrade reaction as presented by Terzaghi[21] is a simpli-

fied method for the solution of settlement problems.

The subgrade reaction is the pressure p per unit of area of the surface of contact between a loaded beam or slab and the subgrade.

The coefficient of subgrade reaction k_s is the ratio between this pressure p at any given point of the surface of contact and the settlement y produced by the application of the load at that point. Therefore,

$$k_s = \frac{p}{y} \ . \tag{20}$$

The value k_s depends on the elastic properties of the subgrade and on the dimensions of the loaded area.

Terzaghi's theory[21] of subgrade reaction is based on the following simplifying assumptions:

1. The ratio $k_s = \frac{p}{y}$ is independent of the pressure p, and

2. k_s has the same value for every point of the surface acted upon by the contact pressure.

In connection with a rigid foundation the relation $k_s = \frac{p}{y}$ leads to the fact that the distribution of the subgrade reaction p over the base of the foundation must be planar since a rigid foundation remains plane when it settles. Hence, we can assume that the subgrade reaction has a planar distribution; this is contrary to the reality. (Refer to Fig. 7.)

In spite of the discrepancy between theory and reality, the theory of subgrade reaction can be used safely in the design of footings. The errors are within the margin of safety, and moreover the results are conservative.

The numerical values of the coefficient of subgrade reaction can either be estimated on the basis of published data from tests or else can be derived from field tests.

The coefficient of subgrade reaction $\bar{k}_{s_1}$ for a square plate with a width of one ft has been selected as a basis from which values for other shapes and sizes may be computed. The following table, as given by Terzaghi,[21] gives values for $\bar{k}_{s_1}$ in tons per cu ft for square plates 1 ft x 1 ft resting on sand. Terzaghi also gives values for $\bar{k}_{s_1}$ for clay; however, the experimental portion of this investigation deals only with sand; therefore, only values for sand are presented here.

TABLE 1.

Values of $\bar{k}_{s_1}$ in Tons/ft^3

Relative Density of Sand,	Loose	Medium	Dense
Dry or moist sand, limiting values	20 - 60	60 - 300	300 - 1000
Dry or moist sand, proposed value	40	130	500

The coefficient k_s for a rectangular plate of width B may be obtained from the relation[21]

$$k_s = \bar{k}_{s_1} \left(\frac{B + 1}{2B} \right)^2 ,$$ (21)

where B is feet.

Moreover, the adjusted values for shape and size may be obtained from the following relations:[21]

$$k_s = \frac{2}{3} \bar{k}_{s_1} \quad \text{for continuous footings}$$ (22)

and

$$\bar{k}_{s_B} = \frac{\bar{k}_{s_1}}{B} \quad \text{for a square footing of width} \quad B. \tag{23}$$

The use of the theory of subgrade reaction has limitations due to the simplifying assumptions upon which it is based. Referring to Fig. 2, the line OA represents the first assumption in the theory of the subgrade reaction; whereas, the curve OC would be the true relationship if loading tests were performed. As seen, therefore, the assumption is valid at best only up to values of p equal to about one-half the ultimate bearing capacity. Moreover, the second assumption states that the subgrade reaction p has the same value under all the contact area of the footing. In reality, the pressure at the rim of the surface of contact is different than at the center as shown in Fig. 7.

A comparison between the values of coefficient of subgrade reaction as determined in this investigation and as given by Terzaghi is shown later.

CHAPTER THREE

TESTING EQUIPMENT

3.1 The Soil Beds

The soil beds were placed in boxes made out of 3/4-in. plywood. Exist-

ing soil mechanics literature indicates that foundation beds must have a

depth and width not less than four to six times the diameter or width of

the footing in order that the boundaries of the container do not affect

the results of load bearing tests.[14, 15] For this investigation the factor

of eight times the diameter was chosen to insure accuracy of the results.

The same depth dimension was also used for the length and width; therefore,

the foundation beds used during this investigation had the following sizes:

18 in. x 18 in. x 19 in. for the 2.22-in. diameter plate

25 in. x 25 in. x 26 in. for the 3.14-in. diameter plate

36 in. x 36 in. x 37 in. for the 4.44-in. diameter plate

The largest box was used during testing of the cone and the two spheres.

The box depth was made 1 in. deeper than required to allow for the larger

initial volume of sand in its loose condition, prior to its vibration.

3.2 Loading Machine

The loading was applied by the use of an unconfined compression testing

machine (Soil Test U-160-A) which was manufactured to be manually operated.

The machine was converted to motor-operated, with a gear to control the rate

of loading. As shown in Fig. 9, the machine, with its top cross bar removed,

was mounted upside down on a rigid steel frame. A double proving ring attach-

ment (Soil Test No. 2124) was fitted on the loading piston so that the applied

UNCONFINED COMPRESSION MACHINE

GEAR-DRIVEN MOTOR

HOIST

DOUBLE PROVING RING

FOOTING ELEMENT

SAND BOX

STEEL FRAME
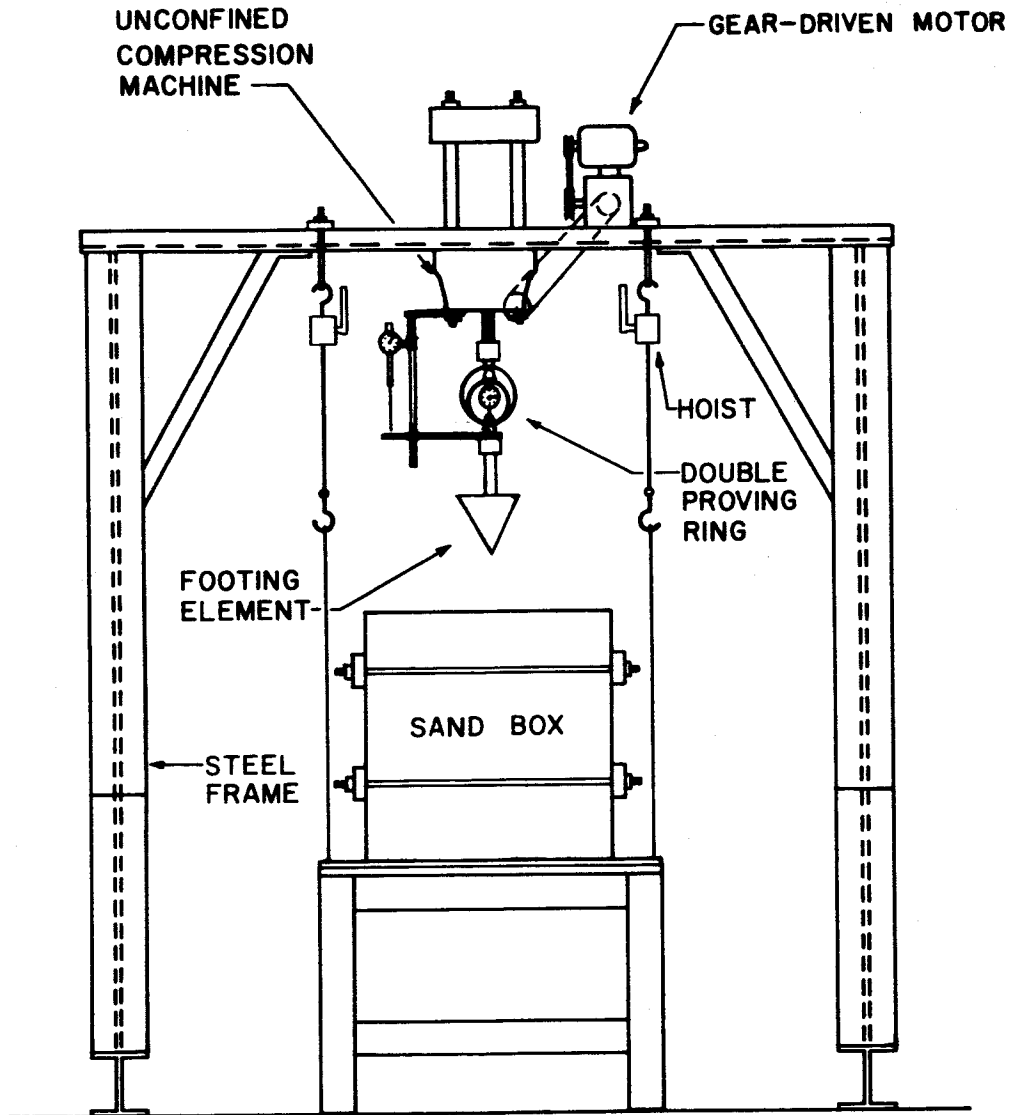
FIG. 9.   TESTING EQUIPMENT
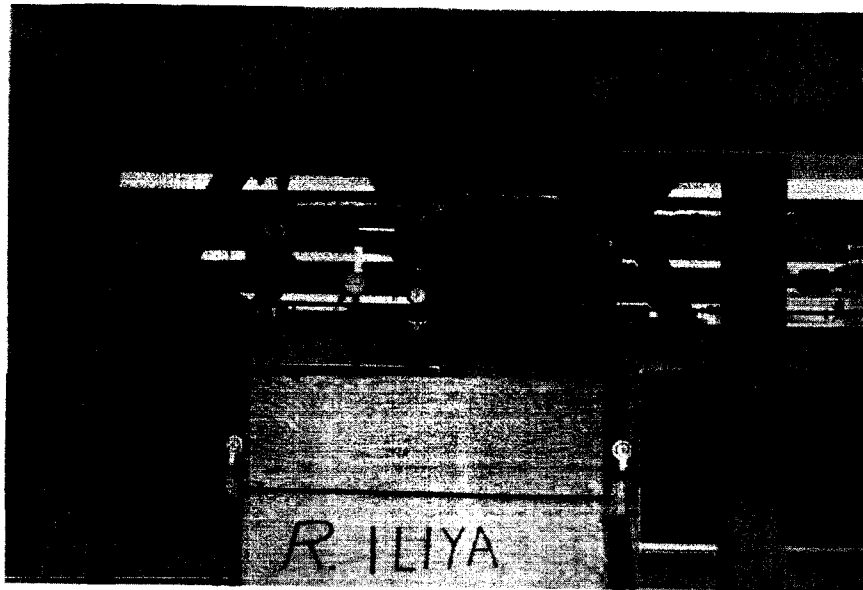
FIG. 9 TESTING EQUIPMENT

load could be accurately measured to a value of about 0.3 lb.

The piston on the loading machine had a 4-in. stroke, which was sufficient to produce ample settlement in all the foundation elements employed in the tests. The settlement measurements were made with an extensometer, with two inches of travel, which was rigidly attached to the body of the loading machine (see Fig. 9).

The loading piston was fitted with a threaded brass head to which the various foundation elements were attached.

3.3 Load Cells

As a control on the density of the soil to be tested, the weight of the prepared foundation boxes had to be measured; and since the weight exceeded the capacity of the existing platform scales in the soil mechanics laboratories, load cells were used. Two manually-operated hoists were mounted on the steel frame to lift the boxes so that they could be weighed by either of two Baldwin SR-4 load cells, having capacities of 600 lb and 6000 lb. Weights were read from a Baldwin SR-4 calibration indicator.

3.4 Vibrator

As the foundation soil had to be in a dense state, a concrete hand vibrator with a flexible shaft was used for densifying the sand. The vibrator was manufactured by the Viber Manufacturing Company, and has a power capacity of 345 watts while in concrete.

CHAPTER FOUR

TESTS - PROCEDURES AND DESCRIPTION

4.1 Sieve Analysis and Classification of the Sand

A sieve analysis using standard procedures was made to determine the grain size distribution, and the resulting curve is shown in Fig. 10.

As seen from the grain size accumulative curve in Fig. 10, the sand tested may be classified as a uniform fine sand. Only 7 per cent of the sand passed the No. 80 sieve.

4.2 Density Control Test

One of the critical factors that influence the results of load-settlement tests is the density of the foundation soil. To assure uniformity in the testing conditions of the foundation soil, proper density control or checks must be maintained for every test.

The sand, being a cohesionless material, is densified best through vibration, and as described in Art. 3.4 a concrete vibrator was used to attain the desired density.

The foundation boxes were calibrated along the depth with marks at 6-in. spacings. The sand was then placed in layers of approximately 6 in. and each layer was vibrated for the specific period of time tabulated in Table 2.
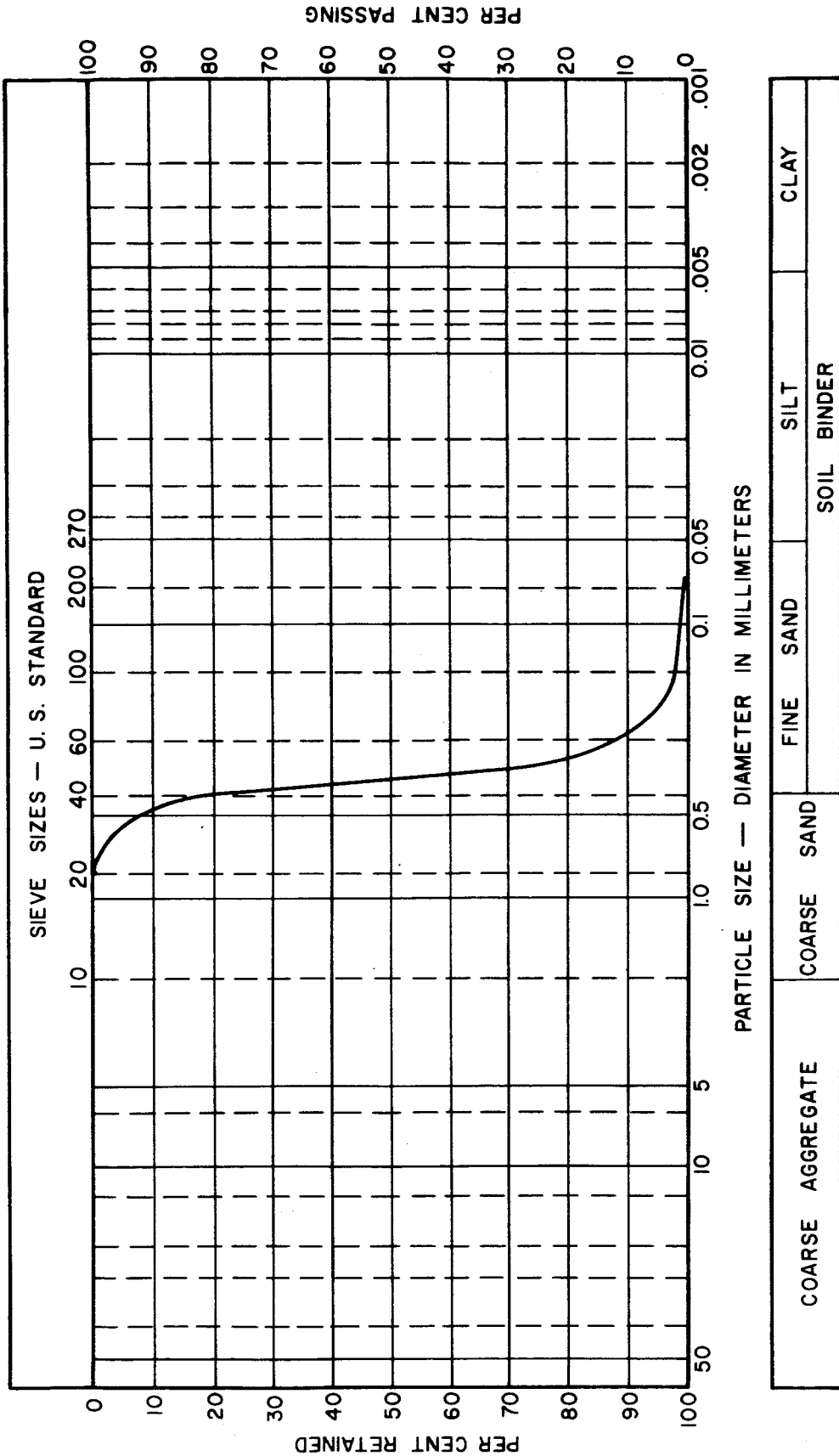
FIG. 10. MECHANICAL ANALYSIS
GRAIN SIZE ACCUMULATIVE CURVE

32

TABLE 2.

VIBRATOR TIME AND POSITIONS

Size of Box in.	Vibrator position	Vibrating Time per Position sec.	Total time per Layer min.
18 x 18 x 19	4 corners	15	1
25 x 25 x 26	4 corners	30	2
36 x 36 x 37	4 corners	30	4
	4 sides	30	

The new height of sand, after vibration, was measured, and the volume was determined. Using the load cell, the sand was weighed and the density was computed. The operation was repeated layer after layer until the box was filled to the required height.

To be sure that the density of the soil did not vary appreciably between the various layers, another type of test was run. One layer after another was scraped from an already full and vibrated box. Then each layer removed was measured for volume and weighed for density computations.

The observed results showed that the density of the sand was controlled within a maximum variation of 4 per cent. Such a variation is thought to be within the accepted precision required for load-settlement tests.

It is of interest to note that the vibration time varied almost directly with respect to the volume of the sand to be densified. The 6-in. layer in the 18-in. x 18-in. box, which measured 1.12 cu ft, was vibrated for one minute to achieve the desired density; while a 6-in. layer in the 36-in. x

36-in. box, which measured 4.50 cu ft, was vibrated for four minutes to achieve the same desired density. The ratio of the volume increase was approximately four times, which agreed with the time ratio of four. Similarly, a 6-in. layer in the 25-in. x 25-in. box, which measured 2.17 cu ft, required two minutes of vibration time to attain the same desired density.

4.3 Determination of the Angle of Internal Friction of the Sand[*]

Vacuum-triaxial tests were run on samples taken from the same sand used in this investigation. The samples were 1.4 in. in diameter and 3.2 in. in height. They were prepared by vibration on a small vibrating platform to attain various densities ranging from the loosest density of 95 lb/ft^3 to the maximum density of 108 lb/ft^3 that was attainable with this sand.

The test speeds were around 0.07 in. per minute under a vacuum up to 10 $lb/in.^2$.

The curve which shows the relation between density and the angle of internal friction of the sand is given in Fig. 11. The density of the sand during the load-settlement tests ranged from 99 to 103 lb/ft^3.

The angle of internal friction as determined is approximately 38.7 degrees, for the average density of 101 lb/ft^3 assumed to apply for all the load-settlement tests. (Refer to Fig. 11.) The probable error in the value of the density was computed for all the load-settlement tests and was found to be 0.8 lb/ft^3.

---

[*]This section is summarized from the unpublished research investigation of Osman I. Ghazzaly, another phase of the entire project mentioned in the preface.
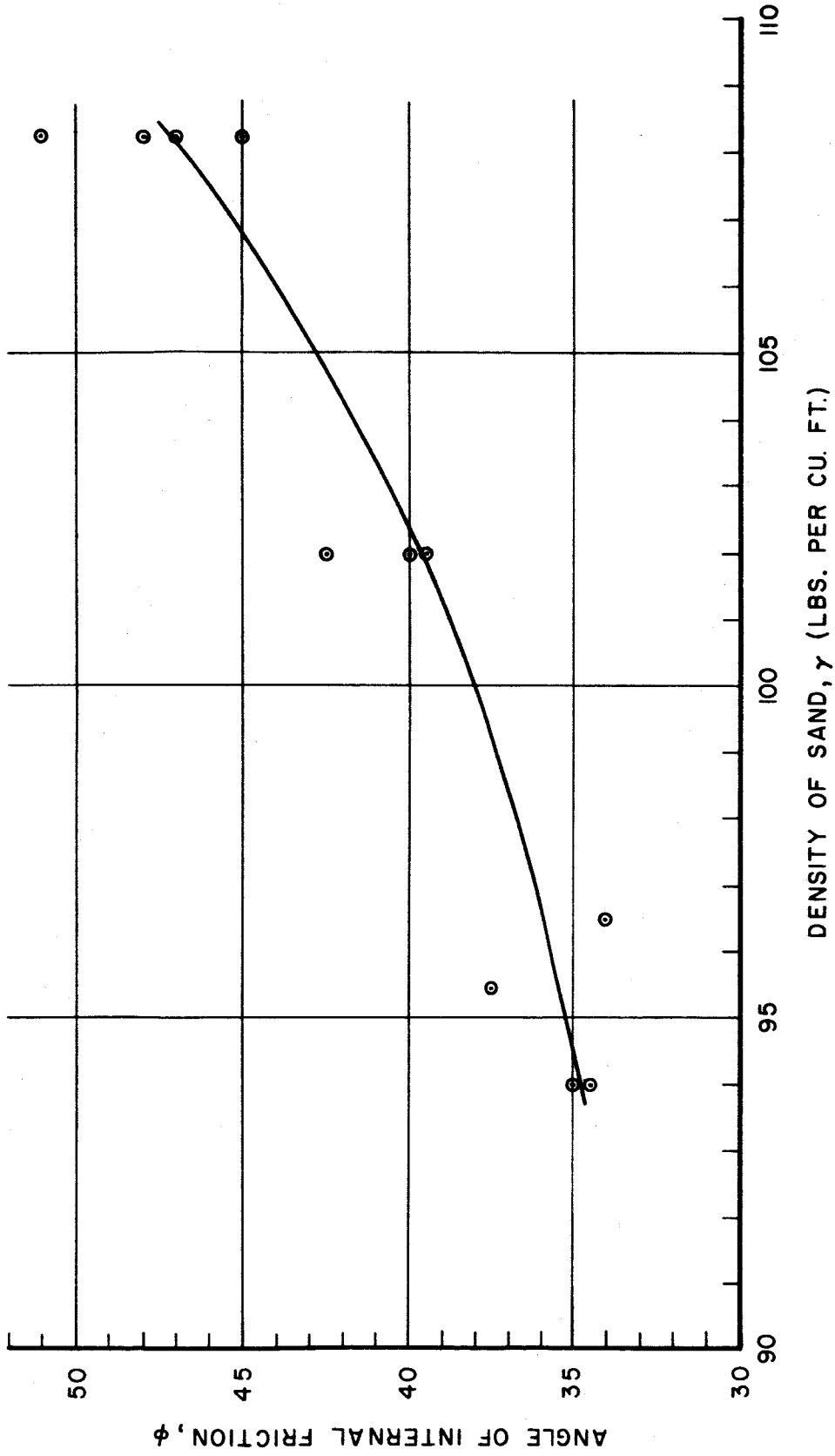
FIG. II RELATION BETWEEN DENSITY OF SAND AND ITS ANGLE OF INTERNAL FRICTION

4.4 Load-Settlement Tests, Standard Procedure for all the Footing Elements

After the soil box was filled with sand in layers, the surface of the top layer was levelled and the layer was vibrated. Since the initial position of the footing element with respect to the soil bed is important, great care was taken to have the surface of the soil bed as level as possible prior to vibration. All attempts to level the soil after vibration disturbed the surface and threw off the results completely. The footing element was brought to a "just touching" position with the surface of the sand, making certain that no load was applied.

The speed of the motor controlling the rate of loading was then adjusted to a constant rate of settlement of approximately 0.07 in. per minute, and after setting both the load and settlement dials to zero, the testing was started. The rate of loading of 0.07 in. per minute was selected because it was slow enough to produce no dynamic effects. While little information is available on the response of footings on sand as a function of the rate of loading, information is available with regard to triaxial testing. The accepted standard loading rate in triaxial compression tests on cohesionless soils for static loading effects is that causing a strain of from 1/4 to 2 per cent per minute.[2] Assuming that a cylinder of soil of about 2 diameters in depth below the foundation element represents the loaded specimen, then the adopted rate of 0.07 in. per minute falls within the accepted standard specification. Triaxial compression tests on one type of cohesionless soil showed only a 10 per cent increase in strength when the duration of time from the start of loading to the time of maximum compressive stress was decreased from 1000 seconds to 0.01 seconds.[2] No difference in results were observed for rates of loading between 1/4 and 2 per cent per minute. Thus, the results

of this test program can be said to be the "static" load conditions, unaffected by the rate of loading.

The load was continued beyond failure, as indicated by a constant load value with an increase in settlement. The test was stopped before any soil started to come over the footing element which would have caused overburden effects.

When the testing was over, the surface of the sand was struck level in order to measure the volume of the sand. The box was then weighed to allow the calculation of the density of the sand.

When all needed data for one test were taken, the soil box was completely emptied, and a new test was started.

CHAPTER FIVE

RESULTS AND DISCUSSION

5.1 Effect of Depth of Soil Bed

The load-settlement tests performed to study the effect of the depth

of the soil bed on the ultimate bearing capacity, the settlement at the

ultimate bearing capacity, and the coefficient of subgrade reaction, were

run in the 18-in. x 18-in. x 19-in. box using the 2.22-in. diameter circular

plate as the foundation element.

The procedure used was the same as that described in Art. 5.4, which

was standard for all load-settlement tests. The observed data are plotted

in Figs. 12, 13, and 14. After studying the plotted data for the ultimate

bearing capacity (Fig. 12), it was felt that the sand might be slipping on

the bottom of the box during the loadings for depths of from two to four

diameters, causing a reduction in the bearing capacity. To remove the

possibility of doubt, a number of tests were performed using a roughened

base for the box. The base was roughened by gluing sand grains to it. The

observed results were the same as those from the previous standard tests.

The fact that there was no increase in load for the tests using the roughened

base may be explained by referring to the theoretical approach[25] in Appendix

A, and noting that the deepest surface at the state of failure was within

the soil even for a depth of two diameters. Therefore, the discontinuity

in the curve in Fig. 12 in the vicinity of a depth of four diameters remains

unexplained.

From an analysis of Fig. 12, which shows the effects of the soil depth
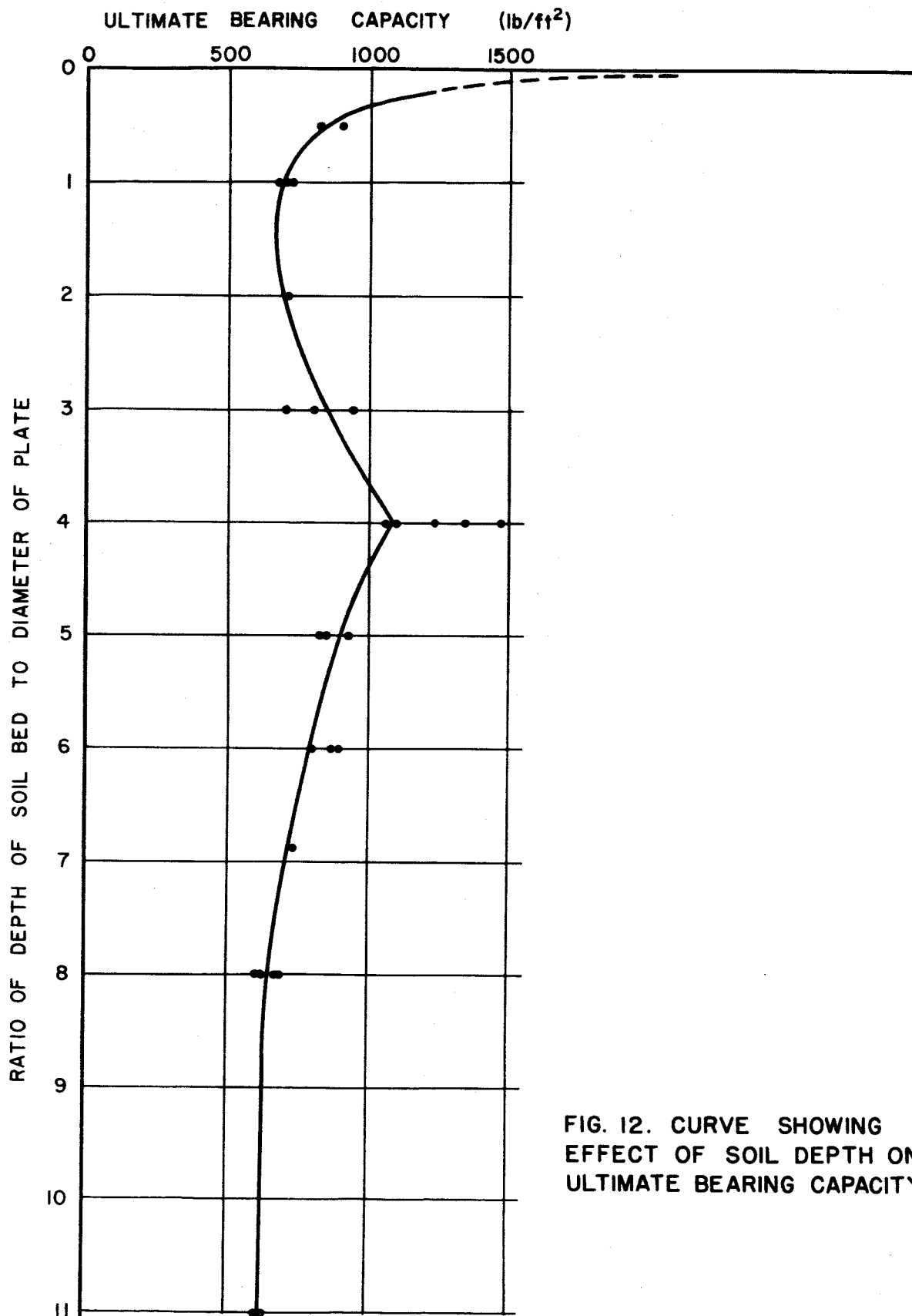
FIG. 12. CURVE SHOWING EFFECT OF SOIL DEPTH ON ULTIMATE BEARING CAPACITY

SETTLEMENT AT ULTIMATE BEARING CAPACITY / DIAMETER
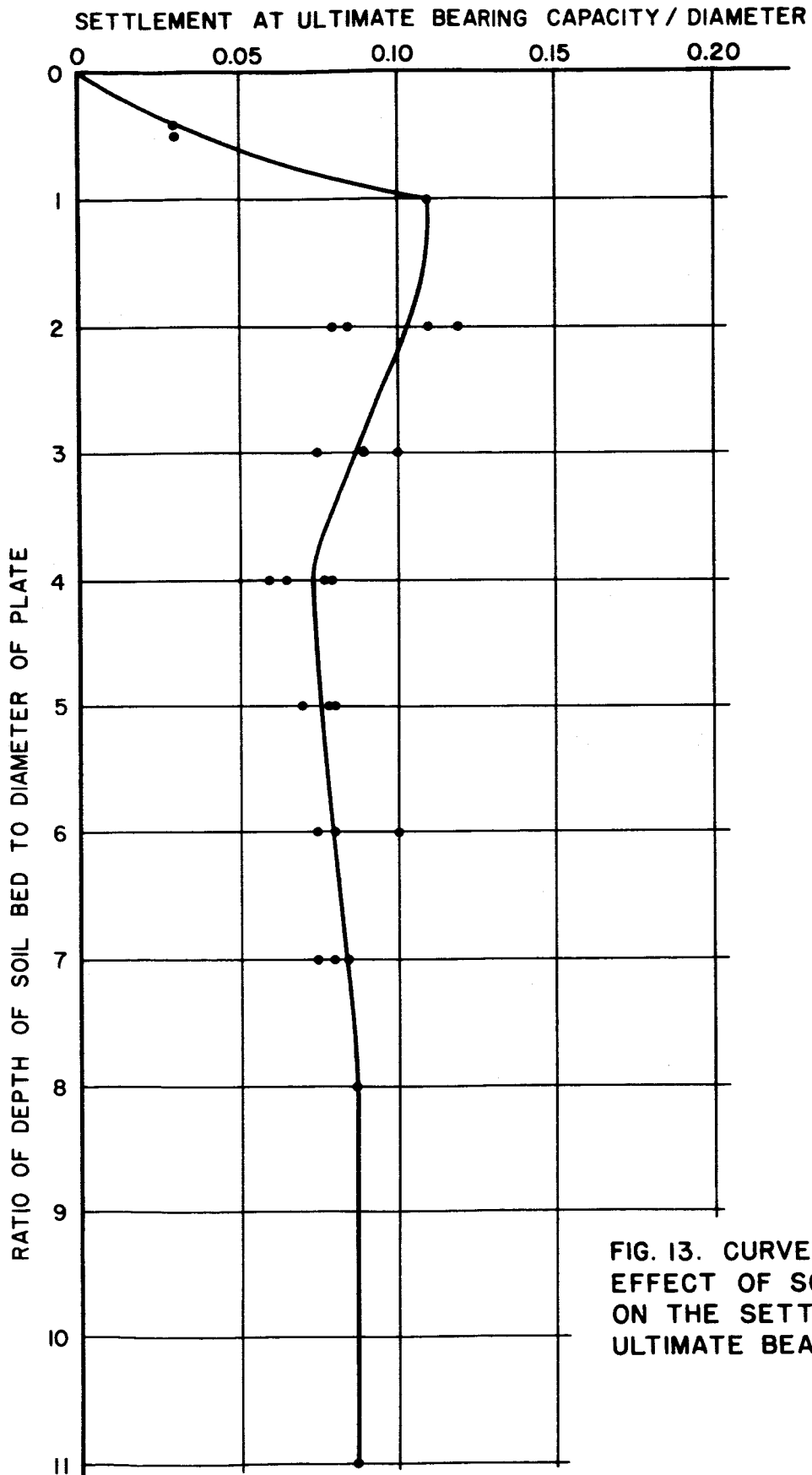
FIG. 13. CURVE SHOWING
EFFECT OF SOIL DEPTH
ON THE SETTLEMENT AT
ULTIMATE BEARING CAPACITY

FIG. 14. EFFECT OF SOIL
DEPTH ON COEFFICIENT
OF SUBGRADE REACTION
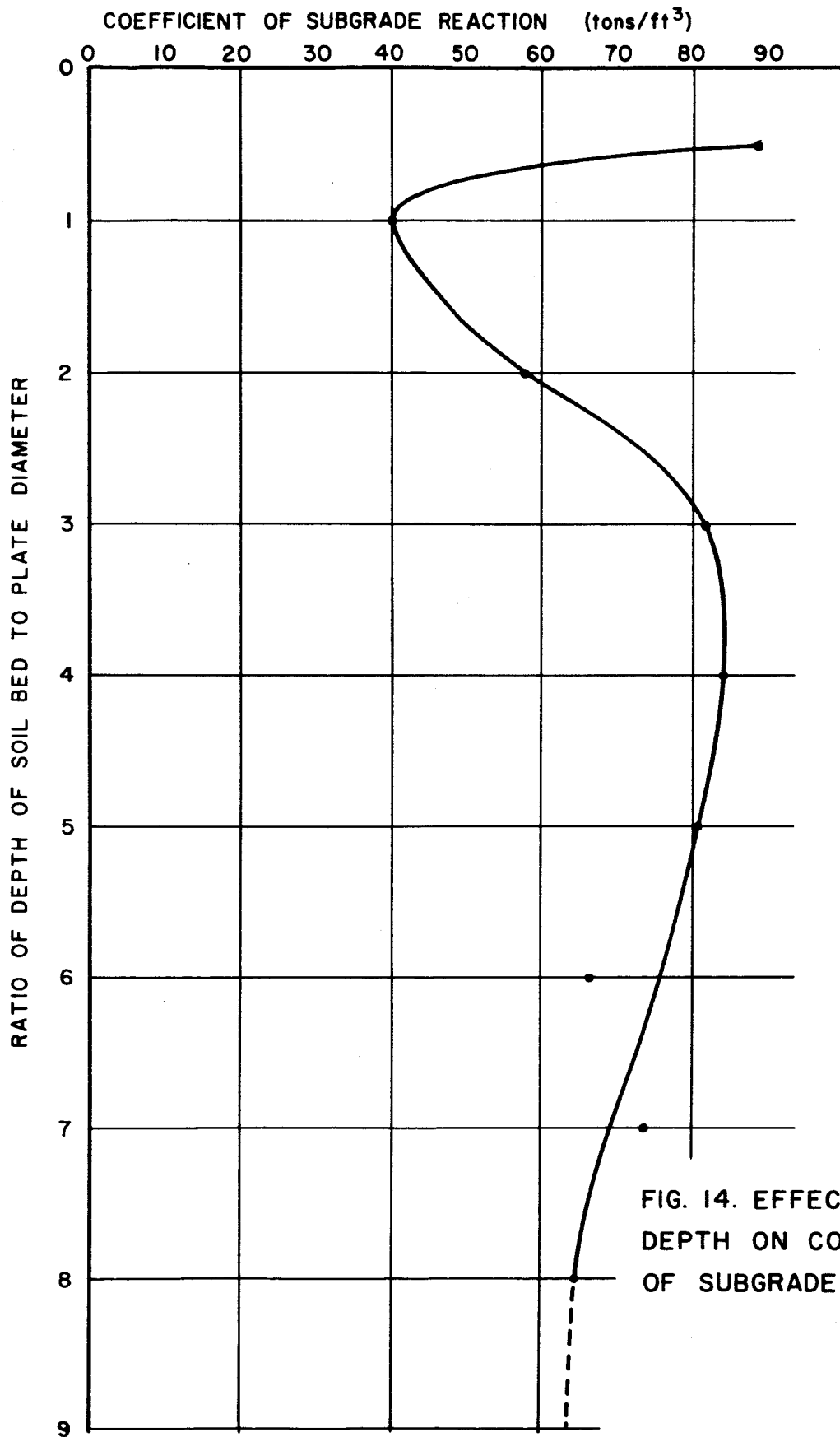
on the ultimate bearing capacity, it may be stated that for load-settlement
tests to be free from any effects of the bottom layers, the thickness of the
soil bed tested must be at least eight times the diameter of the plate used
as the foundation element.

The same anomaly seen in Fig. 12 may also be seen in Figs. 13 and 14.
As may be noted from an examination of the plotted points in Figs. 12 and
13, the unusual results were not due to experimental error since multiple
tests yielded virtually the same values.

Figure 15 shows the percentage error that may result for depths other
than the noted depth of eight times the diameter of the plate. The
expression used in computing the percentage error is

$$E = \frac{\left(V_8 - V_0\right)}{V_8} \times 100$$

where

V_8 = value at depth of eight diameters and below

V_0 = observed value.

Further study of Figs. 12 and 13 shows similarity in behavior in the
neighborhood of 1 to 2 diameters in depth to the depths of 8 diameters and
more. The error in the value of the ultimate bearing capacity, as shown in
Fig. 15, is about +8.5 per cent. Such a value may be of interest where deep
soil beds are not possible. Moreover, a 2-diameter soil depth is relatively
easy to prepare and handle in the laboratory.

It is to be noted here that the soil bed may not behave the same under
dynamic load. Moreover, other soils, even under static load, may behave
in a different manner than did the sand used by this investigation. There-
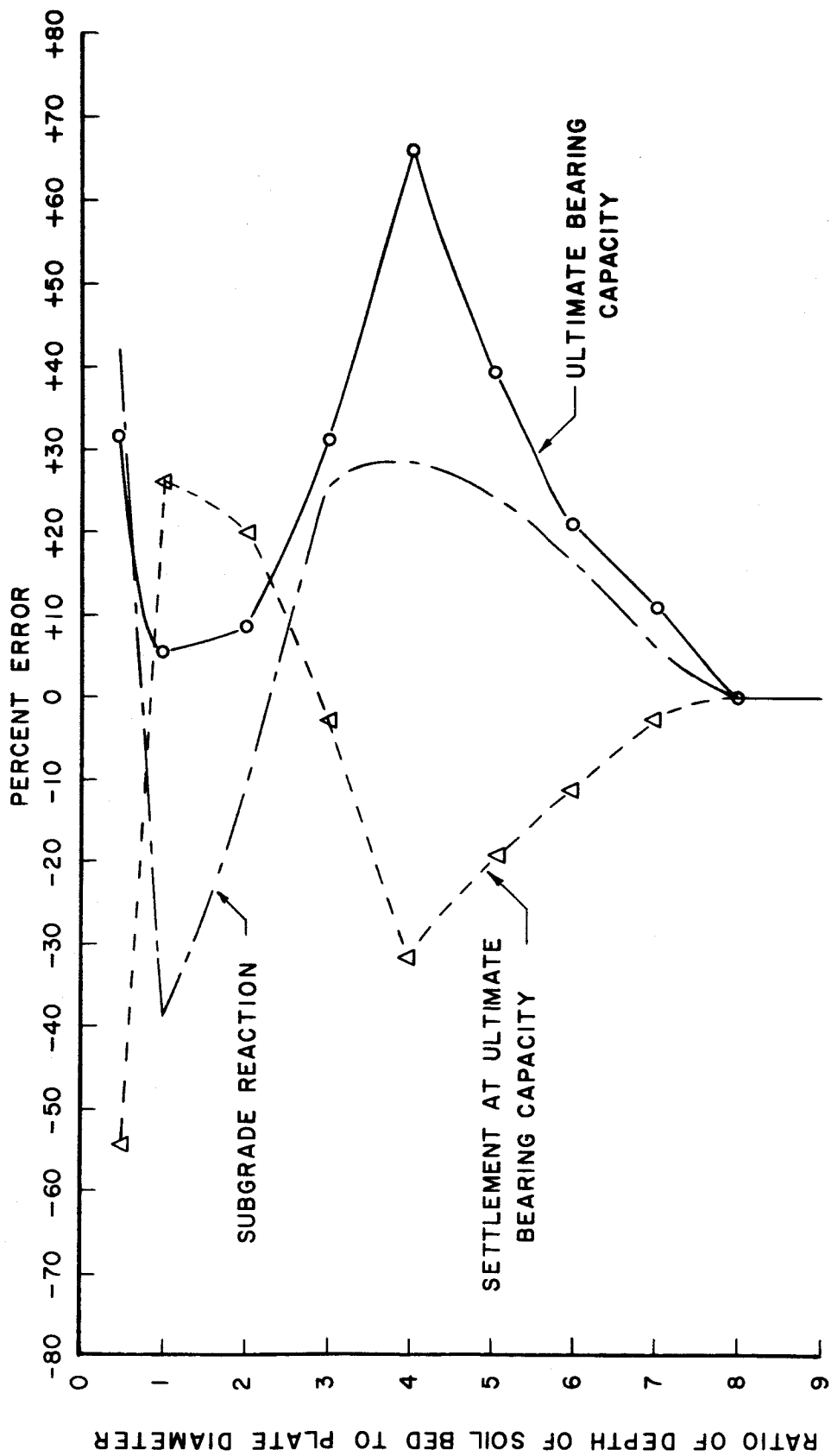
FIG. 15 PERCENT ERROR IN q_u, y AND K AS A FUNCTION OF DEPTH

fore, additional research is recommended on the minimum depth of soil bed which can be used with accuracy for various types of soils and loads.

5.2 Load-Settlement Curves for the Plates

A. Experimental Results.

Load-settlement tests on the three plates (the 2.22 in., the 3.14 in., and the 4.44 in. in diameter) were run in the respective soil boxes as previously discussed, and the observed data were plotted. Thus every plate had a set of load-settlement curves from which an average load-settlement curve was obtained. The average curves were used for the analysis of the results. A typical load-settlement curve for the 2.22-in. diameter plate is shown in Fig. 16. Average load-settlement curves for all the plates are shown in Figs. 17 to 19. The average load-settlement curves were obtained by averaging graphically the results of the individual tests. Eleven tests were performed using the 2.22-in. diameter plate, 5 tests using the 3.14-in. diameter plate, and 7 tests using the 4.44-in. diameter plate.

It is to be noted that the type of soil failure for all the plates was that of the general shear failure, which conforms with the established behavior of shallow footings as discussed in Art. 2.1.

Values of ultimate bearing capacities, the corresponding settlements and the coefficients of subgrade reaction were read from the idealized curves and are tabulated in Tables 3 and 4. The last column in Table 4 will be discussed later.

B. Discussion of Bearing Capacity.

The theory of the bearing capacity of foundations, (refer to Art. 2.2 B), as established by Terzaghi in 1943[22, 23] and which is still widely used, has been thoroughly investigated in this study. Figure 20 shows a
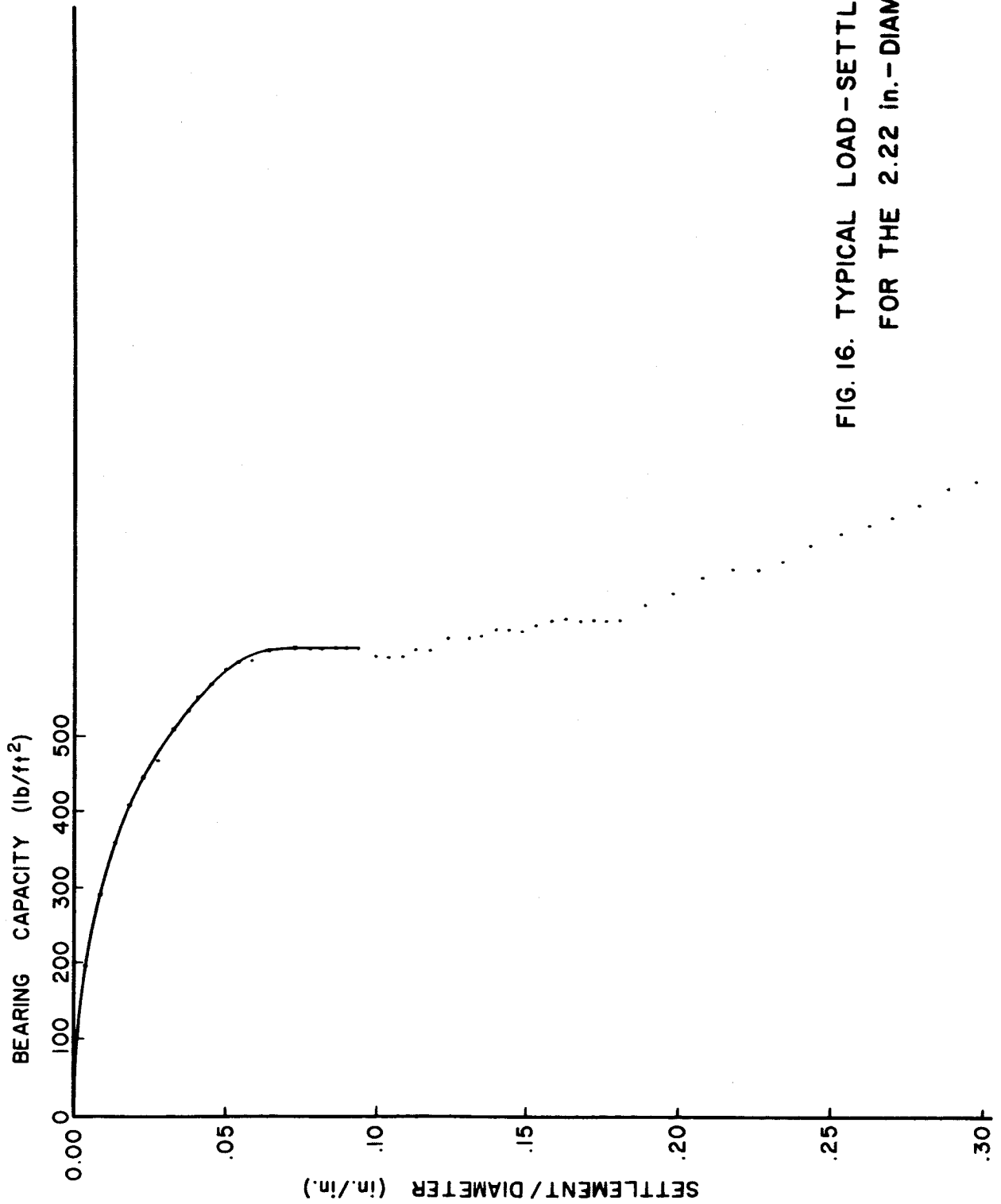
FIG. 16. TYPICAL LOAD–SETTLEMENT CURVE FOR THE 2.22 in.–DIAMETER PLATE
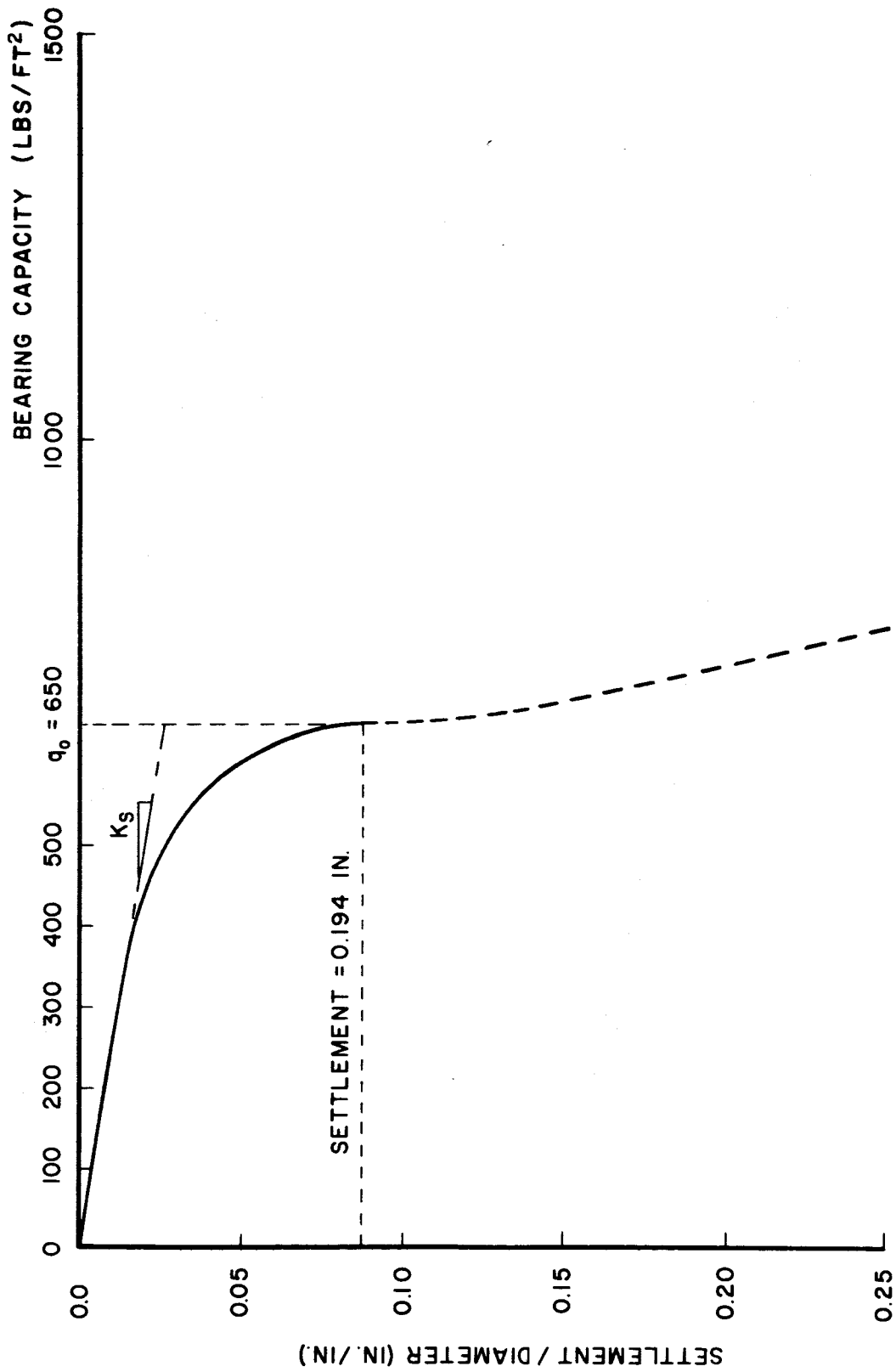
FIG. 17 AVERAGE LOAD-SETTLEMENT CURVE FOR THE 2.22 IN.-DIAMETER PLATE
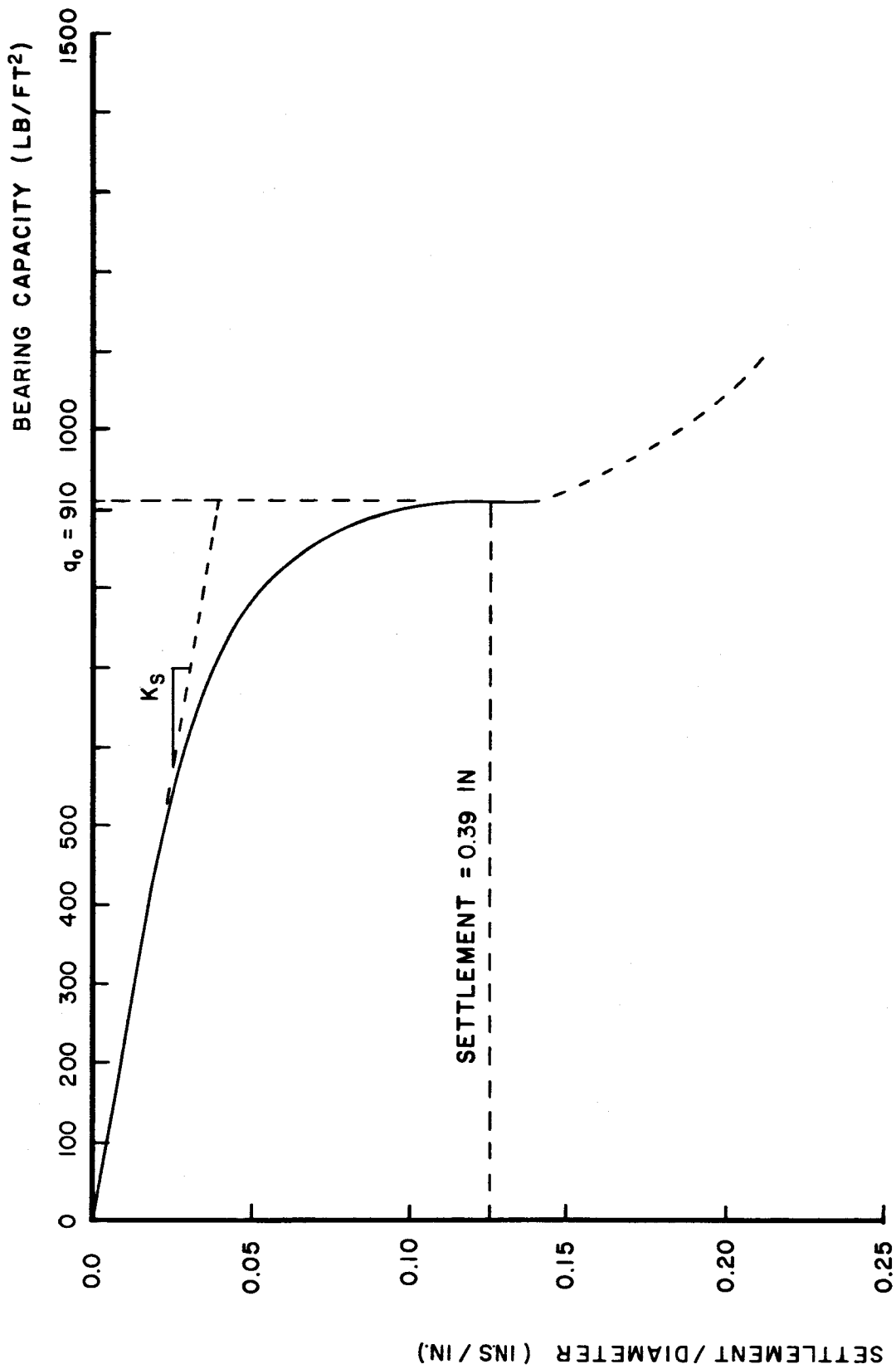
FIG. 18 AVERAGE LOAD-SETTLEMENT CURVE FOR THE 3.14 IN.-DIAMETER PLATE

48
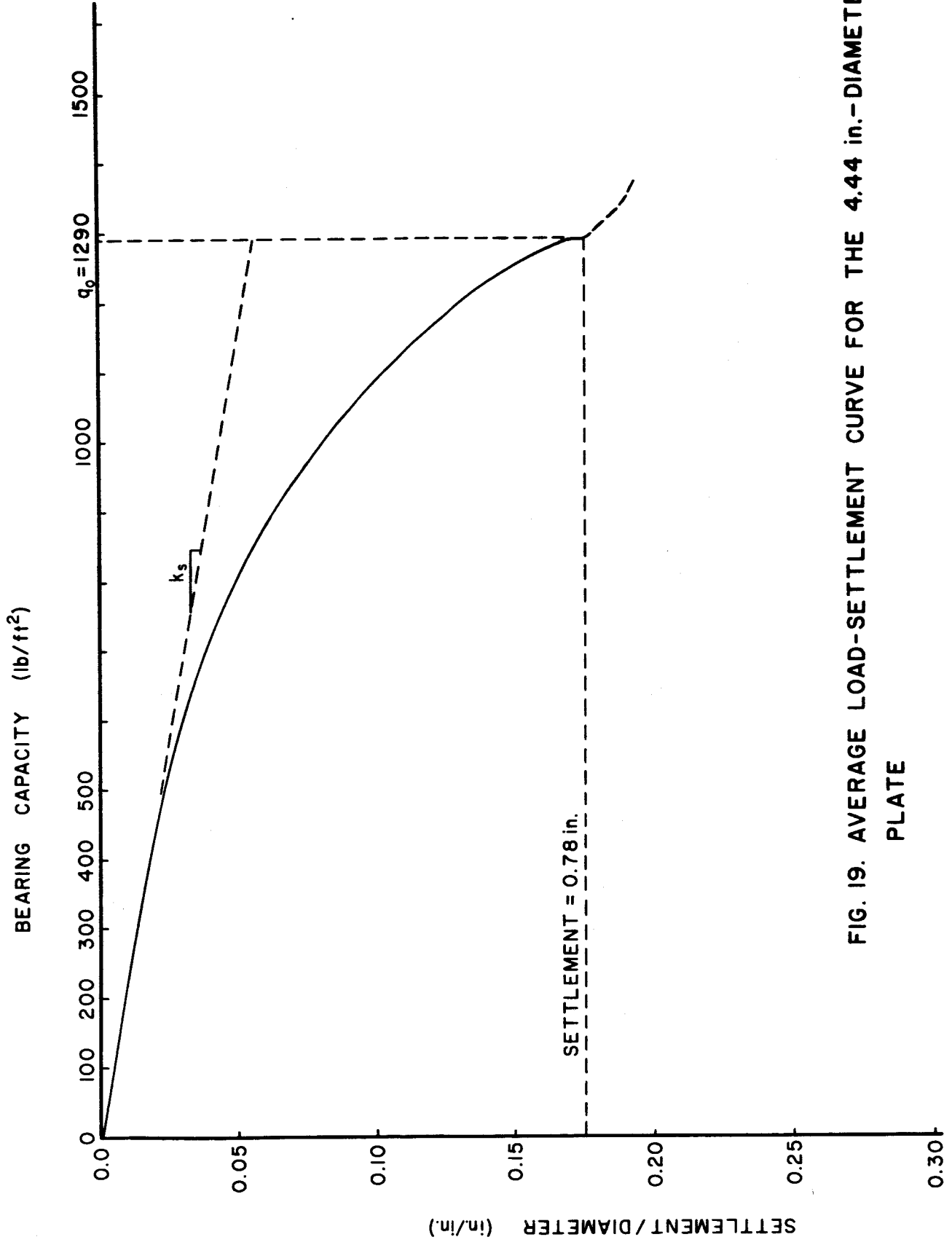
FIG. 19. AVERAGE LOAD-SETTLEMENT CURVE FOR THE 4.44 in.-DIAMETER PLATE

TABLE 3.

ULTIMATE BEARING CAPACITIES AND CORRESPONDING SETTLEMENTS FOR PLATES

Plate Diameter In.	Area of Plate In.^{2}	Ultimate Bearing Capacity lb/ft^2	Ratio of Settlement to Plate Diameter *	Settlement * In.
2.22	3.87	650	0.0875	0.194
3.14	7.74	910	0.125	0.39
4.44	15.48	1290	0.175	0.78

*Values read off the average curves at the points corresponding to the ultimate bearing capacity, i.e., the transition point of the curve to a vertical tangent.

TABLE 4.

COEFFICIENTS OF SUBGRADE REACTION FOR PLATES

Diameter of Plate In.	Ultimate Bearing Capacity* lb/ft²	Corresponding Ratio of Settlement* y/B	Settlement In.	k_s ton/ft³	Ratio of k_s
2.22	650	0.026	0.06	65	$\dfrac{65}{46} = 1.41$
3.14	910	0.038	0.12	46	$\dfrac{46}{32.5} = 1.41$
4.44	1290	0.055	0.24	32.5	$\dfrac{65}{32.5} = 2.0$

*These two values are the coordinates of the point at the intersection of the projection of the initial tangent to the load-settlement curve with the vertical line of the ultimate bearing capacity.

CENTER LINE OF FOOTING

WEDGE IN ELASTIC EQUILIBRIUM

LOG SPIRAL

$45° - \phi/2$

$45° - \phi/2$

$\psi = \phi$

P_1

W

R

P_P

B

ϕ
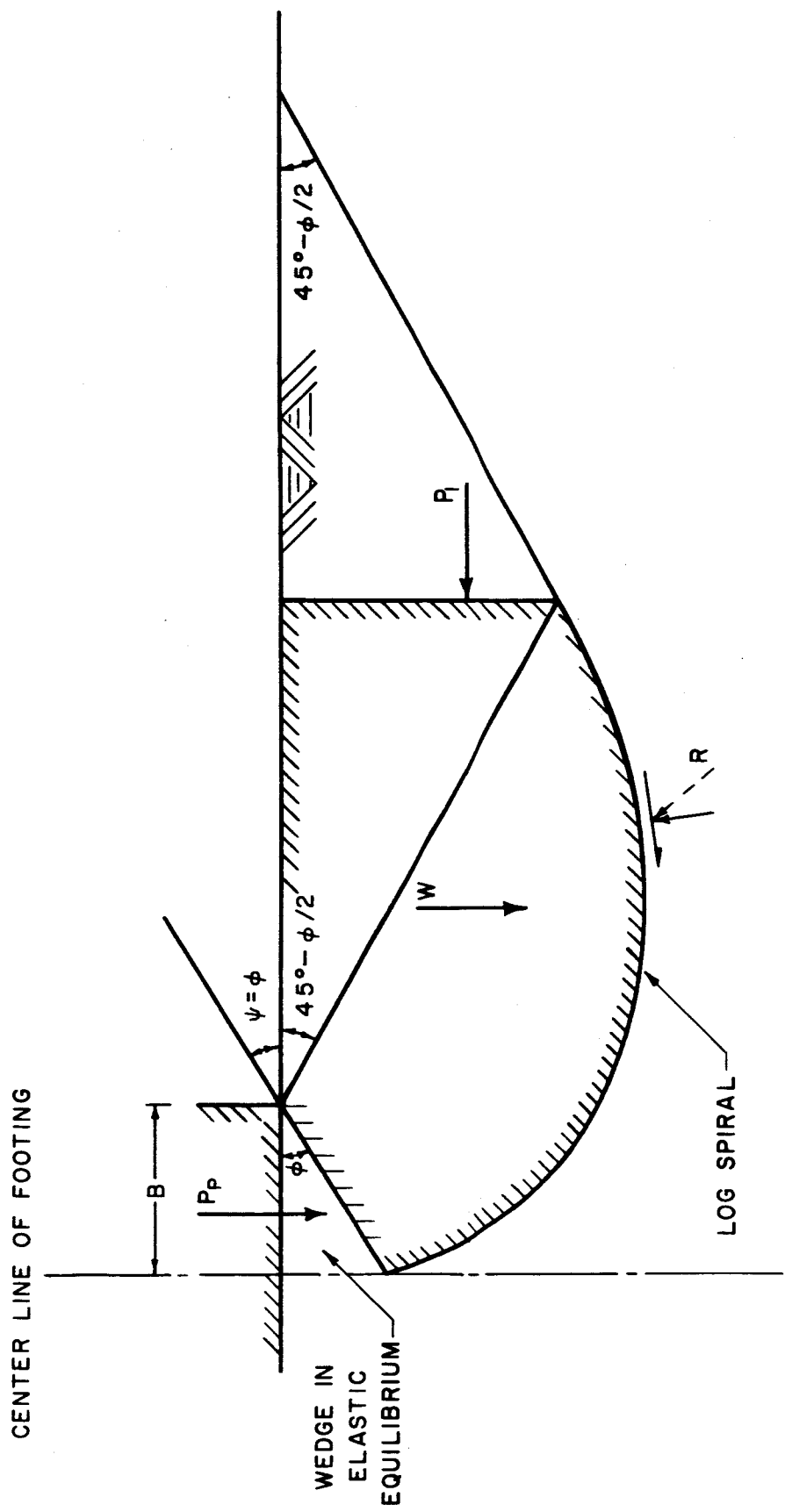
FIG. 20 FREE BODY DIAGRAM BASED ON TERZAGHI'S THEORY FOR STRIP FOOTINGS

freebody diagram of the assumed failure surface, much of which is a log
spiral, under a loaded strip footing on the surface of the soil. The assump-
tions made by Terzaghi and which affect the theoretical value of the ultimate
bearing capacity are hereby discussed.

The central zone beneath the footing is a wedge in elastic equilibrium.
The soil located within this wedge-shaped body remains practically unchanged
in shape as it moves vertically downward with the footing. The lower bound-
ary of this central zone is assumed to rise at an angle to the horizontal
equal to ϕ for a footing with a rough base and at an angle equal to
$45 + \phi/2$ for a footing with a smooth base. Therefore, according to Terzaghi[22,23]
this angle may have any value intermediate between ϕ and $45 + \phi/2$. Such a
wide possibility in the value of the rise angle of the central wedge gives
various and different failure surfaces that affect the bearing capacity.

The effect of the variation in the angle of rise and other factors
mentioned below are studied through the example calculations, shown in
Appendix A. These calculations show the evaluation of the bearing capacity
coefficient N_γ , which is the only coefficient related to the investiga-
tion. (Refer to Eq. 4.)

Figure 7(a) shows the generally accepted pressure distribution under
a rigid footing loaded on the surface of cohesionless soils. While the
pressure distribution shown may be approximated fairly well with a triangle,
at high loads the pressure distribution tends to increase at the center and
the triangle is even a better approximation. Such a pressure distribution
was used by Terzaghi in the theory under discussion. However, pressure
distribution under a footing on sand has not been thoroughly studied by
experiment and there is the possibility that other shapes of pressure dis-

tribution exist under the base of the footing. Therefore, it was decided to study the values of the bearing capacity coefficient N_γ for three types of pressure distribution:

(1) Triangular distribution, with the maximum ordinate under the center of footing, (Terzaghi's assumption);

(2) Uniform distribution;

(3) Triangular distribution with the maximum ordinates under the edges of the footing.

The results from the example calculations in Appendix A are shown in Fig. 21. It can be seen that the assumed pressure distribution under the base has an appreciable effect on the value of the bearing capacity. Further, it can be seen in Fig. 21 that the angle of rise ψ also has an appreciable effect on the value of the bearing capacity. Further discussion relative to the above mentioned point is given later in this section.

Analyzing the results as shown in Table 5, it is to be observed that the ultimate bearing capacity of circular plates varies directly with respect to the diameter of the plate. This can be seen by comparing the ratios of the diameters with the ratios of the ultimate bearing capacities, as tabulated in columns 1 and 3 of Table 5, respectively. This proves the validity of the set expression,[19] (see Eq. 4), that

$$q_0 = \text{constant x B} \tag{24}$$

$$q_0 = \left[0.3\gamma N_\gamma \right] \text{ x B} \tag{25}$$

At this point in the discussion, a study of the theory as compared to
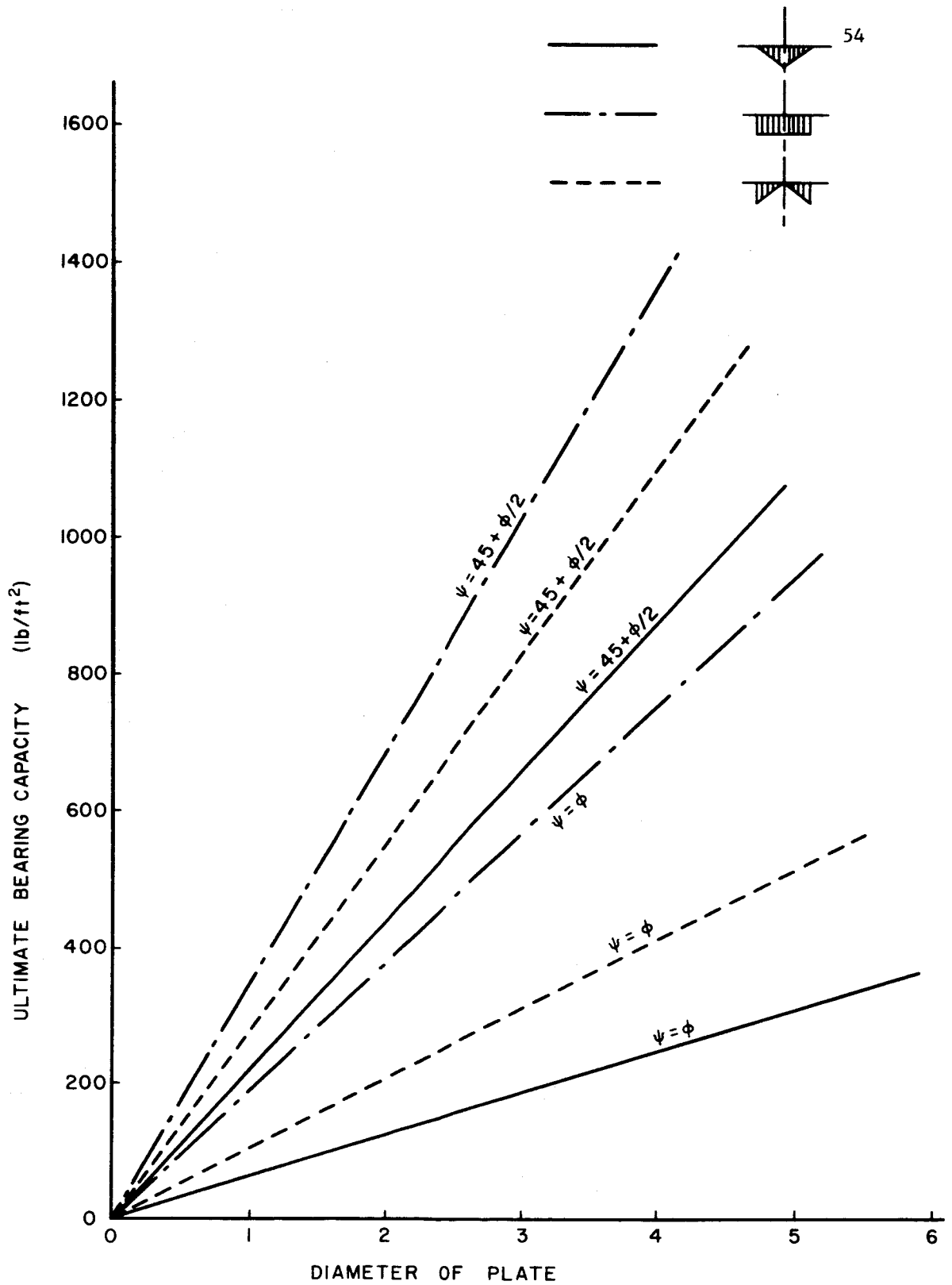
FIG. 21. EFFECT OF ψ AND BASE PRESSURE ON THE ULTIMATE BEARING
CAPACITY FOR A ϕ VALUE OF 32 DEGREES

TABLE 5.

ANALYSIS OF RESULTS OF PLATE TESTS

Ratio of Diameters	Ratio of Areas	Ratio of Ultimate Bearing Capacities	Ratio of Settlements *
$\dfrac{3.14}{2.22} = 1.41$	$\dfrac{7.74}{3.87} = 2.0$	$\dfrac{910}{650} = 1.40$	$\dfrac{0.39}{0.194} = 2.01$
$\dfrac{4.44}{3.14} = 1.41$	$\dfrac{15.48}{7.74} = 2.0$	$\dfrac{1290}{910} = 1.41$	$\dfrac{0.78}{0.39} = 2.0$
$\dfrac{4.44}{2.22} = 2.0$	$\dfrac{15.48}{3.87} = 4.0$	$\dfrac{1290}{650} = 1.9$	$\dfrac{0.78}{0.194} = 4.02$

*Settlements correspond to the ultimate bearing capacity

experimental testing is given. Results of this investigation as well as those of other investigators are used in the study.

With regards to this investigation, the angle of internal friction ϕ of the sand, (Art. 4.3), was 38.7 degrees. The value of the bearing capacity coefficient N_γ from Fig. 6 is 96. Using this value of 96, and the average soil density of 101 lb/ft^3, the theoretical values of the bearing capacity were calculated and tabulated in Table 6.

Tables 7, 8, and 9 show pertinent experimental results of some of the research done on plates by other investigators.[3,10,14] Each of these investigations is discussed briefly to give the background and the procedures followed by each of the authors.

Selig and McKee,[14] Table 7, used uniform Ottawa sand that was kept air-dry throughout the tests. The density of the sand ranged between 96.3 lb/ft^3 and 112.7 lb/ft^3, with an assumed average density of 112.3 lb/ft^3 to apply throughout the experimental program.[14] By means of triaxial shear tests, values of the angle of internal friction ranged from 38 degrees to 41 degrees. The plate experiments were conducted in a box approximately 48 in. square and 36 in. deep, that was built of wood and strapped for added strength. The footings were machined from aluminum plate and the bottoms were knurled. Static loads were applied in increments by a hydraulic jack acting through a calibrated loading ring. The sand was vibrated using a flexible-shaft concrete vibrator.

Davis and Woodward,[3] Table 8, ran their tests on cohesionless sand. The density of the sand was 102 lb/ft^3 and the angle of internal friction was approximately 36 degrees. The soil masses on which the tests were made

TABLE 6.

EXPERIMENTAL VERSUS THEORETICAL RESULTS

(From this study)

Footing Shape	Dimensions In.	* Average Bearing Capacity Load lb/ft^2	** Theoretical Value Using Terzaghi's Equation lb/ft^2	Ratio of Experimental Theoretical
Circular	2.22 diameter	650	538	1.21
	3.14 diameter	910	761	1.20
	4.44 diameter	1290	1076	1.20

*The experimental values are the mean values as read off the idealized average load-settlement curves.

**Values calculated base on an average angle of internal friction of 38.75 degrees and a mean density of 101 pcf.

TABLE 7.[14]

EXPERIMENTAL VERSUS THEORETICAL RESULTS

(From Selig and McKee)

Footing Shape	Dimensions In.	Average Bearing Capacity Load lb/in.^{2}	Theoretical[*] Value Using Terzaghi's Equations lb/in.^{2}	Ratio of $\dfrac{\text{Experimental}}{\text{Theoretical}}$
Square	2 x 2	9.3	9	1.03
	3 x 3	15.1	13.5	1.12
	4 x 4	19.1	18	1.06
Circular	2.26 diameter	9.3	5.3	1.75
	3.39	14.1	7.95	1.77
Rectangular	3 x 6	15.9	11.7	1.36
	3 x 9	17.5	11.7	1.50
	3 x 12	22.5	11.7	1.92
	3 x 15	22.5	11.7	1.92
	3 x 18	21.7	11.7	1.85
	3 x 21	23.1	11.7	2.06

[*]Values calculated by R. A. Iliya based on an average angle of internal friction of 39.5 degrees and a mean density of 112.3 lb/ft^3.

TABLE 8.[3]

EXPERIMENTAL VERSUS THEORETICAL RESULTS

(From Davis and Woodward)

Footing Shape	Dimensions In.	Average Bearing Capacity Load $lb/in.^2$	Theoretical Value Using Terzaghi's Equation $lb/in.^2$ [*]	Ratio of Experimental Theoretical
Rectangular	1 x 24	16.0	14.7	1.09
		16.0	14.7	1.09
		14.0	14.7	0.95
		18.0	14.7	1.23
	1 x 10	22.0	14.7	1.49
		20.0	14.7	1.49
		14.0	14.7	0.95
		16.0	14.7	1.09
		22.0	14.7	1.09
Circular	2 diameter	21	17.7	1.19
		22	17.7	1.24
		23	17.7	1.30

[*]Values calculated by R. A. Iliya based on an angle of internal friction of 36 degrees and a density of 102 lb/ft^3.

TABLE 9.[10]

EXPERIMENTAL VERSUS THEORETICAL RESULTS

(From Meyerhoff)

Footing Shape	Dimensions In.	Average Bearing Capacity lb/ft^2	Theoretical * Value Using Terzaghi's Equation lb/ft^2	Ratio of Experimental Theoretical
Square	1/2 x 1/2	720	388	1.85
	1 x 1	1200	775	1.55
Rectangular	1/2 x 1 1/2	700	486	1.44
	1/3 x 3	1080	486	2.22
	1/2 x 4 1/2	1560	486	3.2
	1/2 x 6	1240	486	2.56
	1 x 3	1640	972	1.69

*Values calculated by R. A. Iliya based on an angle of internal friction of 30.5 degrees, and a density of 106 lb/ft^3.

had horizontal dimensions of from 1-1/2 to 3 ft and the depth was at least

eight times the footing width.

Meyerhoff,[10] Table 9, carried out loading tests in a stiffened steel

tank 18 in. long, 15 in. wide and 18 in. deep, which was filled in 3-in.

thick layers with a clean and dry, medium river sand. The grading lay

between 0.3 and 0.6 mm, with 50 per cent passing a 0.4 mm sieve. Each layer

was tamped with a vibrating hammer and a fairly uniform density was obtained.

The angle of internal friction was 30.5 degrees. The footings were made of

brass, and were loaded by a jack through a proving ring. The load was applied

in small steps, each increment being maintained until the settlement was

complete.

As shown in Tables 7, 8, and 9 the ratios of the experimental results

to the theoretical values of the ultimate bearing capacities ranged from

0.95 to 1.85 for square and circular footings. Higher ratios were observed

for rectangular footings.

Judging from their results it may be stated that the above mentioned

investigators[3,10,14] agreed closely with the theory of Terzaghi.

Referring to the results of this investigation, it may be concluded

that the equation for the ultimate bearing capacity on the surface of

cohesionless soils as given by Terzaghi[18,26] is in close agreement with

the observed load-settlement tests (refer to Table 6 and Fig. 22). As

indicated, the ratio of the experimental results to the theoretically cal-

culated values is approximately 1.20. This difference of 20 per cent may

have been caused predominantly by the following previously discussed factors:

(1) The shape of the failure surface, and the angle of rise of the
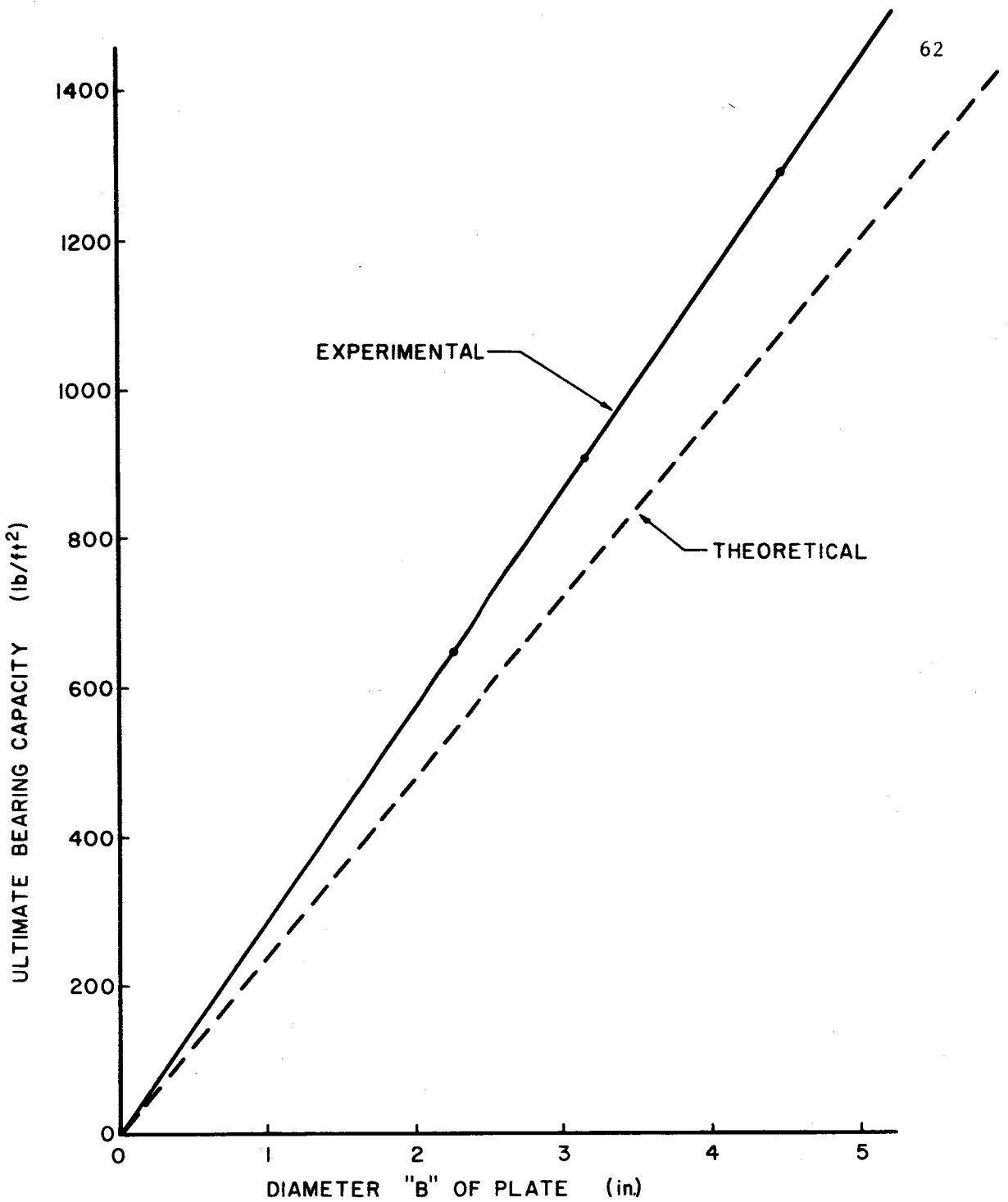
FIG. 22 EFFECT OF SIZE OF DIAMETER ON
THE ULTIMATE BEARING CAPACITY

lower boundary of the central zone beneath the footing.

(2) The pressure distribution at the base of the footing.

(3) The true case of a three-dimensional problem as compared to

the two-dimensional analysis used in developing the theory, and

converted semi-empirically for use on three-dimensional problems.

However, some error may be attributed to the evaluation of the angle

of internal friction, and to possibly experimental procedures.

C. Discussion of Coefficient of Subgrade Reaction.

The theory of subgrade reaction as discussed in Chap. II, Art.

2.4 states that for a loaded area on a given soil the value of the coeffi-

cient of subgrade reaction k_s is a constant and is equal to the relation

$$k_s = \frac{p}{y} \tag{20}$$

Referring to the average load-settlement curves for the three plates,

it can be seen that this relationship holds for each of the plates up to

where the value of p equals to about one-half the ultimate bearing capa-

city. At that point the actual curve for the load-settlement test starts

to deviate from the initial tangent modulus.

The results (refer to Table 4) show that the value of the k_s was

affected by the size of the contact surface of the loaded area. It was

found that the coefficient of subgrade reaction k_s varies inversely with

respect to the diameter of the loaded footing element. This can be seen by

comparing the ratios of k_s from Table 4 with the ratios of the diameters

of the plates from Table 5. Moreover, this relation is used in the theory

of elasticity covered below. The effect of the diameter of the plate on the

coefficient of subgrade reaction is given in Fig. 23.

Values of the coefficient of subgrade reaction for square plates on sand are given by Terzaghi[21] as shown in Table 1. In order to compare values obtained for circular plates from these experiments with values in Table 1, the theory of elasticity will be employed to obtain a correlation factor between values of k_s for circular and square plates.

From the theory of elasticity, the settlement of a loaded area on the surface of a semi-infinite solid is given by the expression (refer to Art. 23)

$$y = q_n \ B \ \frac{1-\mu^2}{E} \ I_\rho \tag{5}$$

since k_s , the coefficient of subgrade reaction is by definition equal to

$$k_s = \frac{q_n}{y} \tag{26}$$

then

$$k_s = \frac{1}{B \ \frac{1-\mu^2}{E} \ I_\rho} \tag{27}$$

The shape factor I_ρ as given by Terzaghi and many others [12,15,24,27] is

I_ρ for a square = 0.56

I_ρ for a circle = 0.7854

therefore, for a circular plate whose diameter is equal to the side of a square, we could write the following relation:

COEFFICIENT OF SUBGRADE REACTION k_3 (tons/ft^3)
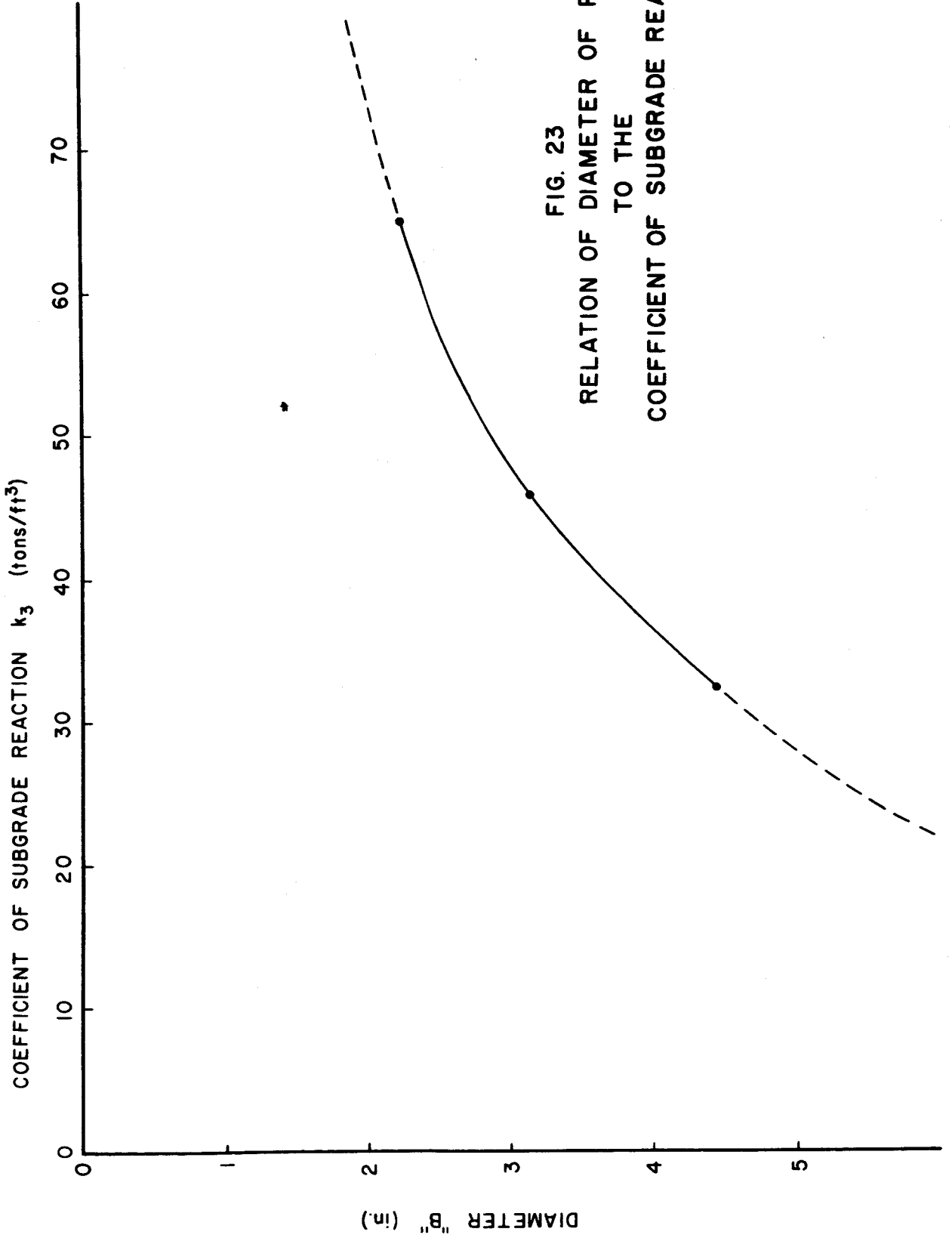
DIAMETER "B" (in.)

FIG. 23
RELATION OF DIAMETER OF PLATE
TO THE
COEFFICIENT OF SUBGRADE REACTION

65

$$\frac{k_s \text{ (circle)}}{k_s \text{ (square)}} = \frac{k^0_s}{k_s} = \frac{\frac{1}{0.7854}}{\frac{1}{0.56}} = 0.713. \tag{28}$$

Adjusting the values proposed in Table 1 the coefficients of subgrade reaction are obtained for a circular plate with a 1-ft diameter, in tons/ft^3, as shown below.

TABLE 10.

VALUES OF $k^0_{s_1}$ IN TONS/FT^3

Relative Density of Sand	Loose	Medium	Dense
Dry or moist sand, limiting values	14-43	43-215	215-713
Dry or moist sand, proposed value	28	93	357

The adjusted values for various size diameters may be obtained from the following relation as discussed above

$$k^0_{s_B} = \frac{k^0_{s_1} \times 1}{B} \tag{29}$$

or

$$k^0_{s_1} = k^0_{s_B} \times B \tag{30}$$

where B is the diameter in feet. Using this relation, the $k^0_{s_1}$, coefficient of subgrade reaction for a circular plate having a 1-ft diameter, should be equal to:

$$\overset{o}{k}_{s_1} = \overset{o}{k}_s (2.22) \times \frac{2.22}{12} = 65 \times 0.185 = 12 \text{ tons/ft}^3$$

if based on the test results of the 2.22-in. diameter plate.

As seen such a value is quite low as compared to the proposed values by Terzaghi, even for loose sand. The condition of the sand used in the investigation may be accurately described as of medium density since the completely loose condition gave a density of 95 lb/ft^3 and the densest 108 lb/ft^3.

Based on the above analysis it may be concluded that the proposed values of the coefficient of subgrade reaction by Terzaghi tend to predict much smaller settlements than actually would occur, which may be serious for structures where the settlement governs the design. This conclusion, of course, is based on very limited data. However, it should be noted that Terzaghi failed to site references, either theoretical or experimental, that would show the derivation of the values proposed in Table 1.

In analyzing the results of the settlements which correspond to the ultimate bearing capacity it is to be noted that the settlement varied directly with respect to the areas of the plates, or to the square of the diameter. (Refer to Table 5.)

5.3 Load-Settlement Curves for the Cone

Seven load-settlement tests using the cone were run in the 36-in. x 36-in. x 37-in. box. A load-settlement curve was plotted for each individual test. From these individual curves an average load-settlement curve was obtained for use in the analysis and comparison with the plates. A typical load-settlement curve and the average load-settlement curve are shown in

Figs. 24 and 25, respectively. The average load-settlement curve was obtained by averaging graphically the results of the eleven tests.

Referring to Fig. 24 it may be observed that the early part of the load-settlement relationship is irregular in that very small loads were developed although the settlement was appreciable. This is thought to be explained by the lack of sensitivity of the loading system to such small loads. In the analyses it is assumed that the curve extends smoothly back to the origin. Even though the irregularity actually exists in the real response of the system, any discrepancy between experiment and theory will be very small because of the very small loads in the early portion of the curve.

From Fig. 24, it can be observed that the load-settlement curve for the cone is almost a straight line; and the curve does not indicate an ultimate load condition as characterized by the curve for a plate. This behavior is, of course, expected from a loaded cone since the cross-sectional area at the plane of the original soil surface increases with settlement.

The loading was carried on until the cone was deep enough in the sand so that the cross-sectional area of the cone at the plane of the original soil surface was equal to the area of the largest plate. Even though failure of the sand, as observed in the plate tests, possibly did not occur, in referring to the ability of the cone to carry load, the term "bearing capacity" is employed. In the case of the cone, the bearing capacity is computed by dividing the observed load by the cross-sectional area of the cone at the plane of the original soil surface.

The bearing capacity values with the corresponding settlements were
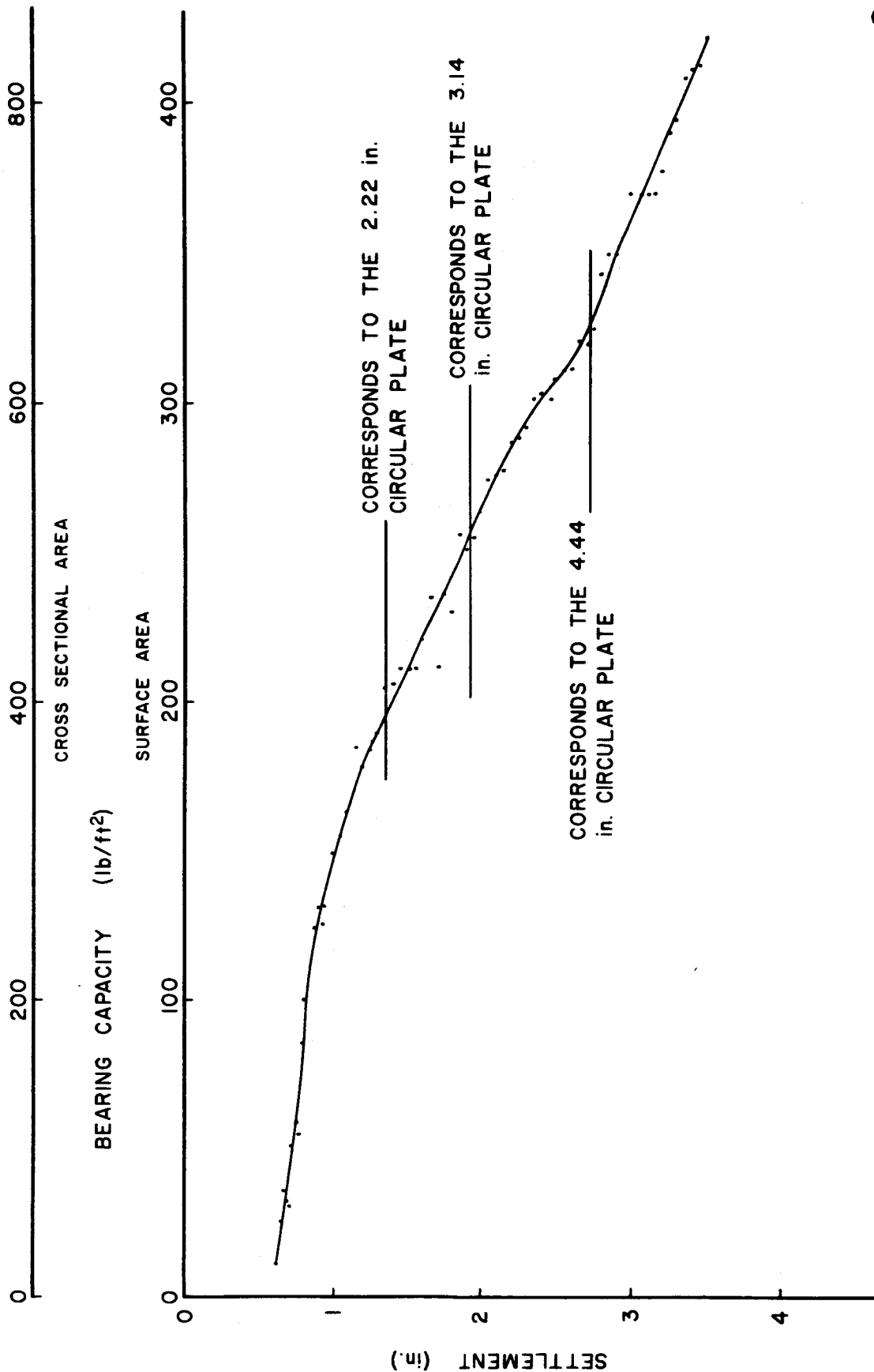
FIG. 24 TYPICAL LOAD-SETTLEMENT CURVE FOR THE CONE

69
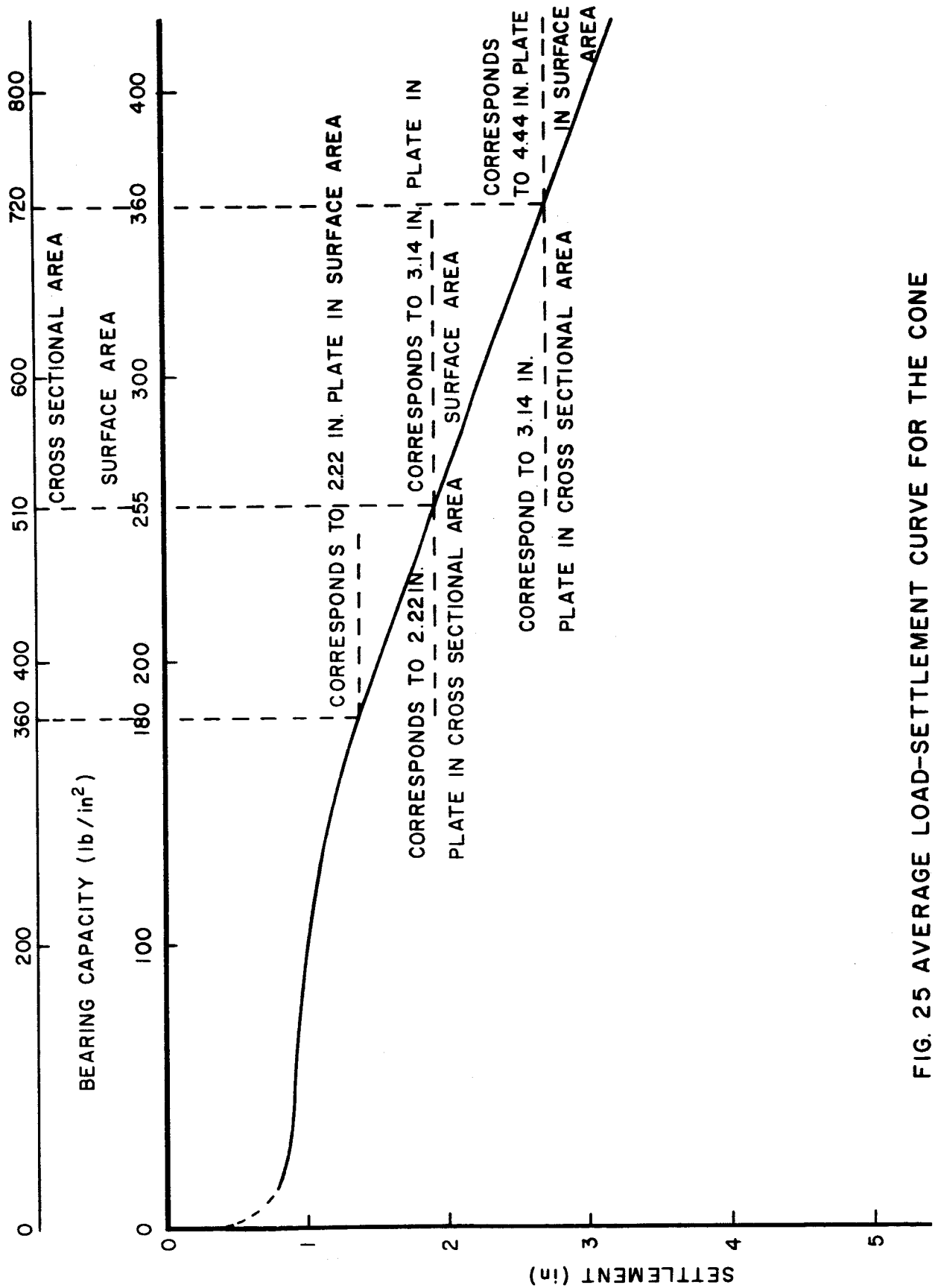
FIG. 25 AVERAGE LOAD–SETTLEMENT CURVE FOR THE CONE

read from the average load-settlement curve and are tabulated in Table 11.

With regard to the theory for the computation of the bearing capacity of a cone on cohesionless soil, the same basic assumptions previously discussed in the theory of plates were used. As before, the computations were made for the two-dimensional case. A numerical example of the computations is presented in Appendix B. A wedge forming an angle equal to ϕ is assumed to develop, as shown in Fig. 37 (see Appendix B). As previously assumed for plates, this wedge of soil moves downward and outward.

The calculations shown in Appendix B were performed using an angle ϕ equal to 32 degrees, the same as was used for the examples of the strip footing. As shown, the value of the bearing capacity coefficient N_γ is equal to 20.8 which is about 0.825 of the value calculated, using the same procedures, for the strip footing. Such a relation agrees very closely with the experimental results where a ratio of 0.79 was observed. (Refer to Tables 12 and 13.)

Using this factor of 0.79, the value of the bearing capacity coefficient N_γ for the cone for sand with an angle of internal friction ϕ equal to 38.7 degrees is 79, which is 0.825 N_γ (plate).

In the following pages expressions for the bearing capacity of a cone are developed.

As seen from Table 12 the bearing capacity of the cone varied directly with respect to the cross-sectional diameter at the plane of the original soil surface. This relation was shown to be typical of circular plates on the surface of cohesionless soil. Therefore, the bearing capacity of the cone may be expressed in the same basic equation form previously pre-

TABLE 11.

SIGNIFICANT RESULTS* OF TESTS ON THE CONE

Settlement In.	Cross-Sectional Diameter In.	Cross-Sectional Area In.^{2}	Bearing Capacity lb/ft^2
1.35	1.56	1.90	360
1.92	2.22	3.87	510
2.72	3.14	7.74	720

*Values read off the average curve.

TABLE 12.

ANALYSIS OF RESULTS OF TESTS ON THE CONE

Ratio of Cross-Sectional Diameters	Ratio of Bearing Capacities	Ratio of Settlement
$\dfrac{2.22}{1.56} = 1.43$	$\dfrac{510}{360} = 1.42$	$\dfrac{1.92}{1.35} = 1.42$
$\dfrac{3.14}{2.22} = 1.41$	$\dfrac{720}{510} = 1.41$	$\dfrac{2.72}{1.92} = 1.42$
$\dfrac{3.14}{1.56} = 2.01$	$\dfrac{720}{360} = 2.0$	$\dfrac{2.72}{1.35} = 2.01$

TABLE 13.

COMPARATIVE RESULTS FOR THE CONE AND PLATES

Based on Cross-Sectional Area			Based on Surface Contact Area		
Ultimate Bearing Capacity of Plate lb/ft^2	Bearing Capacity of Cone lb/ft^2	Ratio Cone/Plate	Ultimate Bearing Capacity of Plate lb/ft^2	Bearing Capacity of Cone lb/ft^2	Ratio Cone/Plate
645	510	$\frac{510}{645} = 0.79$	645	180	$\frac{180}{645} = 0.28$
910	720	$\frac{720}{910} = 0.79$	910	255	$\frac{255}{910} = 0.28$

sented for plates. Since the ratio of 0.79 was observed between the bearing capacity of the cone and the ultimate bearing capacity of the circular plate, the expression for the bearing capacity of the cone may be written as

$$q = 0.24 \ \gamma B N_\gamma \ \text{(plate)} \ \text{lb/ft}^2 \ \text{of cross-sectional area} \qquad (31)$$

where B is the diameter of the cone at the plane of the original soil surface, and N_γ is the bearing capacity coefficient of a circular plate as shown in Fig. 6.

Since for a 30 degree half vertex angle, the relation between the diameter B and the settlement height y is

$$B = \frac{2y}{\sqrt{3}} \qquad (32)$$

the bearing capacity of the cone may be expressed in terms of the settlement y by the following equation

$$q = 0.28 \ \gamma y N_\gamma \ \text{(plate)} \ \text{lb/ft}^2 \ \text{of cross-sectional area} \qquad (33)$$

If the bearing capacity of the cone is to be expressed in terms of the surface contact area, and since the ratio between this bearing capacity and the ultimate bearing capacity of the plate is 0.28 (refer to Table 13), the bearing capacity of the cone in terms of the surface area is given by

$$q = 0.084 \ \gamma B_p N_\gamma \ \text{(plate)} \ \text{lb/ft}^2 \ \text{of surface contact area} \qquad (34)$$

where B_p is the diameter of the equivalent circular plate which has the

same surface area as the surface contact area of the cone.

Since the relation between the diameters of the cone and the equivalent circular plate is equal to

$$B_p = 1.414 \ B_c \tag{35}$$

then, Eq. 34 may be rewritten in the form

$$q = 0.12 \ \gamma B_c N_\gamma \ \text{(plate) lb/ft}^2 \text{ of surface contact area} \tag{36}$$

where B_c is the diameter of the cone at the plane of the original soil surface. Equations 31 and 36 show that the bearing capacity of the cone as expressed in terms of the cross-sectional area is twice that expressed in terms of the surface contact area.

The bearing capacity of the cone may also be expressed using the basic equation for circular plates and the theoretically developed value of N_γ (see Appendix B). Therefore, the bearing capacity of the cone may be given by

$$q = 0.3\gamma B N_\gamma \ \text{(cone) lb/ft}^2 \text{ of cross-sectional area} \tag{37}$$

or expressing it in terms of the settlement y

$$q = 0.345 \ \gamma y N_\gamma \ \text{(cone) lb/ft}^2 \text{ of cross-sectional area} \tag{38}$$

If γ equals 101 lb/ft^3 and N_γ equals 79, the theoretical load-settlement curve for the cone may be plotted as shown in Fig. 26. The difference between the theoretical and experimental curves is reflected by the factors, 0.825 and 0.79 previously discussed on page 69. The closeness of these two curves is thought to represent an acceptable accuracy.
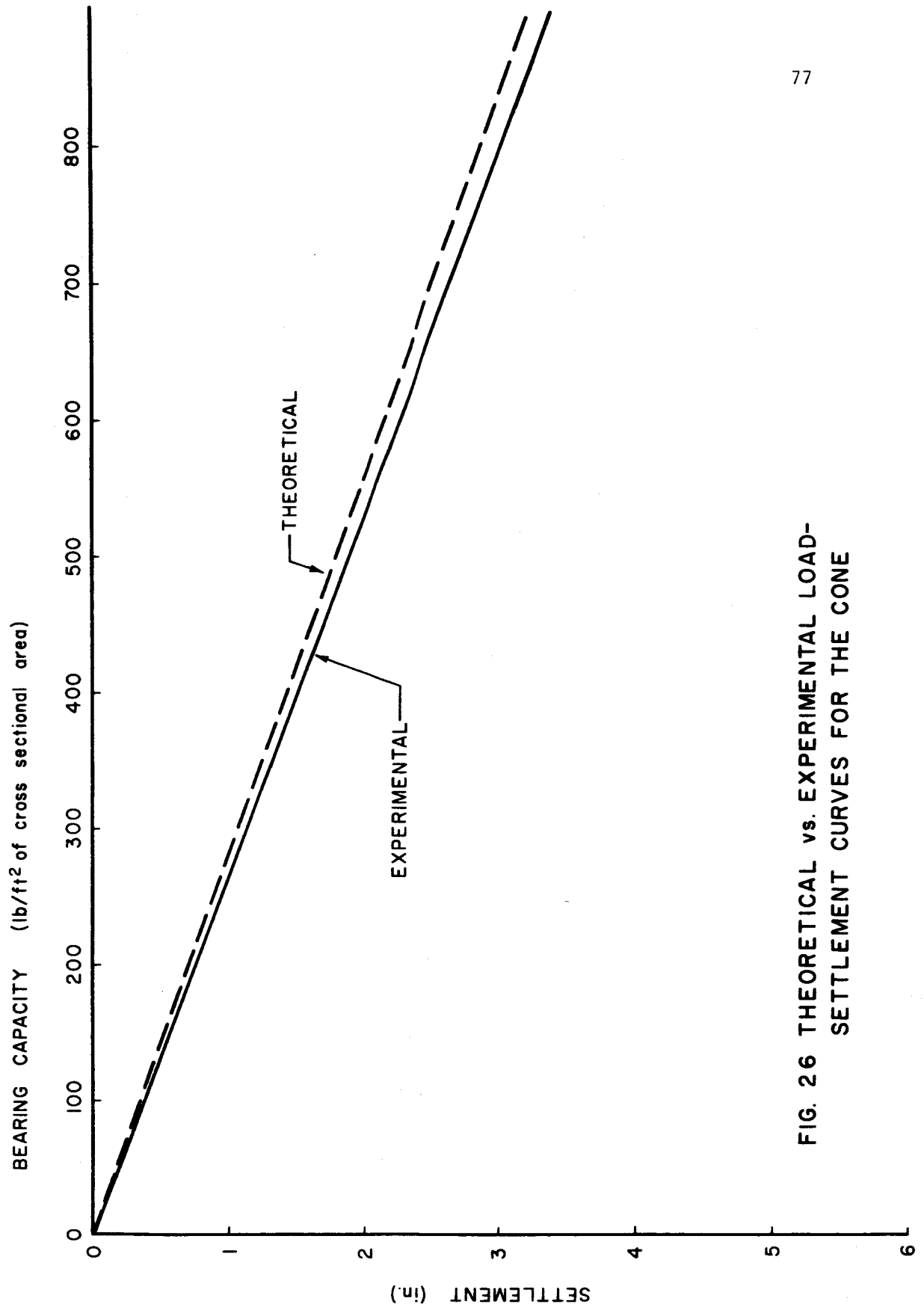
FIG. 26 THEORETICAL vs. EXPERIMENTAL LOAD-
SETTLEMENT CURVES FOR THE CONE

5.4 Load-Settlement Curves for the Spheres

Two spherical foundation elements were tested, with spherical diameters of 3.14 in. and 5 in. The tests were run in the same typical procedure, outlined in Art. 4.4, used on the plates and cone.

A load-settlement curve was plotted for each test, and from these curves an average load-settlement curve was obtained for each of the two spheres. (Refer to Figs. 27 through 30.) The average load-settlement curves were obtained by averaging graphically the results of the individual tests. Eight tests were performed using the 3.14-in. diameter sphere, and 5 tests using the 5-in. diameter sphere.

From Figs. 27 and 29 it may be observed that the early part of the load-settlement relationship is irregular in that very small loads were developed although the settlement was appreciable. This is thought to be explained by the lack of sensitivity of the loading system to such small loads. In the analyses it is assumed that the curve extends smoothly back to the origin. Even though the irregularity actually exists in the real response of the system, any discrepancy between experiment and theory will be very small because of the very small loads in the early portion of the curve.

The load-settlement curves for the spheres were quite similar to those observed for the cone. The curves did not show the ultimate load characteristic as did the plates; this was expected since the cross-sectional area of the sphere increased with settlement.

Similar to the cones, the loading was carried on until the spheres were deep enough in the sand to furnish cross-sectional areas at the plane

FIG. 27
TYPICAL LOAD-SETTLEMENT CURVE
FOR THE
3.14 in DIAMETER SPHERE
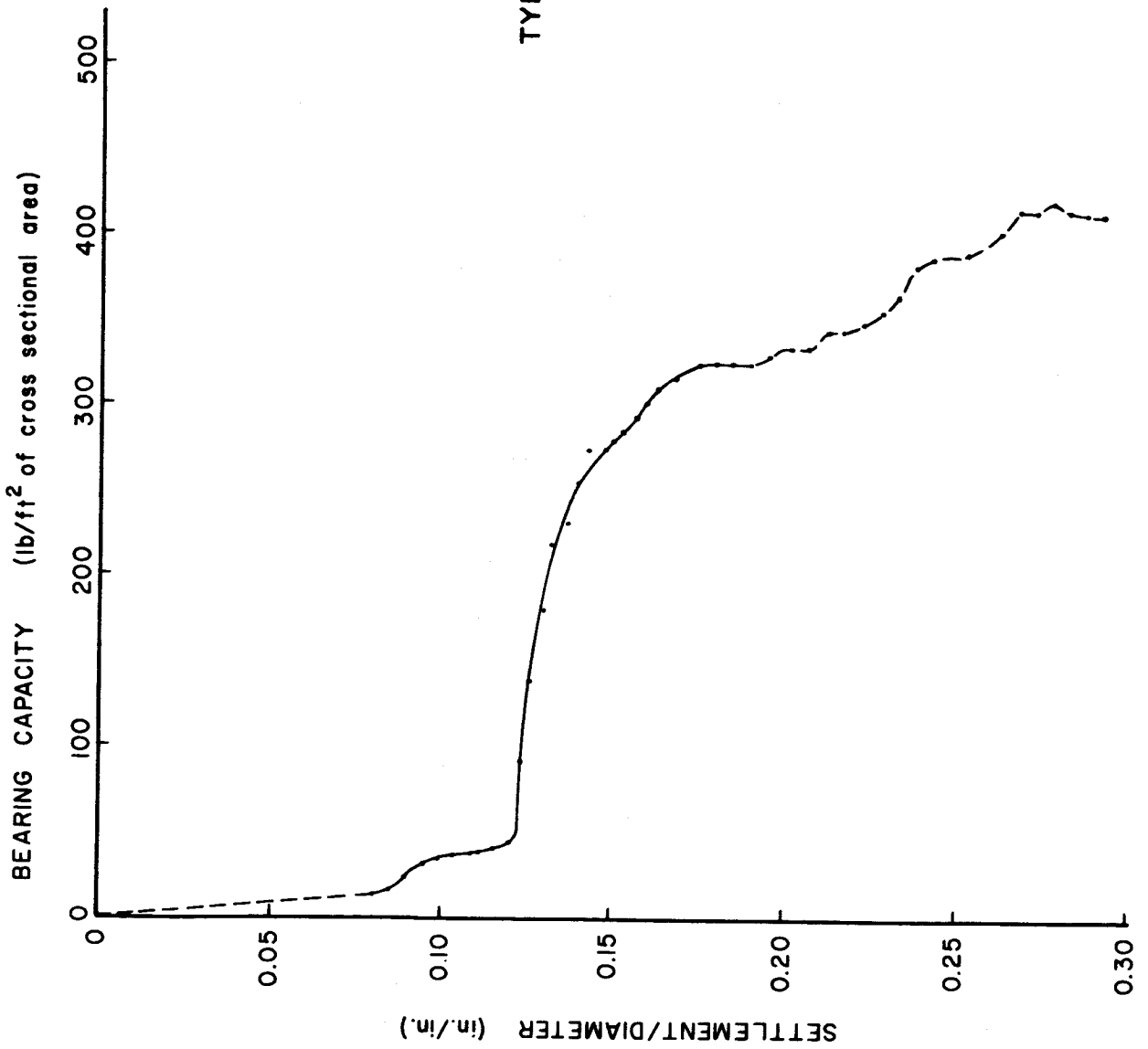
FIG. 28
AVERAGE LOAD-SETTLEMENT
CURVE FOR THE
3.14 in DIAMETER SPHERE
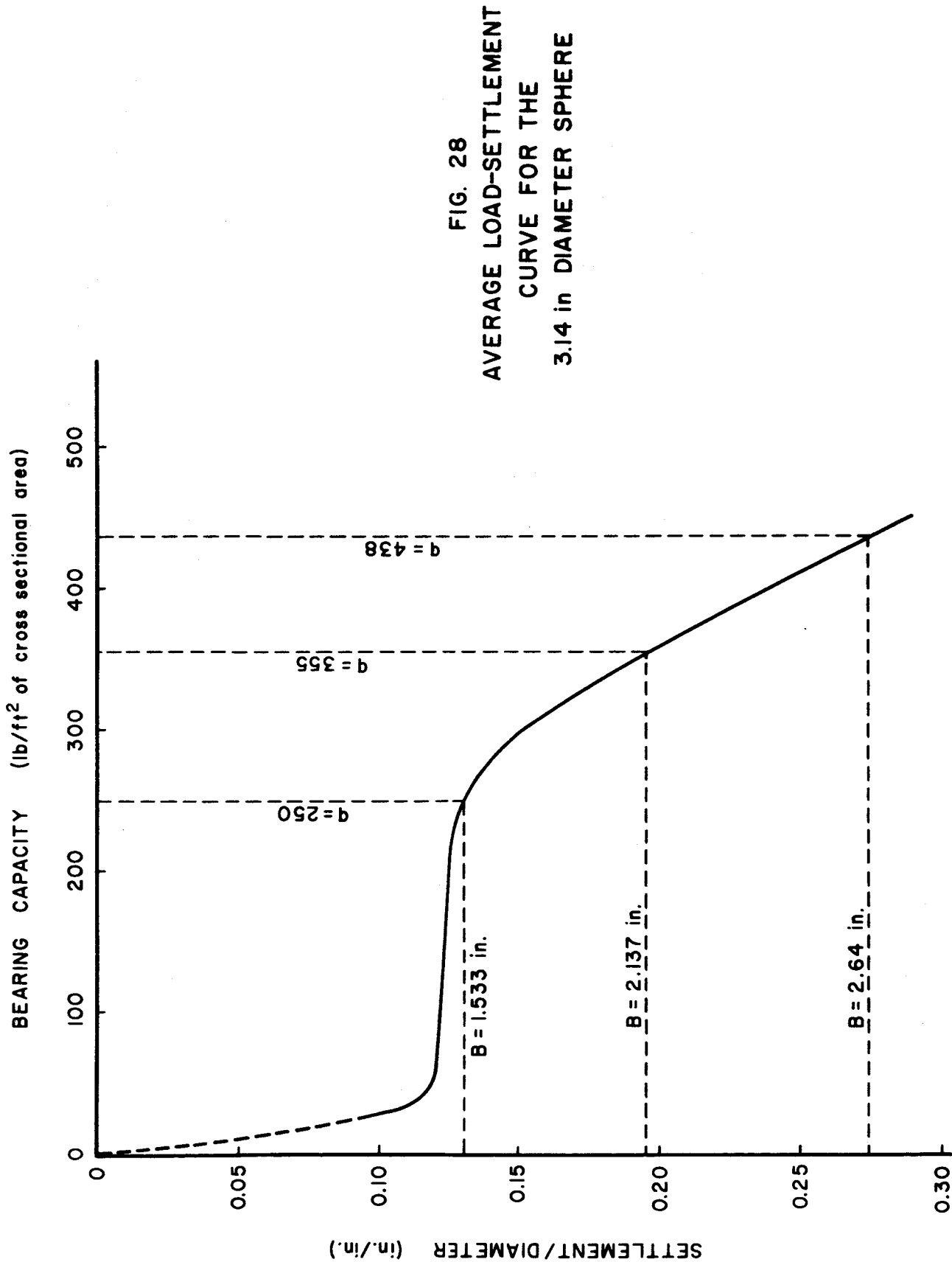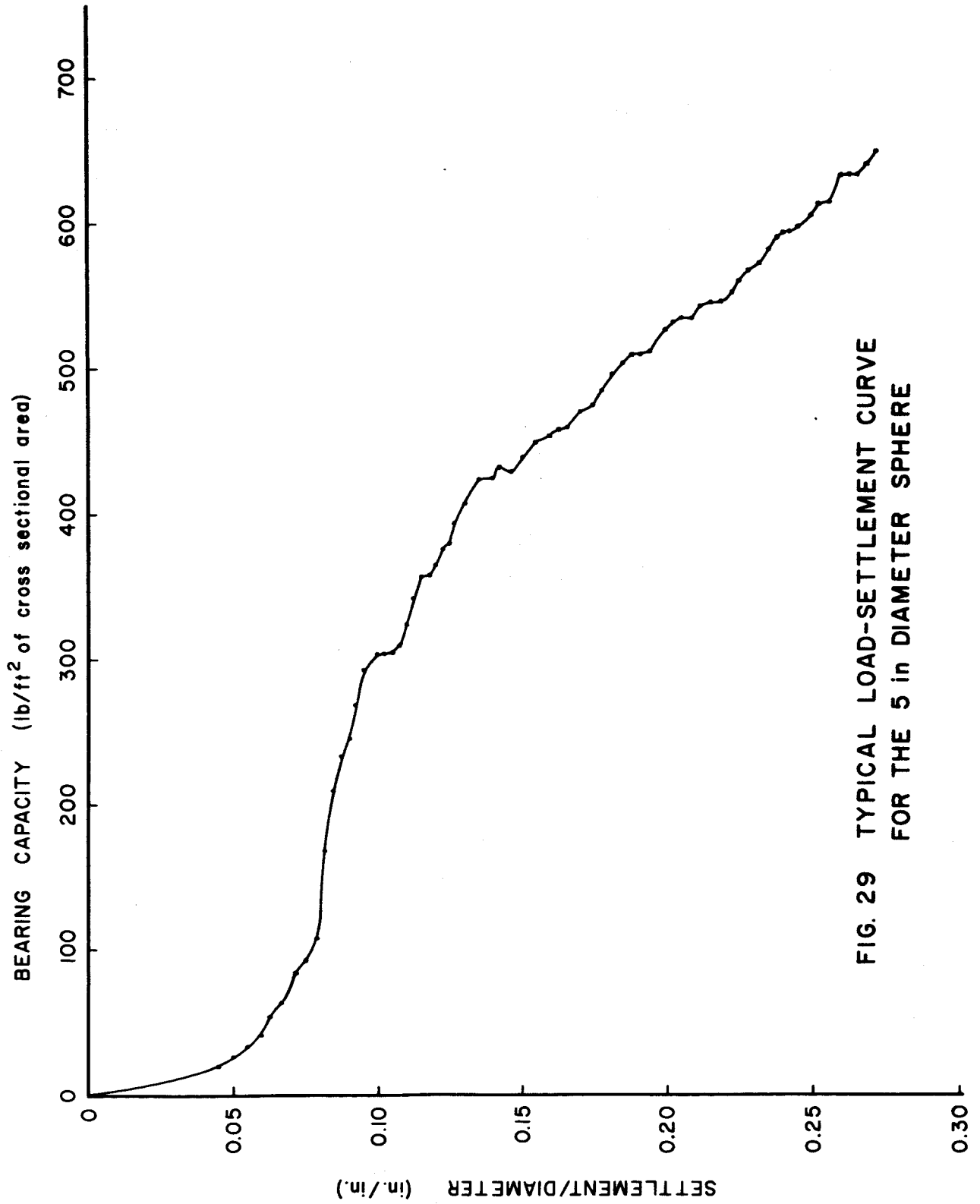
FIG. 29 TYPICAL LOAD-SETTLEMENT CURVE
FOR THE 5 in DIAMETER SPHERE
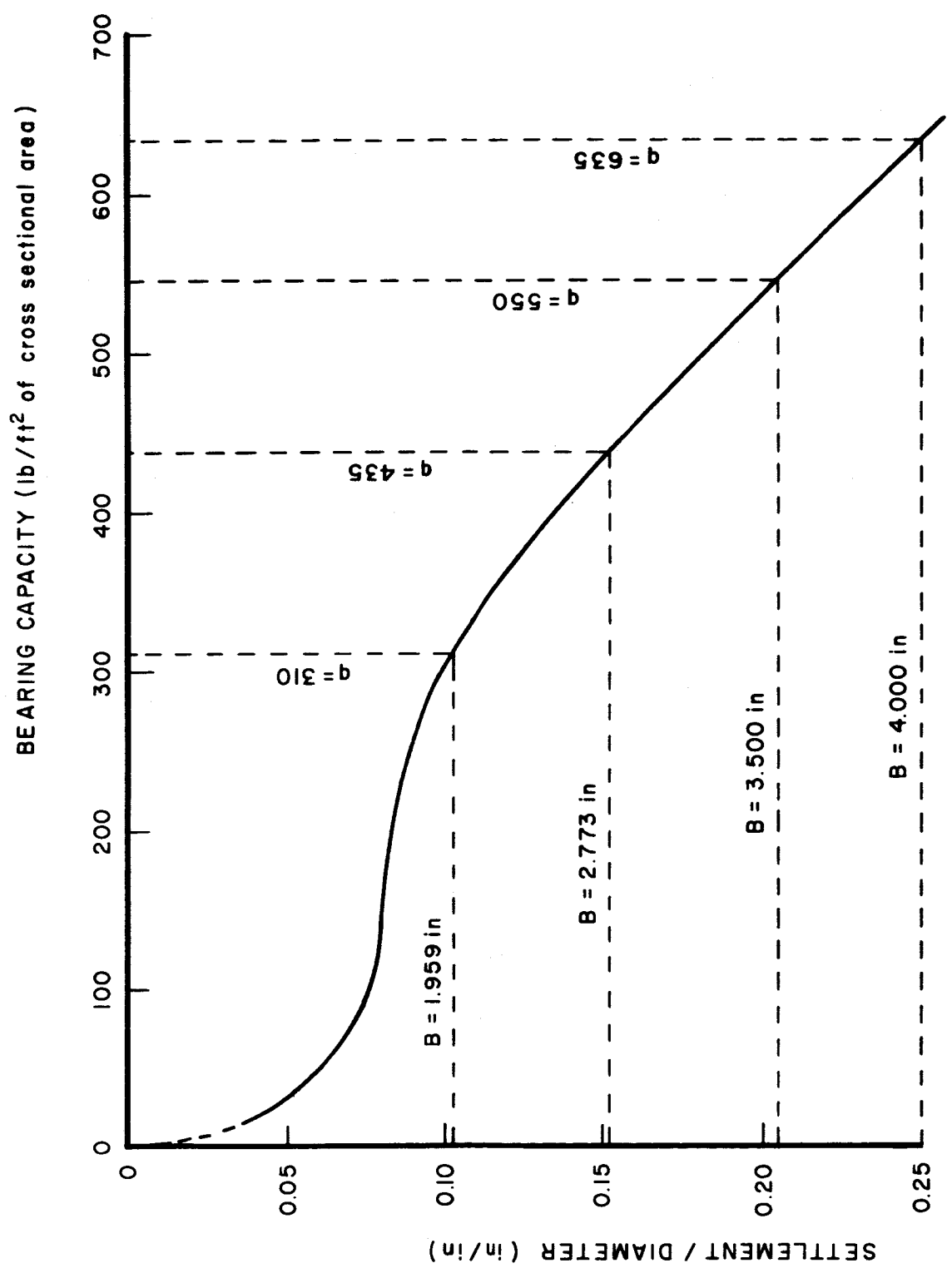
FIG. 30 AVERAGE LOAD-SETTLEMENT CURVE FOR THE 5 in DIAMETER SPHERE

BEARING CAPACITY (lb/ft² of cross sectional area)

SETTLEMENT / DIAMETER (in/in)

q = 635

q = 550

q = 435

q = 310

B = 1.959 in

B = 2.773 in

B = 3.500 in

B = 4.000 in

of the original soil surface equal to those of the plates. The term "bearing capacity" is employed in referring to the ability of the sphere to carry load. It is computed similarly as was the bearing capacity for the cone.

Significant results from the average load-settlement curve are shown in Tables 14 and 15. Analyses of the results are in Tables 16 through 18.

As seen from Tables 16 and 17, the spheres behaved similarly to the cone and plates in that the bearing capacity varied directly with the cross-sectional diameter at the plane of the original soil surface. This relation was true on both the 3.14-in. diameter sphere and the 5-in. diameter sphere. One may probably conclude that the bearing capacity of all foundation elements having circular projected areas varies directly with the diameter of the projected area.

A study of the results of both spheres, (refer to Table 18) revealed that the bearing capacity was not affected by the spherical diameter for the same projected cross section. Of course, to have equal cross-sectional areas with two different spherical diameters, more embedment was required for the smaller sphere. Thus, for the same bearing capacity the settlement of the 3.14-in. diameter sphere was larger than that of the 5-in. diameter sphere.

With regard to the theory for the computation of the bearing capacity of a sphere on cohesionless soil, the same basic assumption previously discussed in the theory of plates were used. As before, the computations were made for the two-dimensional case. A numerical example of the computations is presented in Appendix C. A soil wedge is assumed to adhere to

TABLE 14.

SIGNIFICANT RESULTS* OF TESTS ON THE 3.14-IN. DIAMETER SPHERE

Embedment or Settlement In.	Cross-Sectional Diameter In.	Settlement Per cent of Cross-Sectional Diameter	Cross-Sectional Area In.^{2}	Bearing Capacity* lb/ft^2
0.20	1.533	13.04	1.84	250
0.42	2.137	19.64	3.59	355
0.72	2.640	27.27	5.48	438

*Values read off the Average Curve.

TABLE 15.

SIGNIFICANT RESULTS* OF TESTS ON THE 5-IN. DIAMETER SPHERE

Embedment or Settlement In.	Cross-Sectional Diameter In.	Settlement Per cent of Cross-Sectional Diameter	Cross-Sectional Area In.^{2}	Bearing * Capacity lb/ft^2
0.20	1.959	10.20	3.01	310
0.42	2.773	15.14	6.04	435
0.72	3.50	20.5	9.68	550
1.00	4.0	25	12.58	635

*Values read off the Average Curve.

TABLE 16.

ANALYSIS OF RESULTS OF TESTS ON THE 3.14-IN. DIAMETER SPHERE

Ratio of Cross-Sectional Diameters	Ratio of Bearing Capacities
$\dfrac{2.137}{1.533} = 1.40$	$\dfrac{355}{250} = 1.42$
$\dfrac{2.640}{2.137} = 1.23$	$\dfrac{438}{355} = 1.24$
$\dfrac{2.640}{1.533} = 1.73$	$\dfrac{438}{250} = 1.75$

TABLE 17.

ANALYSIS OF RESULTS OF TESTS ON THE 5-IN. DIAMETER SPHERE

Ratio of Cross-Sectional Diameters	Ratio of Cross-Sectional Areas	Ratio of Bearing Capacities	Ratio of Settlements
$\dfrac{2.773}{1.959} = 1.41$	$\dfrac{6.04}{3.01} = 2.01$	$\dfrac{435}{310} = 1.45$	$\dfrac{0.42}{1.20} = 2.1$
$\dfrac{3.50}{2.773} = 1.26$	$\dfrac{9.68}{6.04} = 1.6$	$\dfrac{550}{435} = 1.26$	$\dfrac{0.72}{0.42} = 1.39$
$\dfrac{4.0}{3.5} = 1.14$	$\dfrac{12.58}{9.68} = 1.3$	$\dfrac{635}{550} = 1.15$	$\dfrac{1.00}{0.72} = 1.39$
$\dfrac{4.0}{1.959} = 2.04$	$\dfrac{12.58}{3.01} = 4.18$	$\dfrac{635}{310} = 2.04$	$\dfrac{1.00}{0.20} = 5.0$
$\dfrac{4.0}{2.773} = 1.45$	$\dfrac{12.58}{6.04} = 2.08$	$\dfrac{635}{435} = 1.46$	$\dfrac{1.00}{0.42} = 2.38$

TABLE 18.

SIGNIFICANT COMPARATIVE RESULTS FOR THE TWO SPHERES

The 3.14-In. Diameter Sphere

Settlement In.	Cross-Sectional In.	Cross-Sectional Areas In.^{2}	Bearing Capacity lb/ft^2
0.42	2.137	3.59	353
0.72	2.64	5.48	425

The 5-In. Diameter Sphere

Settlement In.	Cross-Sectional In.	Cross-Sectional Areas In.^{2}	Bearing Capacity lb/ft^2
0.24	2.137	3.59	340
0.38	2.64	5.48	420

the sphere, forming an angle equal to ϕ with the tangent drawn to the sphere at the soil level. (Refer to Fig. 38). As previously assumed for strip footings and cones, the wedge is in elastic equilibrium and moves with the sphere into the soil.

The calculations shown in Appendix C were performed using an angle ϕ of 32 degrees. The value of the bearing coefficient N_γ calculated is equal to 15 which is about 0.6 of the value calculated for the strip footing.

Such a relation agrees very closely with the experimental results (refer to Table 19) where a ratio of 0.55 was observed. Using this factor of 0.55, the value of the bearing coefficient N_γ for the sphere for sand with an angle of internal friction ϕ equal to 38.7 degrees is 53 which is 0.55 x N_γ (plate).

In the following pages expressions for the bearing capacity of a sphere are developed.

As stated above the bearing capacity of the sphere was observed to vary with respect to the cross-sectional diameter at the plane of the original soil surface. Therefore, the bearing capacity of the sphere, as that of the cone, may be expressed in the same basic equation form previously presented for plates. From Table 19 it is seen that the bearing capacity of the sphere is 0.55 of the ultimate bearing capacity of a circular plate having its diameter equal to that of the sphere at the plane of the original soil surface. Therefore, the bearing capacity of a sphere may be expressed as

$$q = 0.16\gamma B N_\gamma \text{ (plate) lb/ft}^2 \text{ of cross-sectional area} \tag{39}$$

TABLE 19.

SOME COMPARATIVE RESULTS BETWEEN THE PLATE AND SPHERE

Diameter of Plate In.	Ultimate Bearing Capacity lb/ft²	Cross-Sectional Diameter of Sphere	Bearing Capacity of Sphere lb/ft²	Ratio of Bearing of Sphere to Plate
2.22	650	2.22	355	$\frac{355}{645} = 0.55$
3.14	910	3.14	495	$\frac{495}{910} = 0.55$

where B is the diameter of the sphere at the plane of the original soil

surface.

Using the following geometric relation for a sphere

$$B = 2 \sqrt{y(D-y)} \qquad (40)$$

where D is the spherical diameter and y is the settlement the bearing

capacity may then be expressed in terms of the settlement y as

$$q = 0.33\gamma \sqrt{y(D-y)} \; N_\gamma \quad \text{(plate) lb/ft}^2 \text{ of cross-sectional area.} \qquad (41)$$

The bearing capacity of the sphere may also be expressed using the

basic equation for circular plates and the theoretically developed value

of N_γ. (See Appendix C). Thus, the bearing capacity of the sphere is

given by

$$q = 0.3\gamma B N_\gamma \quad \text{(sphere) lb/ft}^2 \text{ of cross-sectional area} \qquad (42)$$

where B is the cross-sectional diameter of the sphere at the plane of

the original soil surface.

Equation 42 may be expressed in terms of the settlement as

$$q = 0.6\gamma \sqrt{y(D-y)} \; N_\gamma \quad \text{(sphere) lb/ft}^2 \text{ of cross-sectional area} \qquad (43)$$

If γ equals 101 lb/ft^3 and N_γ equals 53, the theoretical load-

settle curve for the sphere may be plotted as shown in Fig. 31. The

difference between the theoretical and experimental curves is reflected by

the factors 0.6 and 0.55 previously discussed on page 87. The closeness

of the two curves is thought to represent an acceptable accuracy.
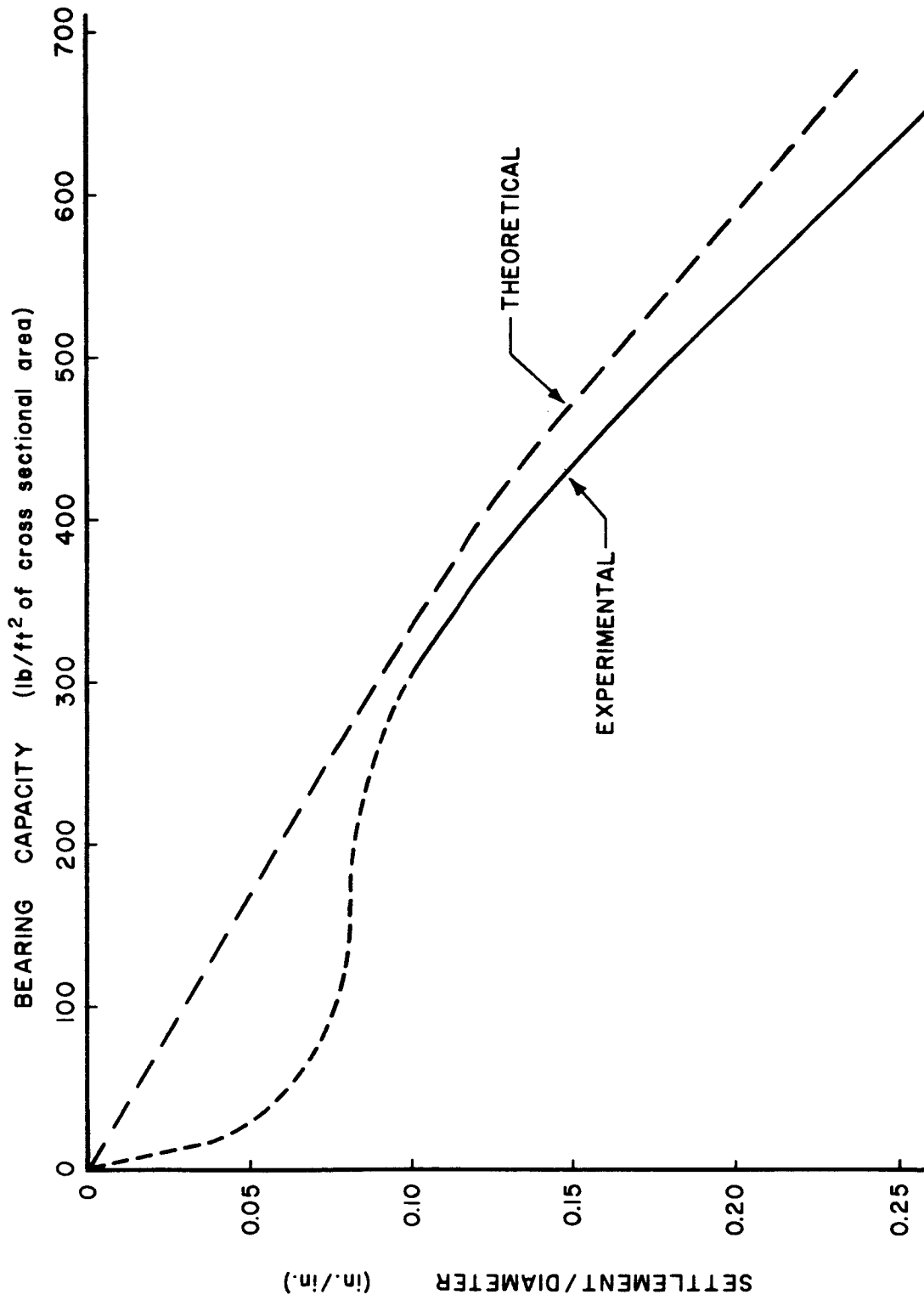
FIG. 31 THEORETICAL vs. EXPERIMENTAL LOAD-SETTLEMENT
CURVES FOR THE 5 in DIAMETER SPHERE

Comparing the bearing capacities of the cone and sphere it was observed that the ratio between the two bearing capacities was

$$\frac{q \text{ (cone)}}{q \text{ (sphere)}} = \frac{0.24}{0.16} = 1.5 \tag{44}$$

for the same equal cross-sectional areas at the plane of the soil surface.

The difference in the behavior of the cone and the sphere, as expressed by the factor 1.5, may be explained by considering the difference in the geometry of the two elements. To obtain the same cross-sectional area at the plane of the original soil surface, much more settlement is required for the cone. Consequently the surface area for the cone is larger than that of the sphere, leading to more bearing capacity for the cone.

5.5 Summary of Experimental Results for the Foundation Elements Tested

The average load-settlement curves obtained from the experimentally observed data for all the foundation elements tested are plotted in Fig. 32.

Though a thorough discussion was given, in separate articles of this chapter, about each of the foundation elements, it is thought helpful to summarize the results.

Referring to Fig. 32, it may be seen that the load-settlement curves of the cone and sphere did not show the ultimate load capacity values as were observed for the circular plates. This, of course, was expected from both the cone and sphere since their cross-sectional areas at the plane of the original soil surface increased with increase in settlement.

Were it possible to increase the load without increasing the cross-sectional area at the plane of the original soil surface, probably the

BEARING CAPACITY (lb/ft^2)
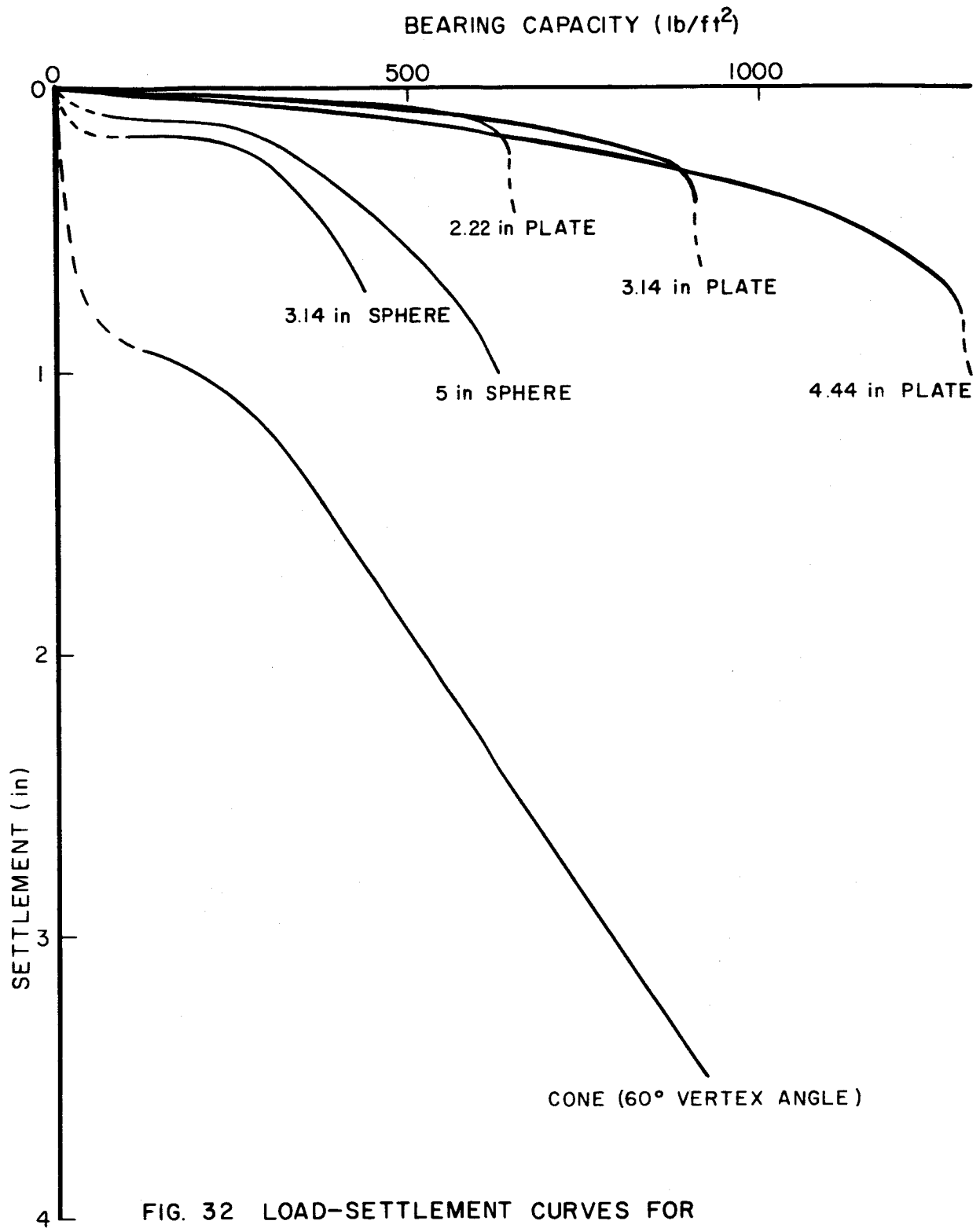
FIG. 32   LOAD-SETTLEMENT CURVES FOR
          PLATES, CONE, AND SPHERES

load-settlement curves would have shown ultimate load conditions similar to those of the circular plates. However, since the theoretical calculations, Appendices B and C, which were based on ultimate failure conditions, agreed closely with the experimentally observed results, the bearing capacity values previously discussed may well be considered as those at the ultimate load. Moreover, this point is only of academic interest since in this investigation the primary interest was the load-settlement relationships.

CHAPTER SIX

LOAD-SETTLEMENT RELATIONS OF FOUNDATION ELEMENTS

IN NON-DIMENSIONAL FORM

6.1 Introduction[1, 4, 7, 11]

Dimensional analysis is a method by means of which we may deduce infor-
mation about a phenomenon described by a dimensional equation, all terms of
which have the same measure formula.

Dimensional analysis is a useful and convenient technique for finding
the quantitative conditions for similarity of behavior.

The use of dimensional analysis in connection with scale models has
proved to be of great importance. Information gained from experiments
using models proved very useful when the mathematical theory was found to
be too difficult. The theory of models founded on the method of dimensions
is indispensable to the modern engineer in planning his experiments.

6.2 Dimensional Analysis in Soil Mechanics[7]

A. Physical Similitude

The following well known considerations of similitude in science
form the basis for the discussion with respect to particular phases of soil
mechanics that are related to the investigation.

Considering a model test that is assumed to be a true picture, at
reduced scale, of a prototype phenomenon, the requirements are:

(1) Geometric similarity: If two, arbitrary, lengths in the

model are designated by L_{1_m} and L_{2_m} and the corresponding

lengths in the prototype by L_{1p} and L_{2p} the geometric similarity is expressed by

$$\frac{L_{1m}}{L_{1p}} = \frac{L_{2m}}{L_{2p}} \tag{45}$$

This fraction gives the linear scale ratio. It means that the ratio of two arbitrary lengths in the model is equal to the same ratio in the prototype, or corresponding ratios L_1/L_2 are equal in model and prototype.

For static phenomenon, only the geometric similarity is of immediate interest, whereas in dynamic problems, the kinematic similarity is also required.

(2) Kinematic similarity: Designating the velocities by V, the kinematic similarity would then be expressed (using the same approach as for the geometric similarity) as:

$$\frac{V_{1m}}{V_{1p}} = \frac{V_{2m}}{V_{2p}} . \tag{46}$$

Though these two expressions form our primary interest for similitude, the physical conditions must be added since it is far from certain that the model would be physically stable, a condition quite sure for the prototype. These physical conditions could be expressed as conditions of equilibrium of the individual particles which are quite evident for the static case. For a dynamic problem inertia forces (mass x negative acceleration) are applied to all particles.

(3) Dynamic Similarity: In the prototype all particles are in equilibrium at any time. Therefore, the system of forces in the model must be a true picture of those in the prototype

so as to fulfill the same conditions. Designating forces by F, the dynamic similarity is expressed by

$$\frac{F_{1,m}}{F_{1p}} = \frac{F_{2m}}{F_{2p}} \cdot \qquad (47)$$

B. Dimensional Analysis Applied to Settlements on Sand

In the development of the basic equation for load-settlement relationships in non-dimensional form a circular foundation element is considered. If the settlement is y due to the load p the foundation element carries per unit of area, then geometric similarity requires that

$$\frac{y_m}{B_m} = \frac{y_p}{B_p} \qquad (48)$$

where B is the diameter of the foundation element.

The most important forces in a problem of settlement on sand are the external load p per unit of area and the unit weight γ of the sand which constitutes the gravitational forces.

If the gravitational stresses in the sand are represented by γB, then the dynamic similarity requires that

$$\left(\frac{p}{\gamma B}\right)_m = \left(\frac{p}{\gamma B}\right)_p \cdot \qquad (49)$$

For proper presentation of the loading test in a dimensionally correct form, Eqs. 48 and 49 may be combined in the form of

$$\frac{y}{B} = f_1\left(\frac{p}{\gamma B}\right) \qquad (50)$$

where f_1 is a dimensionless factor.

If the dimensionless parameter f_1 can be determined in some manner, Eq. 50 can be used to predict the behavior of foundation of various sizes on the surface of different types of sand.

6.3 Non-Dimensional Relations for the Plates, Cone, and Spheres

The non-dimensional approach expressed in Eq. 50 was used in plotting Fig. 33 from the general plot shown in Fig. 32. In using Eq. 50 the value of the sand density γ of 101 lb/ft^3 was employed to compute the gravitational stresses γB.

It may be noted that in plotting Fig. 33 the average curves were used. For the plates and spheres, there was some negligible scatter, which did not show on the scale of the general plot.

Figure 33 shows in non-dimensional form the load-settlement relationships for circular plates, a 60 degree cone, and spheres. It is of significant importance to note that only one curve represents the load-settlement relationships for each of the three types of foundation elements. Therefore, the information contained in Fig. 33 predicts the behavior of any size circular plate, any 60 degree cone, and any size sphere loaded on the surface of a cohesionless sand of the same physical properties as the sand used in this investigation.

Since in general, sands of the exact type used in this investigation will not be encountered, it is important to have procedures for predicting behavior for any sand. The following paragraphs show the developed procedure.

The bearing capacity of the spheres and cone may be expressed as
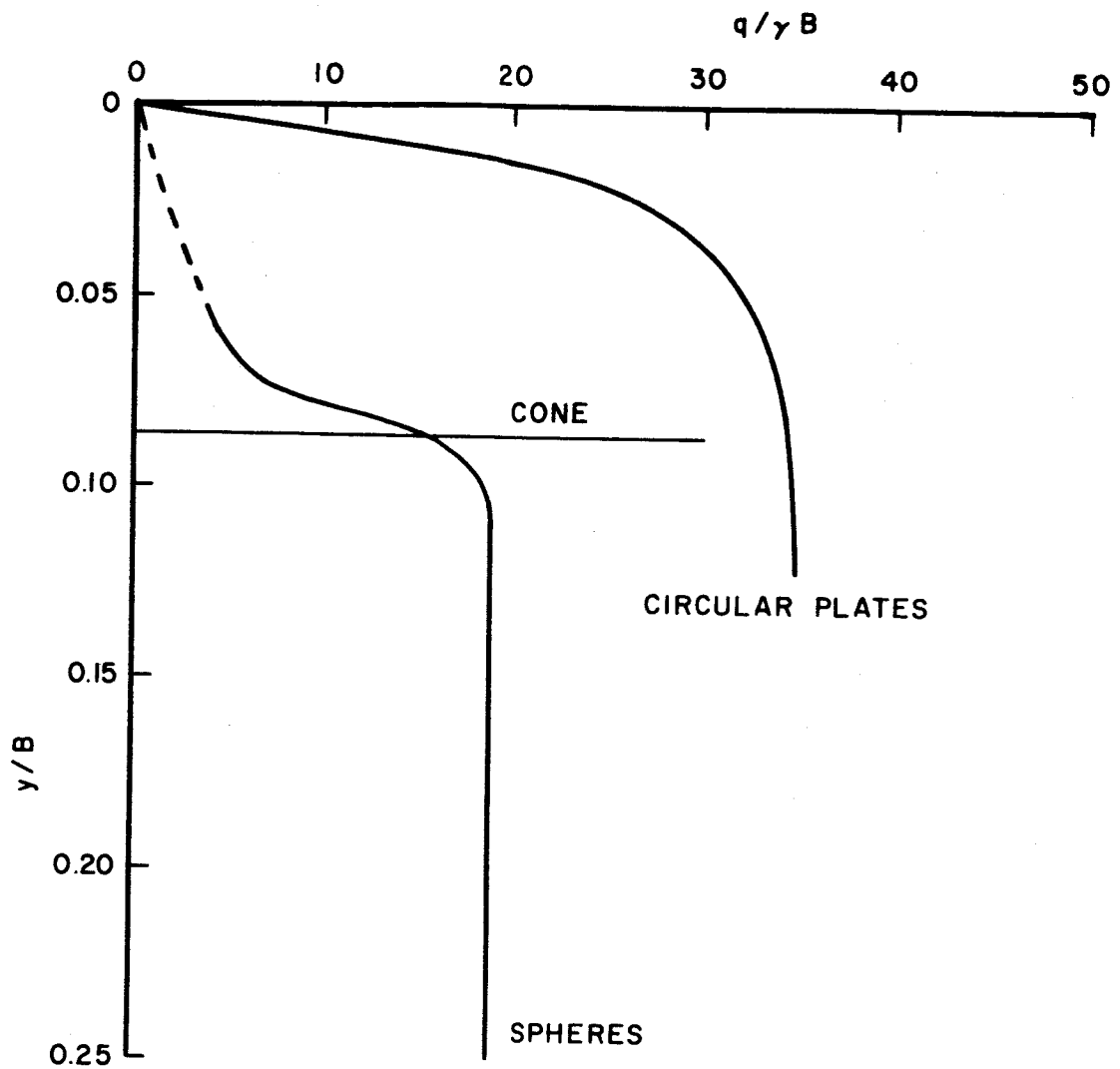
FIG. 33 NON DIMENSIONAL RELATIONS FOR THE CIRCULAR PLATES, SPHERES, AND THE CONE (SAND OF $\gamma = 101$ lb/ft^3)

$$q = \left[\text{Constant}\right] B\gamma N_\gamma \qquad\qquad (51)$$

then the relation

$$\left(\frac{q}{\gamma B}\right) = \left[\text{Constant}\right] N_\gamma \qquad\qquad (52)$$

Therefore, as seen from Eq. 52, the non-dimensional relations for any sphere or 60 degree cone is directly proportional to the value of N_γ which is a function of the angle of internal friction of the sand. (Refer to Fig. 6.) So in using Fig. 33 for various types of sands the values from the curves must be multiplied by the ratio of 96, which is the N_γ for the soil used in this investigation, to the value of N_γ for the new soil as determined from Fig. 6.

For the 60 degree cone the curve will always be a straight line for one value of y/B regardless of the type of sand. As an example, for sand with an angle of internal friction ϕ equal to 32 degrees, the relation $q/\gamma B$ for any 60 degree cone equals the values from Fig. 33 multiplied by 96/28, where 28 is the N_γ of the type of sand. (See Fig. 6.)

Similarly the curve for spheres will always be one vertical line for one type of sand since the relation $q/\gamma B$ is a constant. However, for various types of sand the curve is shifted in proportion to the ratio of N_γ's as explained above.

Analyzing Eq. 50 with respect to the curve for plates, it may be observed that the dimensionless parameter f_1 is a constant and is equal to the slope of the early part of the curve. This relation holds true up to about 1/2 the ultimate value of $q/\gamma B$ at which stage the curve deviates

from this tangent. It is of significance to note that this constant f_1 may be used to compute relations for plates up to 1/2 the ultimate and also to locate the point of intersection between the initial tangent to the curve and the vertical line indicating the ultimate condition. As previously discussed this is possible for any size plate. Equation 52 may be used to obtain the values of the ultimate condition since Eq. 51 represents the ultimate bearing capacity for circular plates. Therefore, for any type of sand, the value of the $q/\gamma B$ at the ultimate must be corrected by multiplying it by the ratio of the N_γ's as shown for the other two elements.

CHAPTER SEVEN

CONCLUSIONS

From the results of this investigation the following observations may be made:

1. The ultimate bearing capacity for circular plates placed on the surface of cohesionless soils varies directly with respect to the diameter of the plate.

2. The bearing capacity of the cone on cohesionless soil, as expressed in terms of the cross-sectional area, varies directly with respect to the cross-sectional diameter at the level of the embedment or settlement. It may be concluded that the ultimate bearing capacity of the cone placed on cohesionless soils behaves similarly to circular foundation elements.

3. The bearing capacity of the sphere on cohesionless soil as expressed in terms of the cross-sectional area varies directly with respect to the cross-sectional diameter at the level of the embedment or settlement.

4. The bearing capacities of any two spheres on cohesionless soil are equal, regardless of size of spherical diameter, at equivalent cross-sectional areas.

5. The ultimate bearing capacity of a cone, whose half vertex angle is 30 degrees, on cohesionless soil is expressed by

$$q = 0.24\gamma\ BN_\gamma\ \text{(plate)}\quad \text{lb/ft}^2\ \text{of cross-sectional area}$$

where B is the cross-sectional diameter of the cone at the level
of the embedment, and N_γ the bearing capacity coefficient for
circular plates

or

$$q = 0.28\gamma\ y\ N_\gamma\ \text{(plate)}\ \text{lb/ft}^2\ \text{of cross-sectional area}$$

where y is the embedment or settlement

or

$$q\text{u} = 0.12\gamma\ B\ N_\gamma\ \text{(plate)}\ \text{lb/ft}^2\ \text{of surface contact area}$$

where B is the diameter of the cone at the level of the settle-
ment that furnishes the surface contact area.

6. Based on the theory developed in this investigation, the bearing
capacity of the cone, whose half vertex angle is 30 degrees, on
cohesionless soil may be expressed as

$$q = 0.30\gamma\ B\ N_\gamma\ \text{(cone)}\ \text{lb/ft}^2$$

or

$$q = 0.345\gamma\ y\ N_\gamma\ \text{(cone)}\ \text{lb/ft}^2.$$

7. The bearing capacity of a sphere on cohesionless soil is expressed
by

$$q = 0.165\gamma\ B\ N_\gamma\ \text{(plate)}\ \text{lb/ft}^2$$

where B is the cross-sectional diameter at the level of the
embedment, and N_γ the bearing capacity coefficient for circular
plates, or

$$q = 0.33\gamma \sqrt{y\,(D-y)} \ \ N_\gamma \ \text{(plate) lb/ft}^2$$

where D is the spherical diameter of the sphere, and y is the settlement or embedment.

8. Based on the theory developed in this investigation the bearing capacity of a sphere on cohesionless soil may be expressed as

$$q = 0.3\gamma \ B \ N_\gamma \ \text{(sphere) lb/ft}^2$$

or

$$q = 0.6 \ \gamma \sqrt{y\,(D-y)} \ \ N_\gamma \ \text{(sphere)} \ \ \text{lb/ft}^2.$$

9. The non-dimensional relationship for load-settlement curves may be expressed as

$$\frac{y}{B} = f_1 \left[\frac{q}{\gamma B} \right]$$

where f_1 is dimensionless parameter.

10. For a specific type of sand there is only one non-dimensional curve for any size circular plate, any size sphere, or 60 degree cone.

11. The equation of Terzaghi for ultimate bearing capacity of circular plates placed on the surface of cohesionless soils is quite accurate as shown by the observed test results.

12. The settlement at the ultimate bearing capacity for circular plates placed on the surface of cohesionless soils varies directly with respect to the area of the plate or the square of the diameter of the plate.

13. The load-settlement relationship for a cone with a 30 degree half vertex angle tested on the surface of a cohesionless soil is a straight line.

14. The coefficient of subgrade reaction k_s is a constant for any one circular plate on any one cohesionless soil only for the values of the subgrade reaction p that do not exceed one-half the value of the ultimate bearing capacity for that plate.

15. The value of the coefficient of subgrade reaction k_s varies inversely with respect to the diameter of the plate loaded as a footing element.

16. The bearing capacities for two equivalent cross sections of the cone and sphere have the ratio of 1.5, which indicates the effect of the surface contact area.

17. The thickness of the sand layer must be at least eight times the diameter of the circular foundation element so as not to have any effects from the lower layer on the ultimate bearing capacity, the settlement at the ultimate bearing capacity, and the modulus of subgrade reaction.

18. If the settlement at the ultimate bearing capacity does not govern the design, the ultimate bearing capacity attained by condition 17 may be developed with a sand layer that is twice the diameter of the foundation element in thickness, and under-lain by a solid strata such as rock. The error introduced is about +8.5 per cent.

19. Maximum ultimate bearing capacity and minimum settlement at the ultimate bearing capacity were observed when the thickness

of the sand layer was four times the diameter of the foundation element and underlain by a solid strata.

APPENDICES

APPENDIX A

APPENDIX A

Steps Used in the Calculations of the Bearing Capacity Coefficient Nγ for

a Strip Footing.

(Refer to freebody diagram, Fig. 34)

Typical steps to be carried out for all the failure surfaces assumed

for trial:

1. Subdivide the soil mass (hatched boundaries) into a convenient

    number of elements and compute the total area and the total moment

    of this area, thus determining the center of gravity.

2. Compute the moment arm d_w, distance of total mass weight (total

    area) from the center of the assumed log spiral surface.

3. Compute the moment arm d_{p_1}, of the passive pressure p_1 which is

    assumed to act at 2/3 the height h from the center of the assumed

    log spiral surface.

4. Compute p_1 from the relation

$$p_1 = 1/2 \ h^2 \ \gamma \left[\tan^2 (45 + \phi/2) \right] = 1/2 \ h^2 \gamma \left[k_{PR} \right]$$

    where h is in terms of r.

5. Compute the total weight W keeping it in terms of γ and r ,

    thus it is equal to $A\left[r^2 \ \gamma \right]$ where A is the total area in

    terms of the scale chosen for r .

6. Enter all previously calculated values in a tabular form, as shown,

    and compute the resisting moment of the soil against failure.

$$M = W \ d_w + P_1 \ d_{p_1}$$

110

(note that both W and P_1, are in terms of $(r^2\gamma)$ and that d_w

and d_{p_1} in terms of r . Therefore, the moment is in terms of

$r^3\gamma$.

7. The moment of the load causing failure is

$$P_p \; d_{p_p}$$

where d_{p_p} is the distance of P_p from the center of the log spiral

surface. (Note that it depends on the pressure distribution at the

base of the footing.)

Thus, compute d_{p_p} in terms of r .

8. Compute P_p from the equilibrium equation

$$P_p = \frac{W \; d_w + P_1 \; d_{p_1}}{d_{p_p}} = C \; \gamma \; r^2 .$$

9. The value of the constant is N_γ .

10. Repeat Steps 1 through 9 for the various assumed failure surfaces,

and plot the results of the values of N_γ . The minimum value would

be the controlling value to be used in determining the load P_p .

112
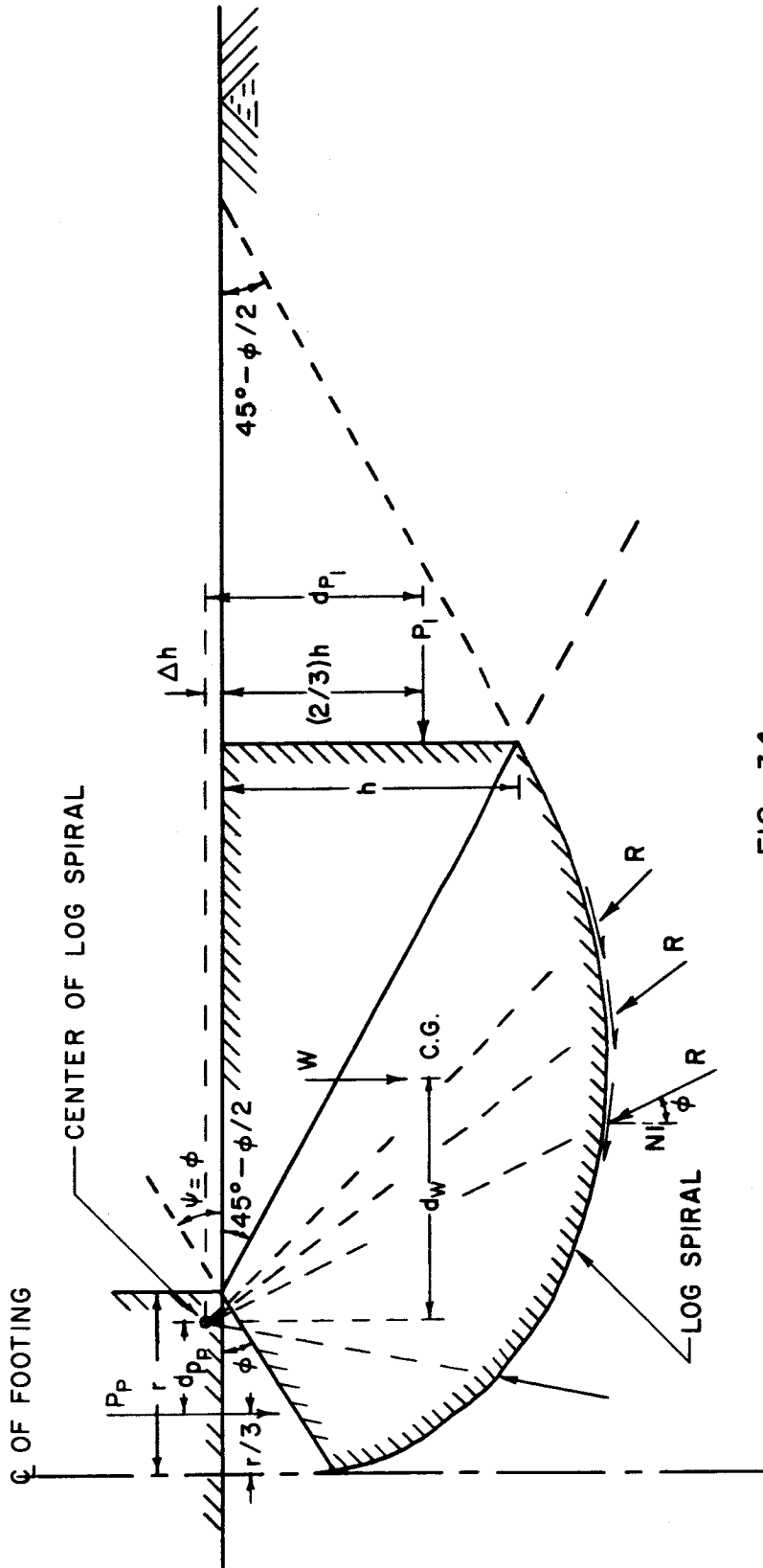
FIG. 34
FREE BODY DIAGRAM *
EQUILIBRIUM EQUATION: $P_P \times d_{P_P} = W d_W + P_l d_{P_l}$

*TERZAGHI'S SOLUTION OF THE BEARING CAPACITY COEFFICIENT N_γ

CALCULATIONS OF THE BEARING CAPACITY COEFFICIENT Nγ FOR A

PLATE FOR $\psi = \phi$

Surface - 1 - (Refer to Fig. 35)

Mean Ordinate	Width	Area	Arm	Moment
10	10	100	5	500
11.6	10	116	15	1740
9.6	5	48	22.5	1080
		264		3320
		-31[*]		-103.33[*]
		233		3216.67

$$C.G. = \frac{3216.67}{233} = 13.81$$

$$d_w = \begin{array}{r} 13.81 \\ -3.50 \\ \hline 10.31 \end{array} = 10.31 \ r$$

$$d_{p_1} = \frac{2}{3} h_1 = \frac{2}{3} \times 8.4 = \begin{array}{r} 5.6 \\ +3.6 \\ \hline 9.2 \end{array} = 0.92 \ r$$

[*]Area of triangular wedge = $\frac{1}{2} \times 10 \times 6.2 = 31$

[*]Moment of triangular wedge = $31 \times \frac{10}{3} = 103.33$
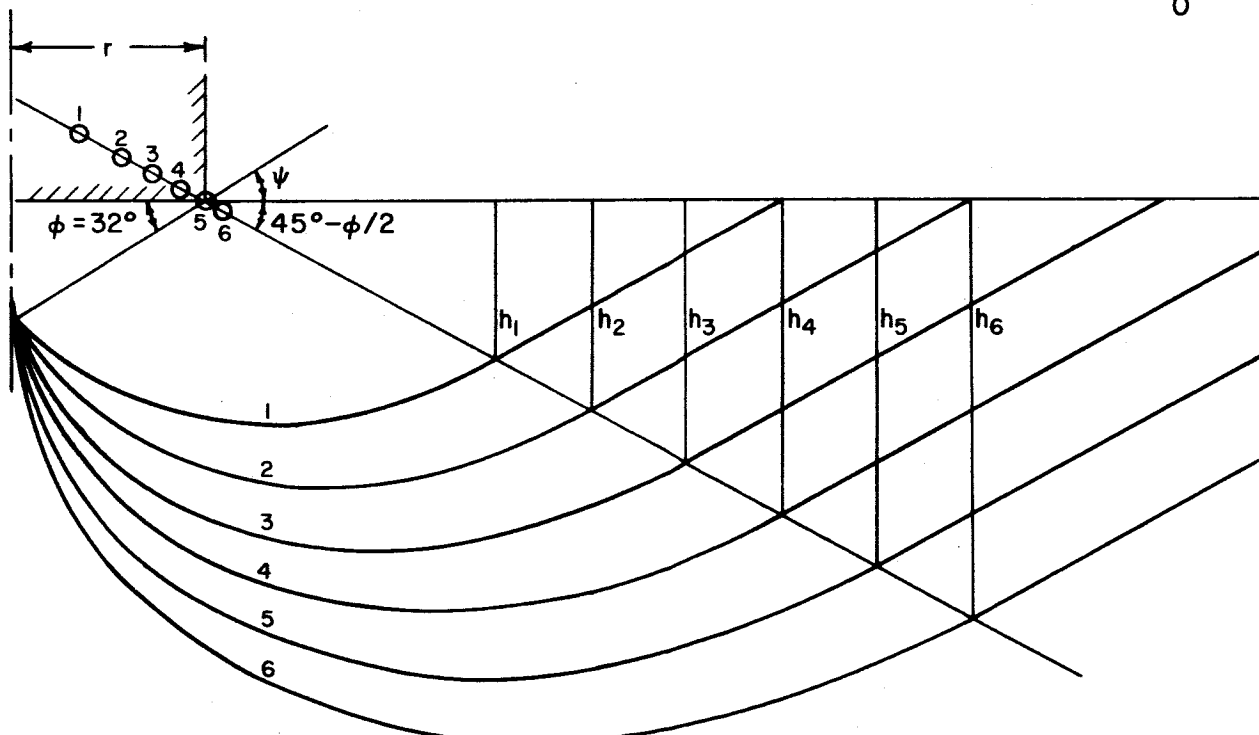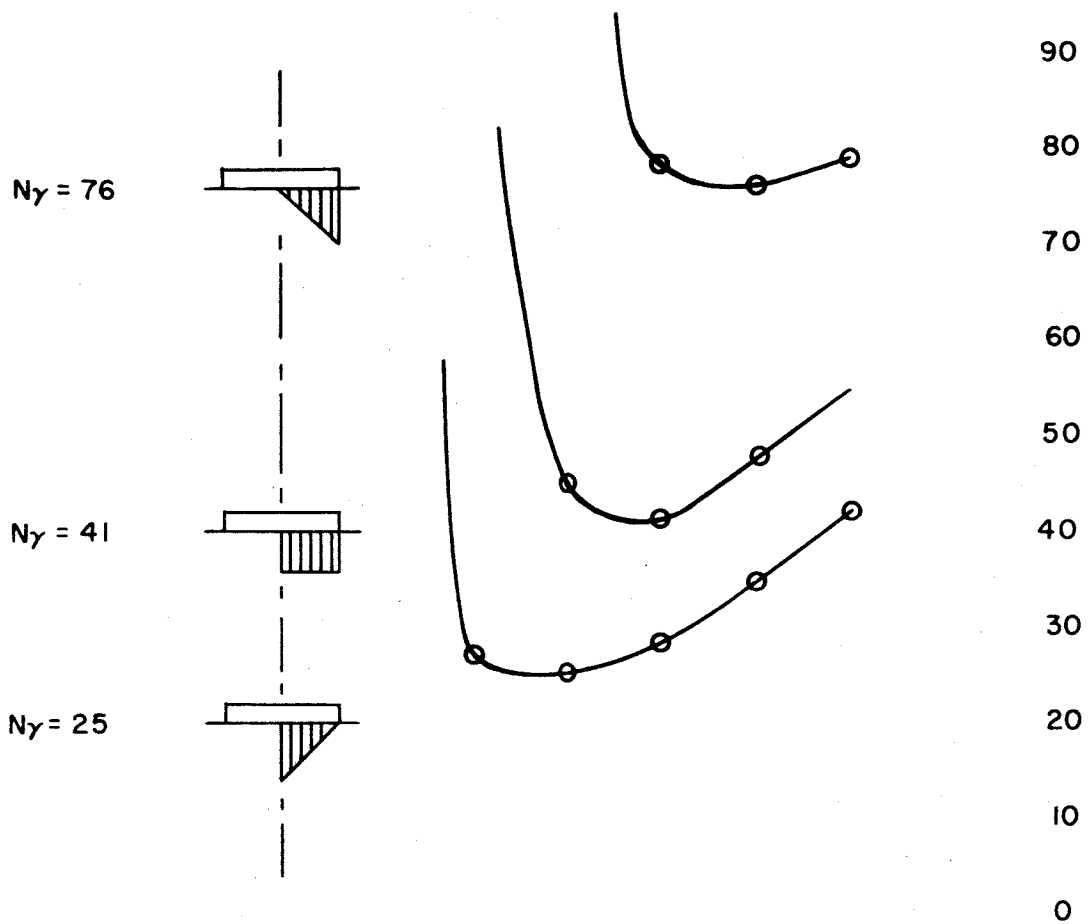
FIG. 35   FAILURE SURFACES FOR A STRIP FOOTING
FOR A RISE ANGLE ψ EQUAL TO ϕ

Surface - 2

Mean Ordinate	Width	Area	Arm	Moment
11.7	10	117	5	585
15	10	150	15	2250
13.2	10	132	25	3300
		399		6135
		-31		-103.33
		368		6031.67

$$\text{C.G.} = \frac{6031.67}{368} = 16.39$$

$$d_w = \begin{array}{r} 16.39 \\ -5.50 \\ \hline 10.89 \end{array} = 1.089 \ r$$

$$d_{p_1} = \frac{2}{3} h_2 = \frac{2}{3} \times 10.8 = \begin{array}{r} 7.2 \\ +2.5 \\ \hline 9.7 \end{array} = 0.97 \ r$$

Surface - 3

Mean Ordinate	Width	Area	Arm	Moment
13.4	10	134	5	670
18	10	180	15	2700
17.7	10	177	25	4425
15	5	75	32.5	2437.5
		566		10232.5
		-31		-103.33
		535		10129.17

$$\text{C.G.} = \frac{10,129.17}{535} = 18.93$$

$$d_w = \begin{array}{r} 18.93 \\ -7.13 \\ \hline 11.80 \end{array} = 1.18 \ r$$

$$d_p = \frac{2}{3} \times h_3 = \frac{2}{3} \times 13.8 = \begin{array}{r} 9.2 \\ +1.5 \\ \hline 10.7 \end{array} = 1.07 \ r$$

Surface - 4

Mean Ordinate	Width	Area	Arm	Moment
15.2	10	152	5	760
20.5	10	205	5	3075
21.3	10	213	25	5325
19	10	190	35	6650
		760		15810
		-31		-103.33
		729		15706.67

$$\text{C.G.} = \frac{15706.67}{729} = 21.55$$

$$d_w = \begin{array}{r} 21.55 \\ -8.55 \\ \hline 13.00 \end{array} = 1.3 \ r$$

$$d_{p_1} = \frac{2}{3} \ h_4 = \frac{2}{3} \times 16.5 = \begin{array}{r} 11 \\ +0.7 \\ \hline 11.7 \end{array} = 1.17 \ r$$

Surface - 5

Mean Ordinate	Width	Area	Arm	Moment
17.3	10	173	5	865
23.5	10	235	15	3525
25	10	250	25	6250
23.5	10	235	35	8225
20.6	5	103	42.5	4377.5
		996		23242.5
		-31		-103.33
		965		23139.17

$$\text{C.G.} = \frac{23139.17}{965} = 23.98$$

$$d_w = \begin{array}{r} 23.98 \\ -9.50 \\ \hline 14.48 \end{array} = 1.448 \ r$$

$$d_{p_1} = \frac{2}{3} \times h_5 = \frac{2}{3} \times 19.2 = \begin{array}{r} 12.8 \\ +0.0 \\ \hline 12.8 \end{array} = 1.28 \ r$$

Surface - 6

Mean Ordinate	Width	Area	Arm	Moment
19.3	10	193	5	965
26	10	260	15	3900
28.3	10	283	25	7075
27.7	10	277	35	9695
24.7	10	247	45	11115
		1260		32750
		-31		-103.33
		1229		32646.67
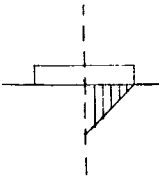
$$\text{C.G.} = \frac{32646.67}{1229} = 26.56$$

$$d_w = \begin{array}{r} 26.56 \\ -10.56 \\ \hline 16.00 \end{array} = 1.6 \; r$$

$$d_p = \frac{2}{3} \, h_6 = \frac{2}{3} \times 21.9 = \begin{array}{r} 14.6 \\ -0.6 \\ \hline 14.0 \end{array} = 1.4 \; r$$

Surface	W	d_w	Wd_w	Pd_{p_1}	M	P_1	d_{p_1}	$\hbar_{PR}$	h^2	h
1	2.33	1.031	2.40	1.06	3.46	1.15	0.92	3.25	0.71	0.84
2	3.68	1.089	4.00	1.84	5.84	1.90	0.97	3.25	1.17	1.08
3	5.35	1.18	6.31	3.31	9.62	3.09	1.07	3.25	1.90	1.38
4	7.29	1.3	9.48	5.17	14.65	4.42	1.17	3.25	2.72	1.65
5	9.65	1.44	13.90	7.68	21.58	6.00	1.28	3.25	3.69	1.92
6	12.29	1.6	19.66	10.92	30.58	7.80	1.4	3.25	4.80	2.19

Plate $- \psi = \phi$

Value of N_γ Based on ▭ Distribution

Surface	d_{p_p}	M	M/d_{p_p}
1	$\dfrac{3.50 - 3.33}{10} = 0.017$	3.46	203
2	$\dfrac{5.50 - 3.33}{10} = 0.217$	5.84	26.8
3	$\dfrac{7.13 - 3.33}{10} = 0.380$	9.62	$\boxed{25.3} \leftarrow$
4	$\dfrac{8.55 - 3.33}{10} = 0.522$	14.65	28
5	$\dfrac{9.50 - 3.33}{10} = 0.617$	21.58	35
6	$\dfrac{10.56 - 3.33}{10} = 0.723$	30.58	42.2

$$\therefore N_\gamma \text{ (min)} = 25.3$$

Value of N_γ Based on
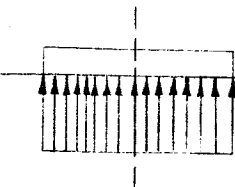
Distribution

Surface	d_{p_p}	M	M/d_{p_p}
1	-	-	-
2	$\dfrac{5.50 - 5.00}{10} = 0.05$	5.84	117
3	$\dfrac{7.13 - 5.00}{10} = 0.213$	9.62	45
4	$\dfrac{8.55 - 5.00}{10} = 0.355$	14.65	41.3
5	$\dfrac{9.50 - 5.00}{10} = 0.450$	21.58	48
6	$\dfrac{10.56 - 5.00}{10} = 0.556$	30.58	55

$$\therefore \ N_\gamma \ (\text{min}) = 41.3$$

Value of N_γ Based on [diagram] Distribution
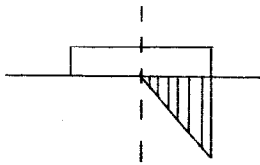
Surface	d_{p_p}	M	M/d_{p_p}
3	$\dfrac{7.13 - 6.67}{10} = 0.046$	9.62	210
4	$\dfrac{8.55 - 6.67}{10} = 0.188$	14.65	78
5	$\dfrac{9.50 - 6.67}{10} = 0.283$	21.58	76
6	$\dfrac{10.56 - 6.67}{10} = 0.389$	30.58	78.5

Calculations of the Bearing Capacity Coefficient N_γ for a

Plate for $\psi = 45 + \phi/2$

Surface 1 (Refer to Fig. 36)

Mean Ordinate	Width	Area	Arm	Moment
12.7	10	127	5	635
14.5	10	145	15	2175
12.2	5	61	22.5	1372.5
		333		4182.5
		-22.5[*]		-37.5[*]
		310.5		4145.0

$$\text{C.G.} = \frac{4145}{310.5} = 13.35$$

$$
\begin{aligned}
d_w \quad &= \quad 13.35 \\
&\quad -3.00 \\
\hline
&\quad 10.35 \quad = \quad 2.07 \ r
\end{aligned}
$$

$$
\begin{aligned}
d_{p_1} = \frac{2}{3} \ h_1 = \frac{2}{3} \times 11 = \quad &7.33 \\
+ \ &1.00 \\
\hline
&8.33 \quad = \quad 1.67 \ r
\end{aligned}
$$

[*]Area of Triangular Wedge = $1/2 \times 5 \times 9$ = 22.5

[*]Moment of Triangular Wedge = $22.5 \times 5/3$ = 37.5
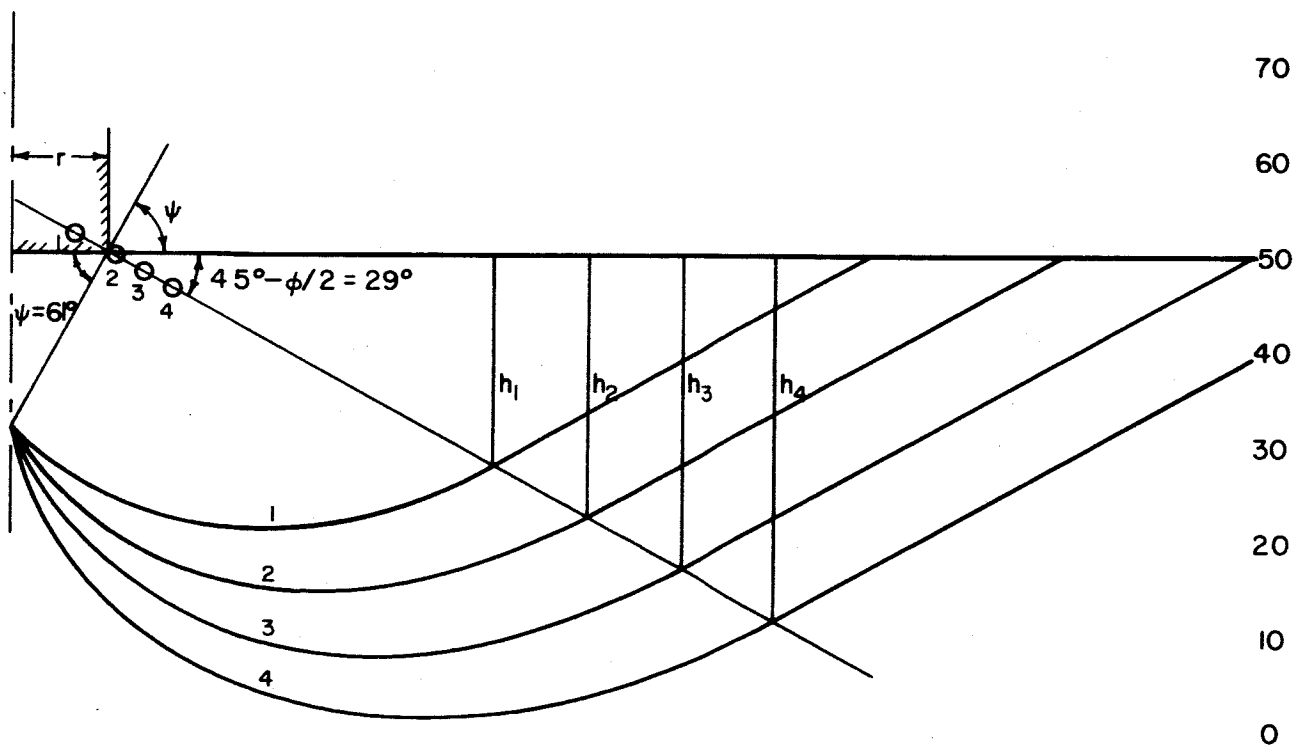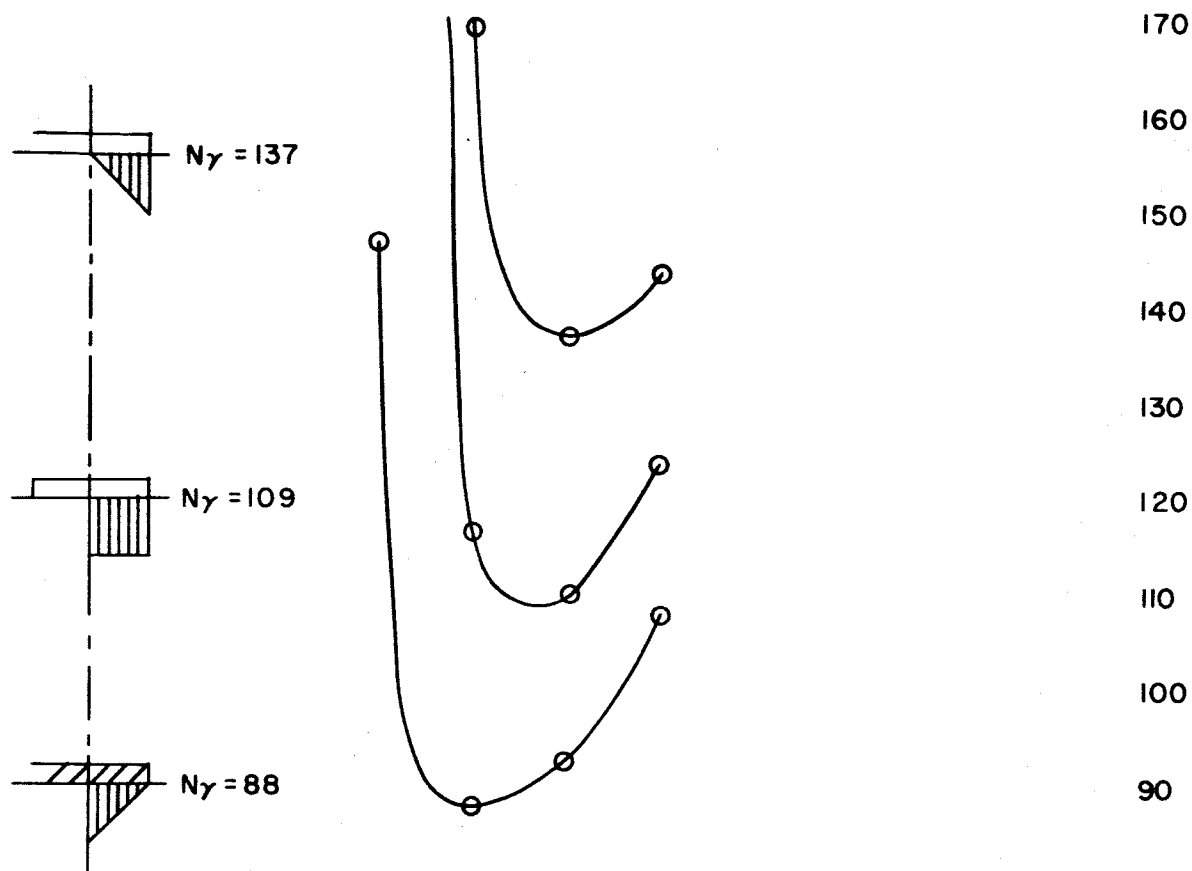
FIG. 36 FAILURE SURFACES FOR A STRIP FOOTING
FOR A RISE ANGLE ψ EQUAL TO $45° + \dfrac{\phi}{2}$

Surface 2

Mean Ordinate	Width	Area	Arm	Moment
14.5	10	145	5	725
17.7	10	177	15	2655
16	10	160	25	4000
		482		7380
		- 22.5		- 37.5
		459.5		7342.5

$$\text{C. G.} = \frac{7342.5}{459.5} = 15.98$$

$$d_w = \begin{array}{r} 15.98 \\ - 5.18 \\ \hline 10.80 \end{array} = 2.16 \ r$$

$$d_p = \frac{2}{3} \ h_2 = \frac{2}{3} \ x \ 13.8 = \begin{array}{r} 9.2 \\ 0.0 \\ \hline 9.2 \end{array} = 1.84 \ r$$

Surface 3

Mean Ordinate	Width	Area	Arm	Moment
16.2	10	162	5	810
20.7	10	207	15	3105
20.3	10	203	25	5075
18	5	90	32.5	2925
		662		11915
		- 22.5		- 37.5
		639.5		11877.5

$$\text{C.G.} = \frac{11877.5}{639.5} = 18.57$$

$$d_w = \begin{array}{r} 18.57 \\ - 6.80 \\ \hline 11.77 \end{array} = 2.35 \text{ r}$$

$$d_p = \frac{2}{3} h_3 = \frac{2}{3} \times 16.5 = \begin{array}{r} 11 \\ - 1.0 \\ \hline 10.0 \end{array} = 2.0 \text{ r}$$

Surface 4

Mean Ordinate	Width	Area	Arm	Moment
18.2	10	182	5	910
23.5	10	235	15	3525
24.2	10	242	25	6050
21.7	10	217	35	7595
		876		18080
		- 22.5		- 37.5
		853.5		18042.5
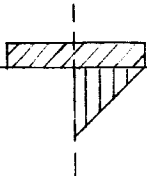
$$\text{C.G.} = \frac{18042.5}{853.5} = 21.14$$

$$d_w = \begin{array}{r} 21.14 \\ - 8.30 \\ \hline 12.84 \end{array} = 2.57 \text{ r}$$

$$d_p = \frac{2}{3} \ h_4 = \frac{2}{3} \times 19.5 = \begin{array}{r} 13 \\ - 1.8 \\ \hline 11.2 \end{array} = 2.24 \text{ r}$$
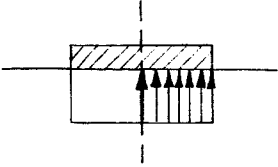
Surface	W	d_w	Wd_w	Pd_{P_1}	M	P_1	d_{P_1}	h_{PR}	h^2	h
1	12.4	2.07	25.7	13.10	38.8	7.85	1.67	3.25	4.84	2.2
2	18.4	2.16	39.7	22.7	62.4	12.35	1.84	3.25	7.6	2.76
3	25.6	2.35	60.1	35.4	95.5	17.7	2.0	3.25	10.89	3.3
4	34.1	2.57	88.0	55.5	143.5	24.75	2.24	3.25	15.21	3.9

Plate $\psi = 45 + \dfrac{\phi}{2}$

Value of N_γ based on Distribution

Surface	d_{p_p}		M	M/d_{p_p}
1	$\dfrac{3.00 - 1.67}{5} = 0.265$		38.80	147
2	$\dfrac{5.18 - 1.67}{5} = 0.702$		62.4	88
3	$\dfrac{6.80 - 1.67}{5} = 1.026$		95.50	92.5
4	$\dfrac{8.30 - 1.67}{5} = 1.326$		143.5	108.5
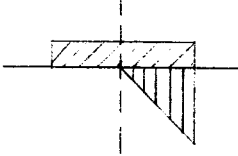
$$N_{\gamma\,(min)} = 88$$

Value of N_Y Based on � Distribution

Surface	d_{p_p}		M	M/d_{p_p}
1	$\dfrac{3.00 - 2.5}{5} =$	0.1	38.8	388
2	$\dfrac{5.18 - 2.5}{5} =$	0.536	62.4	116.5
3	$\dfrac{6.80 - 2.5}{5} =$	0.86	95.5	110
4	$\dfrac{8.30 - 2.5}{5} =$	1.16	143.5	124

$$N_Y \text{(min)} = 110$$

true from curve = 109

Values of N_γ Based on _____ Distribution

Surface	d_{p_p}	M	M/d_{p_p}
1	-	-	-
2	$\dfrac{5.18 - 3.33}{5} = 0.37$	62.4	169
3	$\dfrac{6.80 - 3.33}{5} = 0.695$	95.5	137
4	$\dfrac{8.30 - 3.33}{5} = 0.995$	143.5	144

$$N_{\gamma\,(min)} = 137$$

APPENDIX B

Appendix B

The calculations of the bearing capacity coefficient N_γ for a wedge-shaped foundation element are shown in this appendix (refer to Fig. 37). The proposed failure surfaces, and the procedure followed in the calculations, are based on the theory of Terzaghi previously covered. The steps are the same as those outlined in Appendix A.

Calculations for the Bearing Capacity Coefficient N_γ for a Cone

Surface 2 - (Refer to Fig. 37)

Mean Ordinate	Width	Area	Arm	Moment
21.3	10	213	5	1065
21.7	10	217	15	3255
19.2	10	192	25	4800
		622		9120

$$C.G. = \frac{9120}{622} = 14.66$$

$$d_w = \begin{array}{r} 14.66 \\ + 4.00 \\ \hline 18.66 \end{array} = 1.866 \ r$$

$$d_p = \frac{2}{3} \ h_2 = \frac{2}{3} \times 16.5 = \begin{array}{r} 11.00 \\ + 1.50 \\ \hline 12.50 \end{array} = 1.25 \ r$$

CONE – 30° = HALF VERTEX

50

40

30

20

$N_\gamma = 20.8$

10

Ç OF FOOTING

r

CONE

$45° - \phi/2$

$\alpha = 30°$ $\phi = 32°$

ARC

h_1 h_2 h_3 h_4 h_5

0

1
2
3
4
5
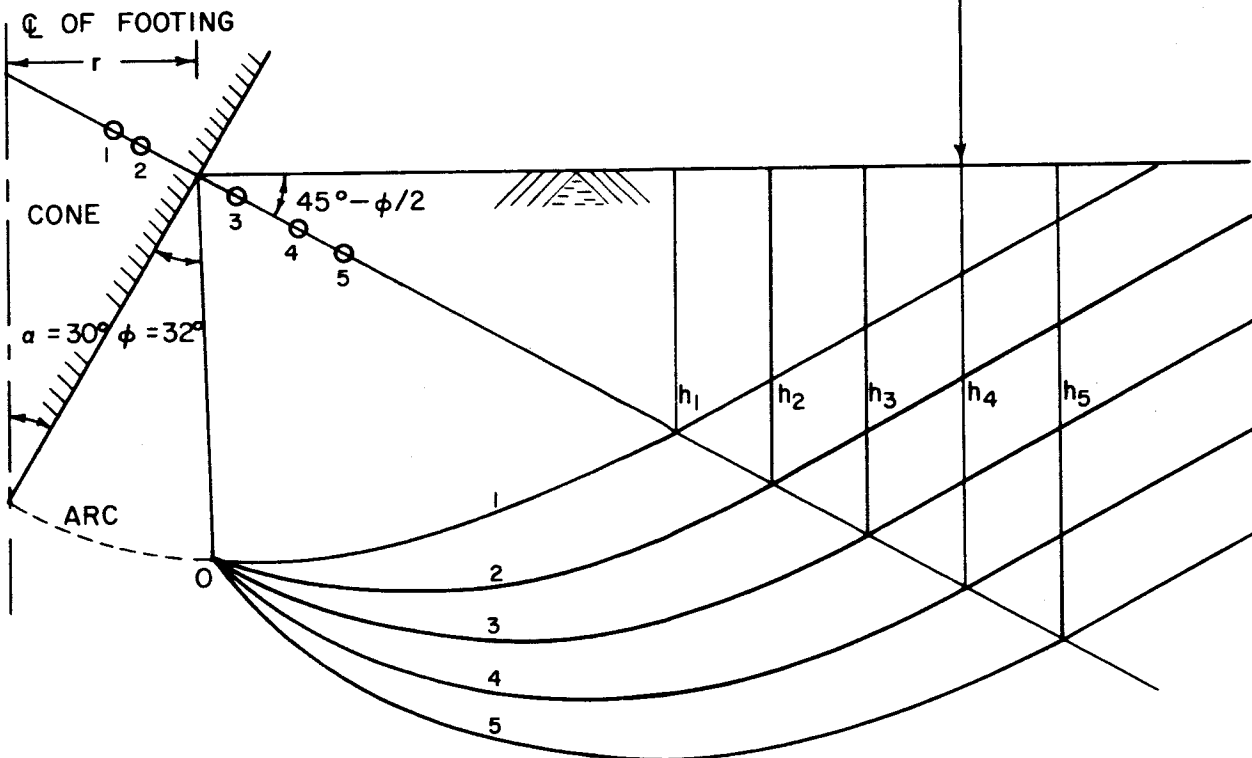
FIG. 37 PROPOSED FAILURE SURFACES FOR A CONE

Surface 3

Mean Ordinate	Width	Area	Arm	Moment
22.3	10	223	5	1115
24.5	10	245	15	3675
23.5	10	235	25	5875
20.7	5	103.5	32.5	3363.75
		806.5		14028.75

$$\text{C.G.} = \frac{14028.75}{806.5} = 17.38$$

$$d_{\text{w}} = \begin{array}{r} 17.38 \\ -\ 1.50 \\ \hline 15.88 \end{array} = 1.588 \ r$$

$$d_{p_1} = \frac{2}{3} h_3 = \frac{2}{3} \times 19.5 = \begin{array}{r} 13.0 \\ -\ 1.2 \\ \hline 11.8 \end{array} = 1.18 \ r$$

Surface 4

Mean Ordinate	Width	Area	Arm	Moment
23.8	10	238	5	1190
27.4	10	274	15	4110
27.5	10	275	25	6875
24.7	10	247	35	8645
		1034		20820

$$\text{C.G.} = \frac{20820}{1034} = 20.14$$

$$d_w = \begin{array}{r} 20.14 \\ -\ 5.00 \\ \hline 15.14 \end{array} = 1.514\ r$$

$$d_{p_1} = \frac{2}{3} \times h_4 = \frac{2}{3} \times 22 = \begin{array}{r} 14.67 \\ -\ 3.00 \\ \hline 11.67 \end{array} = 1.167\ r$$

Surface 5

Mean Ordinate	Width	Area	Arm	Moment
25	10	250	5	1250
29.8	10	298	15	4470
30.8	10	308	25	7700
29.2	10	292	35	10220
26.2	5	131	42.5	5567.5
		1279		29207.5

$$\text{C.G.} = \frac{29207.5}{1279} = 22.85$$

$$
\begin{aligned}
d_w \quad = \quad & 22.84 \\
& -\ 7.00 \\
\hline
& 15.84 \quad = \quad 1.584\ r
\end{aligned}
$$

$$
d_p \quad = \frac{2}{3} \ \times \ h_5 \ = \frac{2}{3} \ \times \ 24.9 \ =
\begin{aligned}
& 16.6 \\
& -\ 3.5 \\
\hline
& 13.1 \ = \ 1.31\ r
\end{aligned}
$$

CONE

Surface	W	d_w	Wd_w	P_1d_1	M	P_1	d_{p_1}	h_{PR}	h^2	h
2	6.22	1.866	11.61	5.55	17.16	4.42	1.25	3.25	2.72	1.65
3	8.06	1.59	12.8	8.02	20.82	6.8	1.18	3.25	3.80	1.95
4	10.34	1.51	15.6	9.1	24.7	7.8	1.167	3.25	4.84	2.2
5	12.79	1.58	20.2	12.8	33.0	9.75	1.31	3.25	6.1	2.49

Surface	d_{p_p}	M	M/d_{p_p}
2	$\dfrac{6.83 - 3.33}{10} = 0.35$	17.16	49
3	$\dfrac{12.0 - 3.33}{10} = 0.867$	20.82	24.2
4	$\dfrac{15.2 - 3.33}{10} = 1.18$	24.7	$\boxed{20.8}$ → Min = N_Y
5	$\dfrac{17.5 - 3.33}{10} = 1.417$	33.0	23.2

APPENDIX C

Appendix C

The calculations of the bearing capacity coefficient N_γ for a strip foundation element with a spherical base are shown in this appendix. (Refer to Fig. 38.) The proposed failure surfaces and the procedure followed in the calculations are based on the theory of Terzaghi previously covered. The steps are the same as those outlined in Appendix A.

SPHERE

$N\gamma._{min.} = 15$

30

20

C OF FOOTING

r

TANGENT

SPHERE

10

$45° - \phi/2 = 29°$

$\phi = 32°$

h_1 h_2 h_3 h_4

0

1

2

3

4
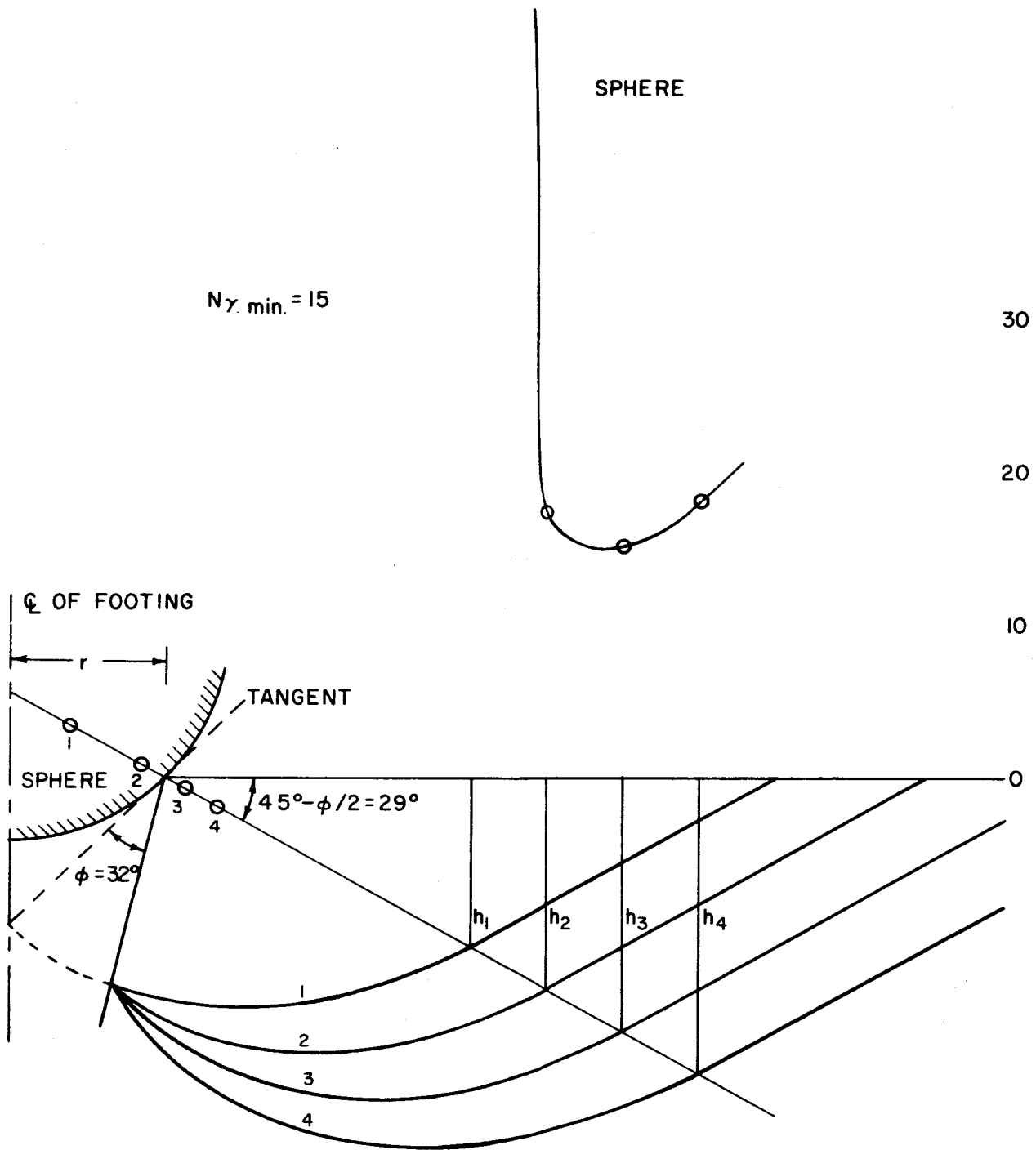
FIG. 38 PROPOSED FAILURE SURFACES FOR A SPHERE

Calculations of the Bearing Capacity Coefficient N_γ for a Sphere

Surface 1 - (Refer to Fig. 38)

Mean Ordinate	Width	Area	Arm	Moment
14.2	3.5	49.70	1.75	86.98
15.1	10	151.00	8.5	1283.50
13.4	10	134.00	18.5	2479.00
		334.70		3849.48
		-23.63*		-27.58
		311.07		3821.90

$$\text{C.G.} = \frac{3821.90}{311.07} = 12.28$$

$$d_w = \begin{array}{r} 12.28 \\ + 3.00 \\ \hline 15.28 \end{array} = 1.528\ r$$

$$d_p = \frac{2}{3}\ h_1 = \frac{2}{3} \times 11 = \begin{array}{r} 7.33 \\ +3.20 \\ \hline 10.53 \end{array} = 1.053\ r$$

*Area of triangular wedge = 1/2 x 13.5 x 3.5 = 23.63

*Moment of triangular wedge = 23.63 x $\frac{3.5}{.3}$ = 27.58

Surface 2

Mean Ordinate	Width	Area	Arm	Moment
14.8	3.5	51.8	1.75	90.65
17.6	10	176.0	8.5	1496.00
17.6	10	176.0	18.5	3256.00
15.2	5	76.0	26	1976.00
		479.80		6818.65
		- 23.63		27.58
		456.17		6791.07

$$C.\ G. = \frac{6791.07}{456.17} = 14.89$$

$$d_w = \begin{array}{r} 14.89 \\ -\ 2.00 \\ \hline 12.89 \end{array} = 1.289\ r$$

$$d_p = \frac{2}{3}\ h_2 = \frac{2}{3} \times 13.8 = \begin{array}{r} 9.2 \\ +0.7 \\ \hline 9.9 \end{array} = 0.99\ r$$

Surface 3

Mean Ordinate	Width	Area	Arm	Moment
15.4	3.5	53.9	1.75	94.33
19.7	10	197	8.5	1674.5
21	10	210	18.5	3885.0
19	10	190	28.5	5415.0
		650.90		11068.83
		-23.63		- 27.58
		627.27		11041.25

$$\text{C.G.} \quad = \quad \frac{11041.25}{627.27} \quad = \quad 17.60$$

$$d_w \quad = \quad 17.60$$
$$\underline{\quad - 5.00 \quad}$$
$$12.60 \quad = \quad 1.26 \ r$$

$$d_{p_1} \quad = \quad \frac{2}{3} \ h_3 \quad = \quad \frac{2}{3} \ \times \ 16.5 \quad = \quad 11.0$$
$$\underline{\quad - 0.7 \quad}$$
$$10.3 \quad = \quad 1.03 \ r$$

Surface 4

Mean Ordinate	Width	Area	Arm	Moment
16.	3.5	56	1.75	98
21.5	10	215	8.5	1827.5
24.2	10	242	18.5	4477.0
23.5	10	235	28.5	6697.5
20.6	5	103	36	3708.0
		851.		16808.0
		- 23.63		- 27.58
		827.37		16780.42

$$\text{C. G.} = \frac{16780.42}{827.37} = 20.28$$

$$
d_w = \begin{array}{r} 20.28 \\ - 7.00 \\ \hline 13.28 \end{array} = 1.328 \ r
$$

$$d_p = \frac{2}{3} \ h_4 = \frac{2}{3} \times 19.5 = \begin{array}{r} 13.0 \\ - 2.0 \\ \hline 11.0 \end{array} = 1.1 \ r$$

SPHERE

Surface	W	d_W	$P_1 d_{P_1}$	M	P_1	d_{P_1}	h_{PR}	h^2	h
1	3.11	1.528	2.07	6.82	1.97	1.053	3.25	1.21	1.1
2	4.56	1.289	3.05	8.93	3.08	0.99	3.25	1.9	1.38
3	6.27	1.26	4.55	12.45	4.42	1.03	3.25	2.72	1.65
4	8.27	1.328	7.48	18.46	6.8	1.1	3.25	3.80	1.95

Surface	d_{P_p}	M	M/d_{P_p}
1	$\dfrac{3.80 - 3.33}{10} = .047$	6.82	145
2	$\dfrac{8.50 - 3.33}{10} = .517$	8.93	17.3
3	$\dfrac{11.50 - 3.33}{10} = 0.817$	12.45	15.2
4	$\dfrac{13.50 - 3.33}{10} = 1.017$	18.46	18.1

REFERENCES

1. Bekker, M. G., Theory of Land Locomotion, p. 457, The University Michigan Press, An Arbor, 1956.

2. Casagrande, A., and Shannon, W. L., "Stress Deformation and Strength Characteristics of Soils Under Dynamic Loads," Proceedings of the Second International Conference on Soil Mechanics, Vol. 5, Paper II d10, pp. 29-34, 1948.

3. Davis, E. H. and Woodward, R. J., "Some Laboratory Studies of Factors Pertaining to the Bearing Capacity of Soils," Reprint No. 6, Proceedings of the Twenty-ninth Annual Meeting of the Highway Research Board, December 1949.

4. Huntley, H. E., Dimensional Analysis, p. 43, MacDonald, London, 1952.

5. Jumikis, A. R., Soil Mechanics, pp. 618-640, Van Nostrand Company, Inc., New Jersey, 1962.

6. Lee, C. E., "The Determination of Pavement Deflections Under Repeated Load Applications," A Dissertation, University of California, 1961.

7. Lundgren H., "Dimensional Analysis in Soil Mechanics," Acta Polytechnica Scandinavica, 237, 1957.

8. Meyerhoff, G. G., "The Ultimate Bearing Capacity of Foundations," Geotechnique, Vol. 2, pp. 301-332, December 1951.

9. Meyerhoff, G. G., "The Tilting of a Large Tank on Soft Clay," Proceedings of The South Wales Institute of Engineers, Vol. LXVII, No. 2, pp. 53-71, 1951.

10. Meyerhoff, G. G., "An Investigation of the Bearing Capacity of Shallow Footings on Dry Sand," Proceedings of the Second International Conference on Soil Mechanics and Foundation Engineering, Vol. 1, Rotterdam, June 21 to 30, 1948.

11. Rayleigh, J. W. S., The Theory of Sound, McMillan and Company, Ltd., London, 1937.

12. Schleicher, F., "Zur Theorie des Baugrundes," Der Bauingenieur, pp. 931-935, 949-952, Heft 48, 1926.

13. Scott, R. F., Principles of Soil Mechanics, p. 447, Addison-Wesley Publishing Company, Inc., Massachusetts, 1963.

14. Selig, E. T. and McKee, K. E., "Static and Dynamic Behavior of Small Footings," _Proceedings of the American Society of Civil Engineers, Soil Mechanics and Foundations Division_, SM6, December, 1961.

15. Skempton, A. W., "The Bearing Capacity of Clays," _Proceedings Building Research Congress_, Division I, Part III, pp. 180-189, London, 1951.

16. Taylor, D. W., _Fundamentals of Soil Mechanics_, John Wiley and Sons, Inc., New York 1948, pp. 572-573.

17. Taylor, D. W., _Fundamentals of Soil Mechanics_, John Wiley and Sons, Inc., New York 1948, pp. 576.

18. Taylor, D. W., _Fundamentals of Soil Mechanics_, John Wiley and Sons, Inc., New York 1948, p. 580.

19. Taylor, D. W., _Fundamentals of Soil Mechanics_, John Wiley and Sons, Inc., New York 1948, p. 584.

20. Taylor, D. W., _Fundamentals of Soil Mechanics_, John Wiley and Sons, Inc., New York 1948, pp. 614-615.

21. Terzaghi, K., "Evaluation of Coefficients of Subgrade Reaction," _Geotechnique_, pp. 297-326, Vol. 5, No. 4, December 1955.

22. Terzaghi, K., _Theoretical Soil Mechanics_, pp. 118-124, John Wiley and Sons, Inc., New York, 1943.

23. Terzaghi, K., _Theoretical Soil Mechanics_, p. 125, John Wiley and Sons, Inc., New York, 1943.

24. Terzaghi, K., _Theoretical Soil Mechanics_, pp. 382-184, John Wiley and Sons, Inc., New York, 1943.

25. Terzaghi, K., and Peck, R. B., _Soil Mechanics in Engineering Practice_, p. 168, John Wiley and Sons, Inc., New York, 1943.

26. Terzaghi, K., and Peck, R. B., _Soil Mechanics in Engineering Practice_, p. 172, John Wiley and Sons, Inc., New York, 1948.

27. Timoshenko, S., _Theory of Elasticity_, McGraw-Hill Book Company, Inc. New York, 1934.

28. Tschebotarioff, G. R., _Soil Mechanics, Foundations and Earth Structures_, pp. 136-137, McGraw-Hill Book Company, Inc, New York, 1951.